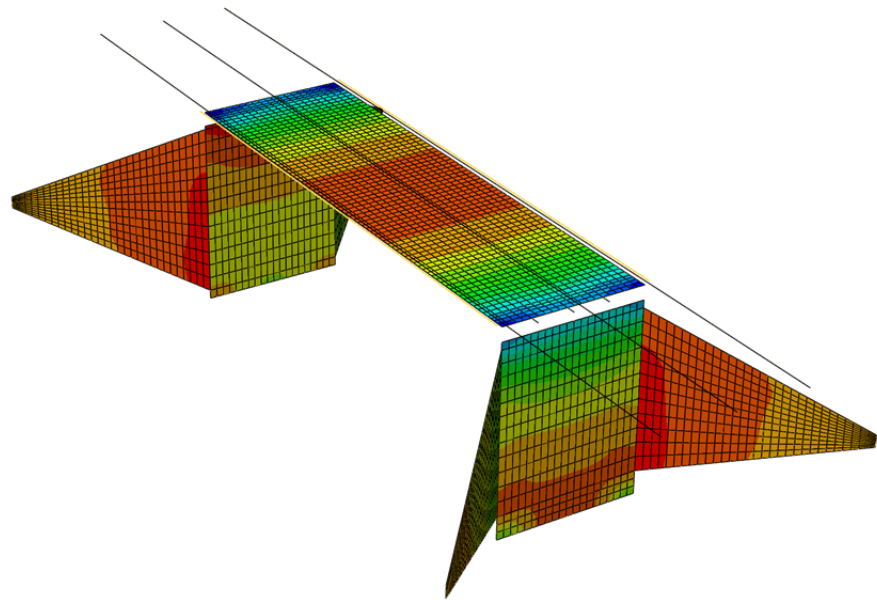


Division of Structural Engineering
Lund Institute of Technology, Lund University

Realistic Modeling of Thermal Effects in Concrete Bridges



Carl Larsson, Gustav Svensson

Avdelningen för Konstruktionsteknik
Lunds Tekniska Högskola
Lunds Universitet 2013



Report TVBK-5223
Lund 2013

LUNDS UNIVERSITY
DIVISION OF STRUCTURAL ENGINEERING
AVDELNINGEN FÖR KONSTRUKTIONSTEKNIK

REPORT:
ISSN 0349-4969
LUTVDG/TVBK-5223(102)

MODELING OF THERMAL EFFECTS IN CONCRETE BRIDGE DESIGN

Master's dissertation by:
CARL LARSSON & GUSTAV SVENSSON

Supervisors:

Oskar Larsson, Dr.
Div. of Structural Engineering

Karl Lundstedt, M.Sc.
Skanska Teknik

Examiner:

Tord Isaksson, Dr.
Div. of Structural Engineering

Lunds University
Division of Structural Engineering
P.O. Box 118
SE-221 00 Lund, Sweden
www.kstr.lth.se

Abstract

Thermal actions have a significant effect on bridge structures and can at some sections account for more than 20% of the reinforcement. Such actions are especially important in certain types of concrete bridges, e.g. portal frame bridges.

Thermal actions differ from other load types considered during bridge design through being a constraining load. A temperature profile can be divided into a uniform part that affect the bridge with a linear expansion and a non-uniform part that will induce an arch shape of the bridge deck.

Using the current building code, thermal actions can account for more than 20% of the total demand of reinforcement at midsection making them so large that they cannot be neglected. This makes thermal actions in bridge design interesting for further investigation.

The current building code in Sweden suggests two approaches for considering temperature differentials during bridge design. The first approach uses a linear temperature distribution through the bridge deck and the second approach uses a non-linear distribution. In this thesis, an analysis using real climate data presented by SMHI is used to determine which of the two approaches is most realistic. A simulation is performed for the year 1986 with data collected in Stockholm, Sweden. Results from this simulation imply that approach 2 will give a more realistic temperature distribution than approach 1.

A second analysis is performed, analyzing a portal frame bridge built in Katrineholm, Sweden. This analysis compares the different approaches from the current building code. Results from the analysis indicate more favorable load effects when using approach 2. Using this approach during bridge design will reduce the total demand of reinforcement.

When using approach 2 stress peaks will arise at top and bottom of a bridge section during analysis. During a load case when the bridge deck is cooled, tensile stresses will rise above the tensile strength of concrete, implying the appearance of cracks. Based on the current building code, two methods are established to handle stress peaks in a bridge structure. Both methods show similar results, indicating that the total demand of reinforcement using approach 2 will rise.

In addition, this report addresses the difficulties of modeling concrete by FE analysis. In the report an isotropic constitutive model is used with no ability to determine possible cracks and will result in overestimated load effects. Another conclusion is that it is not obvious how a temperature load should be applied to a modern 3D model and today's building codes may not be up to date with this.

Keywords:

TEMPERATURE, THERMAL, EUROCODE, SIMULATION, REALISTIC, CONCRETE, BRIDGE, MODELING, EFFECTS, CRACKING, LOAD, DESIGN

Sammanfattning

Temperaturlaster har en betydande lasteffekt på brokonstruktioner. För plattrambroar byggda i betong kan dessa temperaturlaster stå för mer än 20% av armeringsbehovet i vissa sektioner.

De laster som uppstår p.g.a. temperatur skiljer sig från övriga laster vid dimensionering av broar genom att vara en tvångslast. Temperaturlasten är uppdelad i två delar; en jämn del som påverkar hela brobanan genom en jämn längdutvidgning samt en ojämn del som ger upphov till krökning av brobanan. Den totala lasteffekten av de här lasterna är så stor att den ej kan försummas vid dimensionering. Detta gör temperaturlaster intressanta att studera noggrannare vid brodimensionering.

Den nuvarande byggnormen i Sverige föreslår två olika metoder för att behandla den ojämna delen av temperaturlasten. Den första metoden (approach 1) använder en linjär temperaturfördelning över tvärsnittet. Den andra metoden (approach 2) föreslår en olinjär temperaturdistribution. För att evaluera de båda metoderna har en simulering gjorts på ett fiktivt brotvärsnitt med hjälp av klimatdata inhämtad i Stockholm år 1986 av SMHI. Resultaten från denna simulering tyder på att metoden med en olinjär temperaturdistribution för modellering av temperaturlast är mer realistisk än metoden med en linjär temperaturfördelning.

En andra analys är gjord på en plattrambro byggd i Katrineholm. Denna analys jämför de skillnader som uppstår vid dimensionering då de två olika metoderna för temperaturlasten används. Resultaten från analysen visar att det är mer fördelaktigt att använda metod 2 med en olinjär temperaturdistribution. Denna metod ger lägre dimensionerande moment vilket således också ger lägre ett armeringsbehov.

Då den andra metoden används vid brodimensionering uppstår spänningstoppar vid brotvärsnittets över- och underkant. Vid lastfall med avkylning av broplattan uppstår dragspänningar nära ytan som i vissa fall överskrider betongens draghållfasthet. Detta tyder på att sprickor orsakade av temperaturlaster kan förekomma. För att hantera dessa spänningstoppar, har två olika angreppssätt (method A och method B) tagits fram och beskrivits i denna rapport baserat på gällande byggnorm gällande sprickor i betong. Då de båda angreppssätten appliceras och jämförs visar de på liknande resultat som båda indikerar på en ökning av det totala armeringsbehovet. Förutom utvärdering av de olika temperaturprofilerna behandlar rapporten svårigheterna med modellering av betong i en FE-analys. I analyserna används en isotrop konstitutiv modell där det inte finns möjlighet att ta hänsyn till sprickbildning i betongen. Denna förenkling kommer leda till att lasteffekterna av tvångslaster blir överskattade. En annan slutsats som dras från arbetet är att tillvägagångssättet för att modellera en temperaturlast inte är självklart. Det finns ett glapp mellan analyser med 3D modeller och det sätt som temperaturlaster föreskrivs i byggnormen.

Nyckelord:

TEMPERATUR, TERMISK, EUROKOD, SIMULERING, REALISTISK, BETONG, BRO, MODELLERING, LASTEFFEKTER, SPRICKOR, LAST, DIMENSIONERING

*“To myself I am only a child playing on
the beach, while vast oceans of truth lie
undiscovered before me”*

- Isaac Newton

We are proud to finish this final piece on our five year master program in Lund, a time and education that changed us both as individuals. Starting off with a broad idea our further investigations made us realize how much there is to learn. The complexity of the problem have been striking us on a daily basis, leaving us with being proud of at least knowing more in this subject than many around us. We have received much and useful help from many around us during this project. We want to thank our supervisors Dr. Oskar Larsson and M.Sc. Karl Lundstedt who always been helpful and answering our questions. We would also like to thank Dr. Tord Isaksson, M.Sc. Joel Bjerstedt and M.Sc. Rickard Nagy who have been helpful with information and discussions every time we needed their help. Special thanks to classmates, friends and family who supported us and made all these years very enjoyable.

LUND MAY 2013



CARL LARSSON



GUSTAV SVENSSON

Contents

| | | |
|----------|---|-----------|
| 1 | Introduction | 5 |
| 1.1 | Background | 5 |
| 1.2 | Purpose | 5 |
| 1.3 | Methods | 5 |
| 1.4 | Objectives | 6 |
| 1.5 | Scope | 6 |
| 1.6 | Outline of the report | 6 |
| 2 | Temperature loads | 7 |
| 2.1 | Thermal input factors | 7 |
| 2.1.1 | Solar radiation | 7 |
| 2.1.2 | Long wave heat radiation | 8 |
| 2.1.3 | Convection | 9 |
| 2.2 | Temperature loads | 9 |
| 2.3 | Heat transfer | 11 |
| 3 | Concrete | 13 |
| 3.1 | Background | 13 |
| 3.1.1 | Components | 14 |
| 3.2 | Thermal material properties | 14 |
| 3.2.1 | Density | 15 |
| 3.2.2 | Specific heat capacity | 15 |
| 3.2.3 | Thermal conductivity | 15 |
| 3.2.4 | Thermal expansion coefficient | 15 |
| 3.3 | Cracks | 15 |
| 3.3.1 | Micro cracks | 16 |
| 3.3.2 | Crack widths | 16 |
| 3.4 | FE modeling of concrete | 17 |
| 3.4.1 | Material modeling | 17 |
| 3.4.2 | Shell Elements | 18 |
| 4 | Building codes | 21 |
| 4.1 | Loads and Material coefficients | 21 |
| 4.1.1 | Partial coefficients | 21 |
| 4.1.2 | Safety factors | 21 |
| 4.1.3 | Load combination factors | 22 |
| 4.2 | Thermal actions on structures | 23 |
| 4.2.1 | Uniform Temperature component | 23 |

| | | |
|----------|--|------------|
| 4.2.2 | Temperature difference components | 24 |
| 4.2.3 | Temperature difference between different structural elements | 25 |
| 4.3 | Crack widths | 26 |
| 4.4 | Additional building codes | 26 |
| 4.4.1 | TRVR Bro | 27 |
| 5 | Climate simulation of bridge cross section | 29 |
| 5.1 | Portal frame bridge 829 in Katrineholm | 29 |
| 5.2 | Climate simulation | 30 |
| 5.2.1 | Finite element model | 30 |
| 5.3 | Results | 32 |
| 5.3.1 | 100mm paving | 33 |
| 5.3.2 | Comparison between paving thickness | 36 |
| 6 | Temperature effects during bridge design | 39 |
| 6.1 | Temperature load analysis | 39 |
| 6.1.1 | Finite element model | 39 |
| 6.1.2 | Validation of FE-model | 42 |
| 6.1.3 | Temperature modeling | 42 |
| 6.2 | Results | 44 |
| 6.2.1 | Section moments | 45 |
| 6.2.2 | Section forces | 47 |
| 6.2.3 | Results from climate simulation | 48 |
| 6.2.4 | Stresses in cross section | 49 |
| 7 | Crack width limitations | 53 |
| 7.1 | Method for calculating crack widths | 53 |
| 7.1.1 | Method A - Force added manually | 53 |
| 7.1.2 | Method B - Moment added manually | 56 |
| 7.1.3 | Graphical comparison of Method A and Method B | 57 |
| 7.2 | Results | 58 |
| 7.2.1 | Element 1 | 58 |
| 7.2.2 | Element 2 | 59 |
| 8 | Conclusion | 61 |
| 8.1 | Summary of Results | 61 |
| 8.2 | Discussion | 61 |
| 8.3 | Further research | 63 |
| A | Climate Model | I |
| A.1 | Climate model | I |
| B | Case Study | VII |
| B.1 | Validation of model | VII |
| B.2 | Load effects from FE analysis | XI |

Chapter 1

Introduction

1.1 Background

Thermal originates from the latin word 'thermalis' and is the total potential and kinetic energy in an object resulting in a temperature. Thermal actions in concrete bridges started to become an issue in the mid 50s. More advanced analysis methods gave rise to bridges with longer span lengths and multiple supports. However, these bridges started to develop temperature related cracks, noticed in Germany. [Leonhardt et al., 1965]

Thermal actions create major constraining forces in bridges of certain types, e.g. portal frame bridges. These constraining forces are of such magnitude that they cannot be neglected. One issue with thermal actions on a concrete bridge is cracking, most noticed on the south side, that give rise to problems with durability in the serviceability state.

With today's requirements of advanced FE analysis during bridge design, these forces have become so large that questions have been raised if the regulating documents considering bridge design is up to date with today's analysis methods. Dr. Oskar Larsson [2012] treats this issue in his doctoral thesis.

1.2 Purpose

Thermal actions is a significant load for certain types of bridge structures making them interesting to investigate. The purpose is to investigate how these actions are treated in modern bridge design.

The authors vision is to find a way or method for a more realistic simulation of thermal actions and use these input variables for a more realistic bridge design. More specifically this thesis will handle the uneven parts of the temperature distribution over a bridge deck cross section.

1.3 Methods

A literature study for deeper understanding of the subject is performed where the main topics are concrete as material, heat transfer as a process and the finite element theory. Other practical subjects that will be addressed are the bridge as a structure and the existing building codes. A real project will be studied to see how Skanska are working with temperature loads during their design process.

The first analysis, described in chapter 5, is a simulation of temperature distribution in a simple 2D concrete section. Actual climate data collected from SMHI is used. The outcome of this analysis is used as a background for validation and choice of temperature model according to the building code.

The second analysis, presented in chapter 6, will be a comparison using different temperature profiles according to the building code. This analysis is done on a real bridge, provided by Skanska Teknik.

The third part of the analysis is to further investigate how different temperature modeling could cause any other unforeseen problems. This is done by combining result from previous FE simulation and the use of empirical relationships used during concrete design.

For all FE analyses the commercial softwares Scanscot BrigadePlus and Scanscot BrigadeStandard are used. To handle the amount of data from the FE analysis, produce accurate plots and solve equations through iteration, Mathworks MatLAB is used.

1.4 Objectives

The main objective in this thesis is to investigate how a more advanced temperature modeling affects the overall bridge design. It will also be investigated how realistic the temperature loads suggested by the building code are.

1.5 Scope

This thesis will treat temperature loads that occur naturally in bridges. With naturally we mean changes in temperature due to natural processes such as solar radiation, wind, long wave radiation and seasonal variations in temperature. Extreme temperature loads from accidents or fire are not included. Further the analyses is limited to portal frame bridges built with reinforced concrete. The majority of analyses will be done with the finite element method. The concrete will not be treated during its hydration phase. The properties of the concrete in cooling and heating is therefore assumed to be equal. During modeling, concrete will be treated as a linear elastic homogeneous material. In reality this means an uncracked state of the material.

1.6 Outline of the report

This report evaluates how temperature effects suggested in the current building codes affects the design of a concrete bridge structure. A simulation with real climate data has been performed and is presented in chapter 5 to evaluate the different approaches given by the current building code. A comparison using these different approaches in regard to temperature loads is presented in chapter 6.

Surface cracking of the concrete could be a problem when non-linear temperature profiles appear in concrete structures. This is presented in chapter 7. To understand these analyses and use correct input parameters a literature study have been done and is presented. Chapter 2 describes the basics of a temperature load, chapter 3 describes concrete as a building material and chapter 4 describes how temperature loads are treated in the current building codes.

Chapter 2

Temperature loads

2.1 Thermal input factors

All structures are affected by its surrounding temperature. Temperature can cause stresses in two ways, either by a non linear temperature distribution causing eigenstresses or a constraint restricting the structure from moving free. The thermal loads can be divided into a number of factors. This chapter will describe the nature of these phenomena and how they interact with a concrete structure. The described factors are shown in figure 2.1

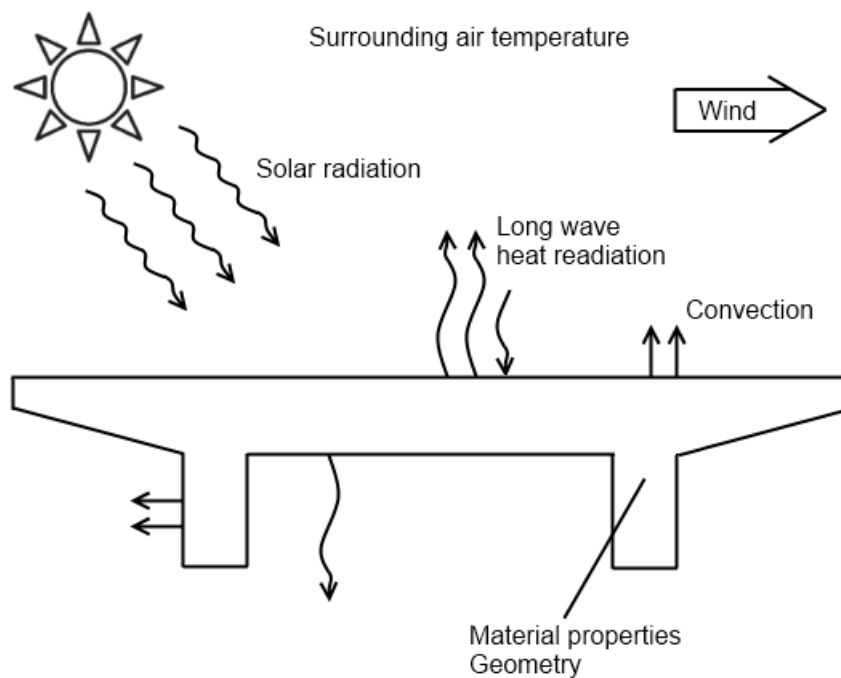


Figure 2.1: Illustration of factors from surrounding climate that affects bridge structures

2.1.1 Solar radiation

Solar radiation is energy emitted from the sun. The radiation flux decreases with distance through dilution. Since the intensity depends on the distance it is changing slightly with season. The solar constant describes the average energy from the sun that reaches the outer boundary of the earth's atmosphere and is according to Incropera et al. [2007] in average $1353W/m^2$. This amount is almost constant, changing from around $1410W/m^2$ in January to $1320W/m^2$ in June [Larsson, 2012]. The radiation from the sun

consists of short wavelength light. The reason that the radiation from the sun has shorter wavelengths than what is referred to as long wave heat radiation from earth is the higher temperature of the sun. The higher the temperature is of the body the shorter the wavelength of its radiation will be. Radiation can be divided into visible light, UV-light and infrared light. A major difference between these are their ability to pass through or be absorbed in the atmosphere. The light can reach the surface of the earth directly or be altered by the atmosphere in different ways. By interacting with the particles the light can be reflected, scattered, refracted or absorbed.

Radiation striking the surface of the earth is called global or total radiation, parts of this is absorbed by vegetation or objects located close to the ground. The ratio of the light that is absorbed or reflected depends on the properties of the material, primary the texture and color. The energy absorbed by the material can be calculated as an absorption coefficient a multiplied with the incident solar radiation G :

$$q_s = a \cdot G \quad [W/m^2] \quad (2.1)$$

Several studies have been performed on the absorptivity of concrete and the results varies from 0.5 [Emerson, 1973] to 0.7 [Branco and Mendes, 1993]. In many cases the concrete is covered by asphalt where the most commonly used absorptivity is 0.9. [Larsson, 2012]

The total light that reaches a surface is called global radiation G :

$$G = I_b + I_d + I_g \quad [W/m^2] \quad (2.2)$$

The light which reaches the ground is either direct light I_b , diffuse light I_d or light that is reflected from another surface I_g . The direct light reaches the surface without being disturbed and its intensity depends on the following reasons:

- Latitude and altitude
- Time of the day and year
- Inclination of the surface

The diffuse light I_d refers to all light that have interacted with any kind of clouds or particles on its way between the sun and the surface and therefore comes with other intensity and/or angle. The amount of diffuse radiation can vary from around 10% of the total light on a clear day to 100% on a cloudy day [Incropera et al., 2007].

Reflected light I_g is light that does not affect the surface, however light can be reflected from other surfaces onto the surface.

2.1.2 Long wave heat radiation

Long wave heat radiation is emitted from all materials with a temperature T greater than absolute zero. All materials emit longwave radiation from its whole volume but a majority is absorbed by nearby molecules. The outgoing radiation from a material is emitted very close to the surface and therefore long wave heat radiation can be considered as a surface phenomenon. The amount of energy that is emitted from a surface is called emissive power E . The upper limit of the emissive power is described by Stefan-Boltzmanns law as

$$E_b = \sigma T_s^4 \quad [W/m^2] \quad (2.3)$$

where σ is the Stefan-Boltzmann constant of $5.67 \cdot 10^{-8} kg/(s^3 \cdot K^4)$. The real emissive power is reduced with a emissivity factor ϵ and the energy emitted from a real surface can then be described as

$$E_s = \epsilon \sigma T_s^4 \quad [W/m^2] \quad (2.4)$$

However, a surface also receives long wave radiation from its surroundings as buildings, trees or clouds. The resulting energy absorbed or emitted to its surroundings can be calculated as the difference in radiation between the surfaces.

$$q_r = E_s - E_{sur} = \epsilon \sigma (T_s^4 - T_{sur}^4) \quad [W/m^2] \quad (2.5)$$

A large part of the surfaces on bridges will exchange long wave radiation with the sky. The incoming radiation can be measured and a fictitious temperature is calculated to consider the sky as a surface according to equation 2.6.

$$T_{sky} = \sqrt[4]{\frac{q_{sky}}{\sigma \epsilon_{sky}}} \quad [^{\circ}C] \quad (2.6)$$

The emissivity factor that describes the relation between the upper limit of radiation described by Stefan-Boltzmanns law and the real radiation from a surface varies between 0.85 and 0.95 for concrete [Threlkeld, 1970]. This variation depends of the color and the texture of the surface.

2.1.3 Convection

Convection, or convective heat transfer, is the transfer of heat from a solid surface to a fluid in motion. In this thesis the convective heat transfer is regarded by the fluid in motion, air, and concrete. The convection process consists of two phenomena; advection and diffusion. Advection is the energy transfer by bulk fluid in motion. Diffusion is the energy transfer within air due to effects of random molecular motion. Diffusion is the main action very close to the surface due to the low velocity of air in this area. Further away from the surface area the advection is the main action. [Incropera et al., 2007]

An important factor for convection is the surrounding air temperature. The surrounding air temperature variations is often described with two sinusoidal cycles. The first cycle is a 24 hour cycle and is the temperature variations of day and night. The second cycle is a 365 day cycle and describes the temperature variations between summer and winter. For both summer and winter, the daily minimum bridge temperature is likely to occur at 05.00 ± 1 hour and the maximum bridge temperature at 15.00 ± 1 hour [Emerson, 1973]. Due to the low thermal conductivity of concrete, see chapter 3, these cycles give rise to stresses in the material. Depending on the size and geometry of the concrete structure, different cycles effects the structure differently.

Air movements occur for different reasons and therefore can convection be divided into two classifications to describe the flow. Natural convection originates from cold air being heavier than hot air. This difference in temperature causes a movement in the air in an effort to reach temperature balance. Forced convection however, is caused by external forces such as wind or fans.[Burström, 2007]

For modeling, the convective heat flux is calculated using Newton's law of cooling:

$$q_c = h_c(T_s - T_{air}) \quad [W/m^2] \quad (2.7)$$

where T_s is the surface temperature, T_{air} is the surrounding air temperature. The convection heat transfer coefficient $h_c(W/(m^2 \cdot ^{\circ}C))$ depends on various variables described above. However, for walls and slabs, h_c can be approximated according to Nevander and Elmarsson [2001] that using the wind speed u as variable.

$$h_c = 6 + 4u \text{ for } u \leq 5m/s \quad [W/(m^2 \cdot ^{\circ}C)] \quad (2.8)$$

$$h_c = 7.4u^{0.78} \text{ for } u > 5m/s \quad [W/(m^2 \cdot ^{\circ}C)] \quad (2.9)$$

The two expressions states that for lower wind speed natural convection is the dominating effect (eq. 2.8). At higher wind speed forced convection is the dominating effect (eq. 2.9).

2.2 Temperature loads

The different actions causing heat flux have been explained earlier in this chapter. However, the reason for treating temperature loads are strains caused by variations in temperature. If the structure is restricted to move strains are directly proportional to stresses. Depending on the distribution of temperature the effects are different. A temperature profile can be divided into four parts according to Eurocode 1991-1-5 [CEN, 2009], see figure 2.2.

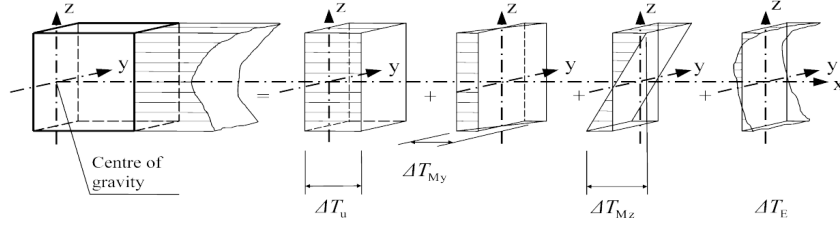


Figure 2.2: Schematic figure over the components creating the resulting temperature profile [CEN, 2009]

The first part ΔT_u is the uniformly distributed temperature component. This will make the whole bridge expand or contract, see figure 2.3. Structures that are tied to the ground or restricted to move will develop stresses when this is occurring. The traditional way to treat this type of load is to assume a initial temperature when the stresses are set to be zero. Any change in temperature from this level will then induce stresses. For a bridge that is free to move or have properly designed expansion joints this will only create strains in the structure.

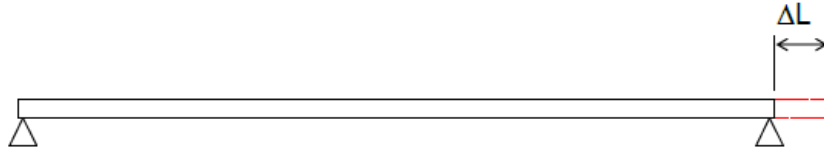


Figure 2.3: Deformation shape from a uniform temperature increase

The second and third parts are ΔT_{My} and ΔT_{Mz} which are linear temperature differences about the z-z and y-y axis. For a structure that is free to move these will cause the structure to bend, see figure 2.4. For a restricted structure these temperature effects results in load effects.



Figure 2.4: Deformation shape from a positive linear temperature difference

The fourth part of the temperature load is a non-linear temperature difference component ΔT_E . This temperature component will induce self equilibrated stresses even on a simply supported beam that is free to move. There is no deformation shape that allows the strains that this temperature distribution would give. Therefore eigen-stresses are introduced. These are not resulting in any net load effects [CEN, 2009].

To separate a given temperature distribution into these components a general method is used. The uniform component are calculated according to equation 2.10.

$$\Delta T_u = \frac{1}{h} \sum_{i=1}^n T_i h_i \quad [^{\circ}C] \quad (2.10)$$

Where h_i is the thickness of the section h_i and T_i is the average temperature in the section h_i . The linear gradient is calculated according to equation 2.11

$$\Delta T_{Mz} = \frac{12}{h^2} \sum_{i=1}^n T_i h_i x_i \quad [^{\circ}C] \quad (2.11)$$

Where x_i is the distance from the center of gravity of the whole section and the center of gravity for the section h_i .

The non-linear temperature component is calculated by subtracting the uniform and the linear distribution from the total temperature distribution.

$$\Delta T_E = T_{tot} - T_{avg} - \Delta T \quad [^{\circ}C] \quad (2.12)$$

Another effect that can cause stresses is temperature differences between different structural elements. The bridge deck is usually in connection with air on both top and bottom while the retaining walls or the wings are partially or fully covered with soil. This difference is in reality a result of an ongoing heat flux between a soil with more stable temperature and a surface against the air where the temperature can change suddenly.

The load effects from temperature is highly dependent on the material properties and the stiffness of the structure. A higher thermal expansion coefficient and a stiffer structure will cause greater stresses. The thermal input factors affects the material according to equation:

$$\sigma(y) = E\alpha\partial T(y) \quad [Pa] \quad (2.13)$$

This is further treated in chapter 3.4.1.

2.3 Heat transfer

For a concrete structure in its serviceability state, heating or cooling will take place at the surface that will result in an uneven temperature distribution in the bridge section. This difference in temperature, called temperature gradient, will cause energy to flow to the cooler parts of the structure. A three-dimensional heat flow can be described with Fourier's law as :

$$\rho c \frac{\partial T}{\partial t} = k \left(\frac{\partial^2 T}{\partial x^2} + \frac{\partial^2 T}{\partial y^2} + \frac{\partial^2 T}{\partial z^2} \right) + q_v \quad (2.14)$$

where ρ is the density (kg/m^3), c is the specific heat capacity ($J/(kg \cdot ^\circ C)$). $\partial T/\partial t$ is the change in temperature over time ($^\circ C/s$) and k is the thermal conductivity of concrete ($W/(^\circ C \cdot m)$). The factors $\partial^2 T/\partial x^2$, $\partial^2 T/\partial y^2$ and $\partial^2 T/\partial z^2$ are the second spatial derivatives of temperature in the x-,y- and z-directions. q_v is the heat generated in the concrete due to i.e. hydration, however this is not considered in this thesis.[Incropera et al., 2007]

For FE analysis the strong formulation for a three-dimensional heat flow is described in Ottosen and Petersson [1992] as:

$$div(\mathbf{D}\nabla T) + Q = 0 \text{ in region A} \quad (2.15)$$

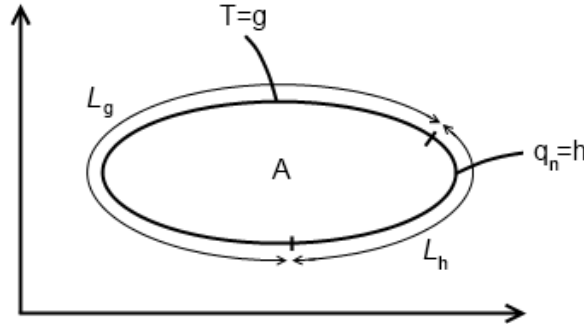


Figure 2.5: Two-dimensional region A with boundary $L = L_h + L_g$

with boundary conditions:

$$q_n = \mathbf{q}^t \mathbf{n} = h \text{ on } L_h \quad (2.16)$$

$$T = g \text{ on } L_g \quad (2.17)$$

where \mathbf{n} are the direction cosines of the unit outward vector normal to the boundary surface

$$\mathbf{n} = \begin{bmatrix} n_{xx} \\ n_{yy} \\ n_{zz} \end{bmatrix}$$

and \mathbf{q} is the energy depending of the temperature change and k the thermal conductivity constant ($W/(^{\circ}C \cdot m)$) in the x-, y-, and z-direction.

$$\mathbf{q} = \begin{bmatrix} -k_{xx} \frac{\partial T}{\partial x} \\ -k_{yy} \frac{\partial T}{\partial y} \\ -k_{zz} \frac{\partial T}{\partial z} \end{bmatrix} \quad [W/m^2]$$

In equation (2.15), Q is the rate of heat transferred to the unit volume per unit time and is divided in to three parts.

$$Q = Q_s + Q_c + Q_r \quad [W] \quad (2.18)$$

where

- Q_s is the flux from incident solar radiation
- Q_c is the convection heat transfer
- Q_r is the long-wave radiation heat transfer

Chapter 3

Concrete

The components of concrete is presented to emphasize the complexity of concrete modeling. The thermal input factors described in chapter 2 affects different types of structures differently dependent on the properties of its materials. This chapter describes concrete as material. The chapter also describes the cracking behavior in concrete and specifically discusses thermal properties and considerations taken when modeling concrete in a finite element model. The material properties are directly connected to the loads caused by thermal effects and are therefore essential to control and understand them.

3.1 Background

Concrete is a material that have been used for a very long time. Buildings have been found with materials similar to concrete dated a few hundred years B.C. In modern structures concrete is almost exclusively reinforced. By reinforcing the concrete it can handle tension and thus bending moments. Figure 3.1 shows the different components of reinforced concrete.

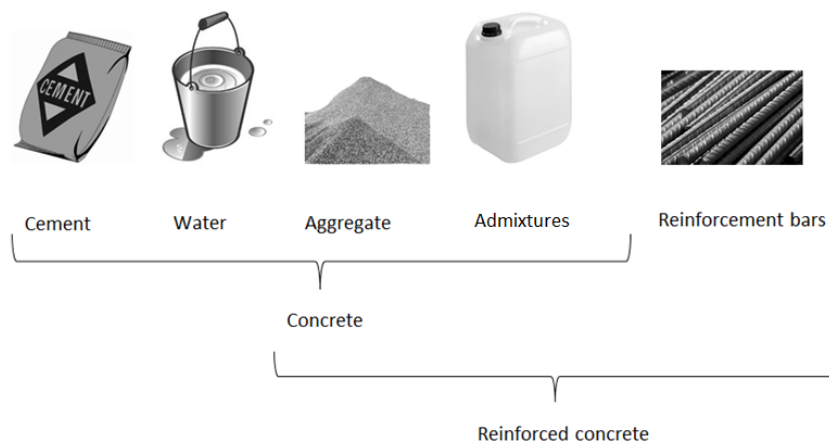


Figure 3.1: Illustration of components in reinforced concrete

The components of concrete can be mixed in various ways to achieve different types of concrete. Concrete is commonly classified by its compressive strength in MPa, e.g. C25, C30 and C45. In addition concrete mass is classified by a number of more factors, i.e. exposure and consistence classification. Common for bridges in Sweden is concrete graded C45 with the exposure classification XF, which defines the materials ability to resist freezing. [CEN, 2005]

3.1.1 Components

3.1.1.1 Cement

The essential component of concrete is cement which acts as a bonding agent. Cement is a broad concept but the most commonly used is Portland Cement. It is a hydraulic binding agent, characterized by its ability to harden in reaction with water. In Sweden modern cement was first manufactured 1872 in Lomma. Cement has its origin from limestone that is burnt in special ovens together with clay. There are many types of cement with different properties.

3.1.1.2 Water

Water is added to chemically harden the cement. The relation between the amount of water and cement is called water-cement ratio.

$$w/c - ratio = \frac{m_{water}}{m_{cement}} \quad [-] \quad (3.1)$$

A high water-cement ratio indicates a concrete that is easily processed at the work site but on the other hand more problems with shrinking and lower strength. A low water-cement ratio is generally more compact with higher strength but requires more vibration and is more difficult to process.

3.1.1.3 Aggregate

Aggregate is the main part of concrete and the word is a general term for rock material used for concrete manufacturing. The term includes all grain sizes that are used in concrete. To get a high strength it is desirable to include all grain sizes, this will fill as much empty space between the larger grains as possible. A lot of research and testing have been done to establish which distribution of grain sizes is optimal for different applications. Depending on its geographical location the aggregate can be of different minerals, in Sweden most minerals are of good quality. The choice of aggregate in the concrete have the largest effect of the total expansion coefficient α , see section 3.2.4.

3.1.1.4 Admixtures

The use of admixtures in concrete has increased rapidly the last decades. They are used to modify the properties of the concrete in different ways. The most commonly used is a plasticizer that can reduce the w/c-ratio without giving the downside properties of lower water content. Other common admixtures are accelerators or retarders who can make the concrete harden faster or slower, air entrainments that reduce damage from freeze and thaw cycles and different kinds of mineral admixtures. There are many other admixtures, chemical and mineral, not mentioned here.

3.1.1.5 Reinforcement bars

Reinforcement bars gives the concrete the ability to take tensile stresses, a necessity when variable loads are applied to the structure. The reinforcement bars is a large part of the cost when reinforced concrete is used. The absolutely most common material used is steel. The amount of reinforcement in a construction varies but a common share for bridges is 1-5% of the total concrete volume.

3.2 Thermal material properties

In equation (2.14) three material properties are stated that affects heat transfer in a material,

- Density ρ (kg/m^3)
- Specific heat capacity c ($J/(kg \cdot ^\circ C)$)
- Thermal conductivity k ($W/(kg \cdot ^\circ C)$)

In addition to these properties, the volumetric thermal expansion coefficient α is of importance during temperature analysis of concrete.

Concrete is a material with a low thermal conductive capacity compared to other load carrying building materials. This causes an uneven temperature distribution in the material since it cannot conduct heat to the cooler parts rapidly enough. Some temperature loads, stated in chapter 2, will give a non-uniform spatial temperature distribution in the material. This temperature distribution will give rise to strains and stresses due to the thermal expansion, explained in equation 2.13. [Larsson, 2012]

3.2.1 Density

Density describes a materials mass per unit volume according to equation 3.2

$$\rho = \frac{m}{V} \quad [kg/m^3] \quad (3.2)$$

For concrete, density is mostly affected by the largest elements in the concrete mass, the aggregate. In Sweden aggregate has a typically solid density of $p_k = 2650kg/m^3$ according to Burström [2007].

For the combined concrete mass with standard aggregate, a common value of ρ according to a literature study published in Larsson [2012] is $\rho = 2400kg/m^3$

3.2.2 Specific heat capacity

The specific heat capacity describes the amount of heat that is required to change the temperature of the material, explained by equation 3.3

$$c = \frac{Q}{\Delta T} \quad [J/(kg \cdot ^\circ C)] \quad (3.3)$$

The specific heat capacity for concrete is affected by the water-cement ratio, temperature and moisture content in the concrete. For concrete in bridges a common value is $c = 900J/(kg \cdot ^\circ C)$. [Larsson, 2012]

3.2.3 Thermal conductivity

Thermal conductivity is a material property which describes the ability to conduct heat. For example, materials with low thermal conductivity are often used as thermal insulation.

For concrete, the thermal conductivity is dependent on the density and composition of the material. The conductivity of the different elements and the moisture in the concrete also affects the total thermal conductivity.

A value of $k = 2.5 W/(kg \cdot ^\circ C)$ is appropriate for concrete in bridges. However, temperature differentials is highly dependent of the thermal conductivity, and a lower value will produce a larger temperature differential and vice-versa. [Larsson, 2012]

3.2.4 Thermal expansion coefficient

The thermal expansion coefficient describes a materials tendency to a change in volume in response to a temperature change. This change in volume depends on the particles change in energy at different temperatures. For example, a higher temperature will cause the particles to move more freely and thereby take a larger volume into account. Hydrated concrete is considered to have the same properties both for heating and cooling. An advantage with using steel as reinforcement in concrete is the similar thermal expansion coefficients for concrete and reinforcement bars. For reinforced concrete, the thermal expansion coefficient according to Eurocode is $\alpha = 1 \cdot 10^{-5} m/(m \cdot ^\circ C)$. [CEN, 2009]

3.3 Cracks

Cracks appear in almost all concrete structures. The reason for this is the low tensile strength of concrete. Tensile stresses are added up from many different loads, where temperature is one among many. Depending on its depth and width a crack can effect the durability or load capacity of the structure. However, cracks usually have greatest effect on durability. Cracks generated from temperature effects can be divided into two categories according to Cementa [1997]

- Cracks through the whole section
- Surface cracks

Cracks that appear through the whole section are usually developed as a result of restraining forces in the structure. Temperature could cause these cracks if no expansion joints allow the structure to contract and a uniform decrease in temperature appears. Tensile stresses will be developed throughout the whole section and therefore cracks can appear. These cracks can easily be identified; they often appear perpendicular to the bridge direction of motion.

As the name indicates, surface cracks appear locally close to the surface. One reason for them to develop is if the temperature close to the surface decreases faster than the temperature in the middle of the cross section. This could happen during nighttime when outgoing radiation from the structure is greater than incoming, or when the air temperature drops quickly. Another common source of surface cracks is dehydration. These cracks appear 1-3 hours after casting and are caused by fast dehydration of the concrete at the surface. [Cementa, 1997]

3.3.1 Micro cracks

When high tensile stresses arise in concrete non-linear phenomena will appear. These phenomena is dependent on micro cracks that softens the concrete [Cementa, 1997]. Softening of the concrete will reduce the tensile stresses appearing from restraint. When stresses are calculated without considering these effects, the stresses will be overestimated.

Micro cracks can also be developed during casting and hydration. This may be caused by different volume change of the concrete mass and the aggregate. Thereby, micro cracks will appear before external loads are applied. [Cementa, 1997]

3.3.2 Crack widths

Crack width, w , is defined as the width of the crack at the surface of the concrete. This width is not constant but often larger close to the surface and smaller at the reinforcement, see figure 3.2.

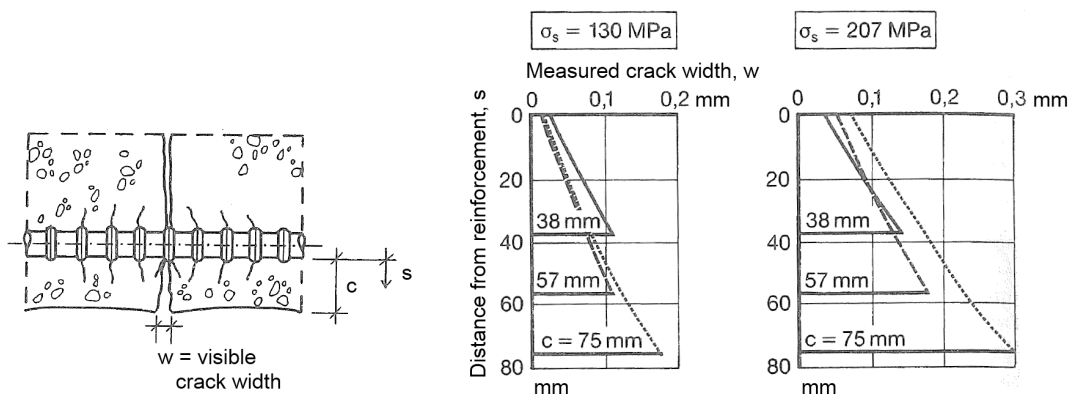


Figure 3.2: Reduction of crack width from the surface to the reinforcement layer as a function of the stresses in the reinforcement σ_s and concrete cover c , according to Cementa [1997]

Due to the maximum crack width appearing at the surface of the concrete, it is possible to identify cracks visually. Cracks widths larger than $0.05 - 0.1\text{mm}$ are visible when the concrete is moistened [Cementa, 1997]

3.4 FE modeling of concrete

3.4.1 Material modeling

As illustrated in figure 3.1, reinforced concrete consists of two materials, the concrete mass and the reinforcement steel. Steel can be considered as a homogeneous material and its material properties are well defined. The concrete mass however, consists of several components which lead to difficulties when defining material properties. Figure 3.3 describes the behavior of the tensile material properties of reinforced concrete.

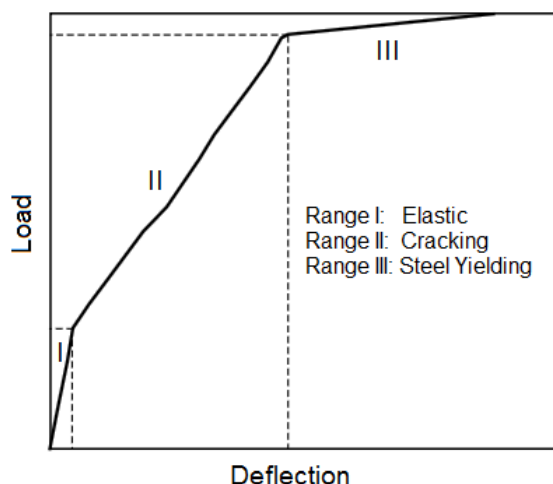


Figure 3.3: Typical load-displacement response of reinforced concrete. [Kwak and Filippou, 1990]

In the first range, the tensile stresses are below the tensile strength of concrete. The material shows a fully elastic behavior. In the second range, the stresses exceed the tensile strength of the concrete. This results in cracking of the concrete and the reinforcement steel will start to take load. In this range the material shows a non-linear behavior. The last range is when the reinforcement steel starts to yield.

For accurate results during FE analysis, it is of great importance to describe the material properties and capture the material behavior in a constitutive model. As figure 3.3 shows, the material have a highly non-linear response. In addition to this, material properties of concrete differ in short- and long-term due to environmental and material effects. In other words, a realistic and accurate constitutive model of reinforced concrete is advanced and analysis with such a model would be computational heavy.

One way to treat concrete in FE analysis is to assume that Hooke's law is applicable. Equation 3.4 shows the constitutive relationship in a linear relation with stress and strain tensors. [Ottosen and Ristinmaa, 2005]

$$\sigma_{ij} = D_{ijkl}\varepsilon_{kl} \quad [Pa] \quad (3.4)$$

where

$$D = \frac{E}{(1+v)(1-2v)} \begin{bmatrix} 1-v & v & v & 0 & 0 & 0 \\ v & 1-v & v & 0 & 0 & 0 \\ v & v & 1-v & 0 & 0 & 0 \\ 0 & 0 & 0 & \frac{1}{2}(1-2v) & 0 & 0 \\ 0 & 0 & 0 & 0 & \frac{1}{2}(1-2v) & 0 \\ 0 & 0 & 0 & 0 & 0 & \frac{1}{2}(1-2v) \end{bmatrix} \quad [Pa]$$

With this assumption, the FE analysis cannot result in a realistic material behavior; however this type of analysis will still result in accurate load effects. These load effects can easily be used in calculations based on traditional formulas during design.

In this thesis, a simple material model based upon Young's modulus of concrete is used. For investigation of constraining stresses caused by a temperature distribution in a concrete bridge deck, it is important to have this simplified material model in mind. A reinforced concrete deck is per definition in a cracked state, otherwise the reinforcement would be of no use. However, cracked concrete has a significantly lower effective Young's modulus, and equation 2.13 states a direct relationship between Young's modulus and stress. In other words, with this material model, constraining stresses will be larger in a FE analysis than in reality.

3.4.2 Shell Elements

Shell elements are widely used for finite element analysis of structures because of their ability to translate (u, v, w) and rotate at the nodes (θ) . Due to these abilities displacement and stress analysis are possible. Figure 3.4 visualizes a shell element that is defined by four nodes and a corresponding thickness.

A shell element is a combination of a 2D solid element and a plate element. In-plane effects are described by the 2D solid element formulation and off-plane effects are described by the plate element formulation [Liu, 2003].

The main benefit of using this type of elements is that the analysis is much more time-effective than using for example a solid element. There is a reduced number of nodes and elements and it is possible to use only one shell element over a certain thickness. Other, more practical benefits when modeling with shell elements is that they are easy to mesh.

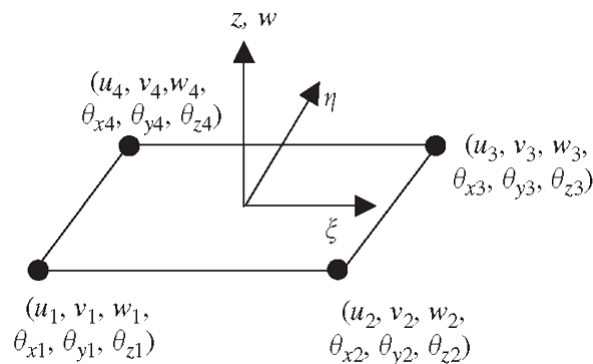


Figure 3.4: Illustration of a shell element

When using shell elements, it is important to know that the formulation of shell elements is based on the assumption of a thin element. For some geometries and analysis, solid elements, beam elements or frame elements are more suitable. [Ottosen and Petersson, 1992]

3.4.2.1 Shell elements in Scanscot BrigadePlus

In the commercial finite element software Scanscot BrigadePlus three types of shell elements are defined; thin, thick and general-purpose shell elements. Thin shell elements are used where plate formulation is required, when shear flexibility is negligible. Thick shell elements are used when the shear flexibility is not negligible. The general-purpose shell element is a combination of the thin and thick shell element formulations. [Systèmes, 2011]

The most used type is the general shell element. Shell elements can be rectangular, triangular or any other shape that is a combination of nodes. To each element, a number of integration points and an integration rule is stated. Temperature points, independent from the integration points may also be defined for a shell element. This gives the possibility to study a certain temperature distribution within a specific shell element, see figure 3.5 where t is the thickness of the shell element.

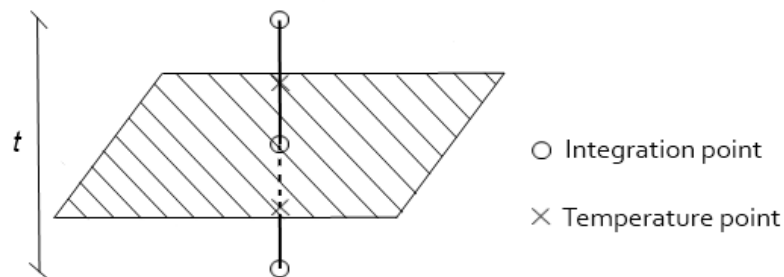


Figure 3.5: Illustration of temperature points and integration points in a general shell element

Chapter 4

Building codes

The origin of thermal loads is a combination of heat transfer processes, material properties and climate variations which have been explained in chapter 2 and 3. Based on these basics, building codes have been developed throughout the years to set up certain regulations and recommendations in the subject. This chapter will treat some basics regarding load combinations and safety factors required for any structural design. In addition a deeper review of how thermal actions and crack width calculations are treated in the code is included.

In Sweden, the main building code for the design of bridges is Eurocode. For specific areas or numerical values, a National Annex complement the Eurocode. In addition, the main client of bridges in Sweden, Trafikverket, has their own code documents complementing the Eurocode and National Annex. These documents is called TRVR Bro and TRVK Bro. In 2011 these documents replaced the older TR Bro 2009 and TK Bro 2009.

This chapter will only approach certain areas of the building codes necessary to understand for analyses performed in this thesis.

4.1 Loads and Material coefficients

To account for uncertainties in material properties or the magnitude of the loads, various coefficients are used to increase or reduce these values. The coefficients are given in the codes and those used in this project will be presented in this section.

4.1.1 Partial coefficients

During design of structures, the material strength value are decreased to account for uncertainties in the material strength. Eurocode treats this with partial coefficients , according to

$$f_{\alpha d} = \frac{f_{\alpha k}}{\gamma_{\alpha}} \quad [-] \quad (4.1)$$

where $f_{\alpha k}$ is the characteristic strength and γ_{α} is the partial coefficient for the specific material. Table 4.1 shows the partial coefficients of reinforced concrete [CEN, 2005]. The different values depends on statistical testing of the material type.

| Material | γ_{α} |
|---------------------|-------------------|
| Concrete | 1.5 |
| Reinforcement steel | 1.15 |

Table 4.1: Partial coefficients

4.1.2 Safety factors

A structural part is assigned a safety class depending on the probability and consequence of failure. For structures where the consequences are lower the design load might be reduced in ultimate limit state.

| Safety class | γ_d | |
|--------------|------------|--|
| 1 | 0.83 | Low risk of serious bodily injury |
| 2 | 0.91 | Moderate risk of serious bodily injury |
| 3 | 1.0 | High risk of serious bodily injury |

Table 4.2: Safety factors according to Boverket [2008]

4.1.3 Load combination factors

When the loads are applied on the structure three types of combination factors are used. The primary factor refers to the coefficient for the leading load, the load causing the most adverse load effect. If any other load is leading, the load is considered secondary and is given the coefficient in the secondary column in tables 4.3, 4.4 and 4.5. For some cases there could be a third and fourth coefficient, then the second most adverse load gets the secondary coefficient etc. Some loads are causing deformations that should be fully implemented with its respective primary or secondary coefficient but the resulting load effect can be reduced. This simulates different Young's modulus in the same load combination. The force coefficient in table 4.3, 4.4 and 4.5 reduces section forces, stresses and reaction forces. The reduction factor is calculated according to:

$$\psi_{red} = \frac{1}{1 + \varphi} \quad [-] \quad (4.2)$$

For temperature loads specifically this factor is 0.769. According to Bro 2004 [Vägverket, 2004] the creep factor φ for temperature loads can be set to 0.3. This was changed and in the current code TRVK Bro [Trafikverket, 2011b] the temperature load effects from uneven temperature should not be reduced for creep. Since the bridge analyzed in this thesis was investigated and designed according to TK bro 2009 [Banverket and Vägverket, 2009a] and TR bro 2009 [Banverket and Vägverket, 2009b] a reduction has been used here.

In current codes no recommended value on the creep factor is given, the value from Bro 2004 is however still commonly used in lack of other values. The current code TRVK Bro clearly states that it is not allowed to reduce the uneven temperature load, but states nothing regarding the even temperature load. The interpretation is therefore that it is allowed to reduce the even temperature load (chapter 6.1.3 in Eurocode 1991-1-5 [CEN, 2009]) but not the uneven temperature (chapter 6.1.4 in Eurocode 1991-1-5 [CEN, 2009]). This was also concluded by Dr Oskar Larsson [Larsson, 2012].

4.1.3.1 Ultimate Limit State

Ultimate limit state is the designing load combination meant to prevent failure in the structure. Table 4.3 lists the coefficients used for the Ultimate Limit State (Transient) load combination.

| Load | Primary | Secondary | Force |
|-------------------|---------|-----------|-------|
| Deadweight | 1.2 | 1.0 | 1.0 |
| Earth pressure | 1.1 | 1.0 | 1.0 |
| Shrinkage | 1.2 | 0 | 0.345 |
| Surface load | 1.32 | 0.9 | 1.0 |
| Support Yielding | 1.0 | 0 | 0.345 |
| Road Vehicle Load | 1.5 | 1.125 | 1.0 |
| Temperature Load | 1.5 | 0.9 | 0.769 |

Table 4.3: Ultimate Limit State factors (Transient) [CEN, 2010]

4.1.3.2 Serviceability Limit State

The Serviceability limit state load combinations are used to design the structure for durability and serviceability purposes. Table 4.4 and 4.5 lists the coefficients used for the Serviceability Limit State load combinations.

| Load | Primary | Secondary | Force |
|------------------|---------|-----------|-------|
| Deadweight | 1.0 | 1.0 | 1.0 |
| Earth pressure | 1.0 | 1.0 | 1.0 |
| Shrinkage | 1.0 | 0 | 0.345 |
| Surface load | 1.1 | 0.9 | 1.0 |
| Support Yielding | 1.0 | 0 | 0.345 |
| Temperature Load | 0.5 | 0.5 | 0.769 |

Table 4.4: SLS Quasi-permanent factors [CEN, 2010]

| Load | Primary | Secondary | Force |
|-------------------|---------|-----------|-------|
| Deadweight | 1.0 | 1.0 | 1.0 |
| Earth pressure | 1.0 | 1.0 | 1.0 |
| Shrinkage | 1.0 | 0 | 0.345 |
| Surface load | 1.0 | 0.9 | 1.0 |
| Support Yielding | 1.0 | 0 | 0.345 |
| Road Vehicle Load | 1.0 | 0.75 | 1.0 |
| Temperature Load | 1.0 | 0.6 | 0.769 |
| Wind Load | 1.0 | 0.3 | 1.0 |

Table 4.5: SLS Characteristic factors [CEN, 2010]

4.2 Thermal actions on structures

Eurocode contains regulations of how the temperature loads should be treated during design of bridge structures. The climate can, as described in chapter 2, affect the bridge in various ways. Simplifications have been made to lump these effects together to a temperature distribution depending on the minimum and maximum shade temperatures. The following types of temperature effects are to be considered in Eurocode:

- Uniform temperature components
- Temperature difference components, primarily vertical but in some cases also horizontal
- Temperature differences between structural components

4.2.1 Uniform Temperature component

The uniform temperature component in the bridge is an evenly distributed temperature that will cause the full bridge to expand or contract. These movements will give rise to stresses in the structure if it is constrained to move. A recommendation of the temperatures to be used have been stated, these bridge temperatures depends on the minimum and maximum shade air temperatures where the structure is erected. Recommendations of temperatures are stated in the national annex in SS-EN 1991-1-5 [CEN, 2009]. For places with high altitude or other special circumstances these temperatures can be altered. A method to calculate a specific value for the site from statistics is also presented in the code.

The correlation between shade air temperature and effective bridge temperature is shown in figure 4.1. This correlation is performed on investigations made on bridges in United Kingdom.

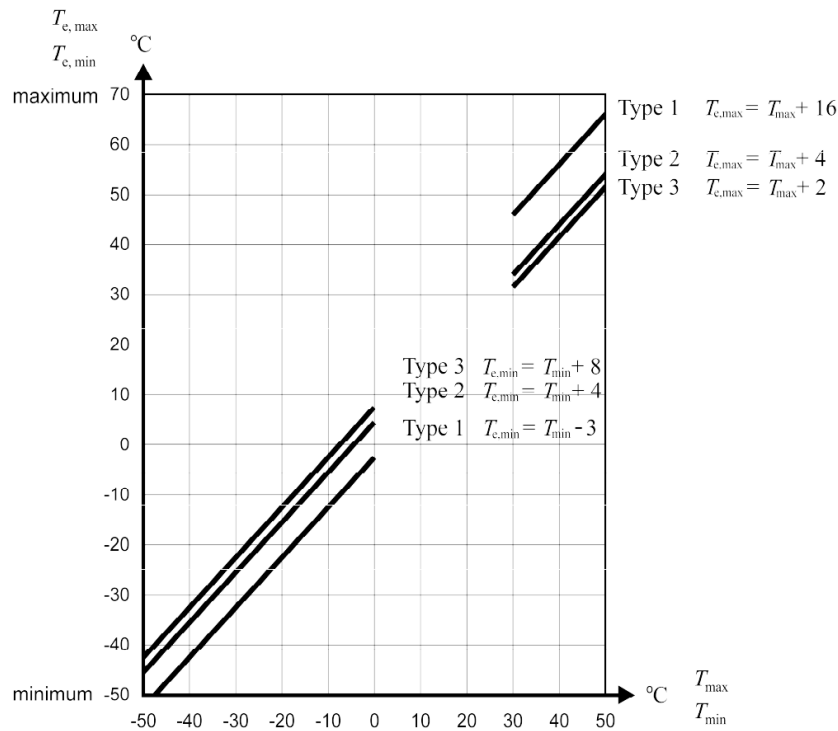


Figure 4.1: Eurocode 1991-1-5 [CEN, 2009] describes the correlation between shade air temperature and effective bridge temperature

The graph for type 3 in figure 4.1 is based on 48 hour mean values of the shade air temperature and the measured bridge temperature. Different time periods have been used for different bridge types due to the materials different conductive capacity. There are four types of bridge categories based on the deck type:

- Type 1 - Steel deck
- Type 2 - Composite deck
- Type 3 - Concrete deck
- Type 4 - Wooden deck with bearing parts of wood

4.2.2 Temperature difference components

Temperature differences could be both vertical and horizontal. Eurocode gives a rather vague statement that the horizontal component should be treated where it needs to be considered. This component could be applicable when one side of the structure is more exposed to sunlight than the other. When this is valid a recommended gradient of 5°C should be applied between the outer edges of the bridge.

The difference in temperature between the top and bottom of the bridge deck surface may produce effects on the structure due to:

- Restraint of free curvature due to the form of the structure
- Friction at rotational bearings
- Non-linear geometric effects

The temperature distribution should be modeled and can be described by two different approaches. These approaches will be deeper investigated in this project and is therefore presented further. In Trafikverkets Författningssamling [Trafikverket, 2011a] it is stated that both approaches are recommended for bridges in steel, concrete and composite bridges. For type 4 bridges only approach 1 is allowed.

4.2.2.1 Approach 1

Approach 1 uses a vertical linear component. This linear component should give section forces equivalent to a realistic non-linear temperature distribution. The load should be considered for both warm top with cold bottom and cold top with warm bottom. Recommended values for different types of bridges are given in table 6.1 in Eurocode 1991-1-5 [CEN, 2009].

| Type of Deck | Top warmer than bottom | Bottom warmer than top |
|---|------------------------|------------------------|
| | $T_{M,heat}$ (°C) | $T_{M,cool}$ (°C) |
| Type 1: Steel deck | 18 | 13 |
| Type 2: Composite deck | 15 | 18 |
| Type 3: Concrete deck: - concrete box girder - concrete beam - concrete slab | 10 15 15 | 5 8 8 |
| NOTE 1: The values given in the table represent upper bound values of the linearly varying temperature difference component for representative sample of bridge geometries. | | |
| NOTE 2: The values given in the table are based on a depth of surfacing of 50 mm for road and railway bridges. For other depths of surfacing these values should be multiplied by the factor k_{sur} . Recommended values for the factor k_{sur} is given in Table 6.2. | | |

Figure 4.2: Eurocode 1991-1-5 gives recommendations on temperature difference components for different types of bridge decks for roads, foot and railways bridges

As stated in figure 4.2 these values are only valid for a surfacing of 50mm. Eurocode gives recommended coefficients to modify these gradients to the current surfacing situation.

4.2.2.2 Approach 2

Approach 2 uses a temperature distribution to combine the linear and the non-linear temperature differences. The distribution of temperatures varies depending on bridge type. For concrete bridges there are two cases, one for warm top and cold bottom and one for the reversed case. The suggested temperature profiles are shown in figure 4.3. This temperature profile includes a small part of the uniform temperature component. If this means that the uniform temperature load can be reduced is not stated in code.

There are corrections to these temperatures in the national annex depending on thickness of the deck and thickness of the paving layer. A thicker paving will result in a smaller gradient whereas a thicker cross section will result in a larger gradient.

4.2.3 Temperature difference between different structural elements

To take into account boundary conditions, such as soil or water against a support or different materials and/or colors of elements Eurocode states that a temperature difference should be applied between different elements where this could cause adverse load effects [CEN, 2009]. These effects should be in addition to the other temperature effects and the values prescribed are:

- 15 °C between main structural elements
- 10 °C and 20°C for light and dark color respectively between suspension/stay cables and deck (or tower)

This temperature difference could be applicable between support and a bridge deck where the boundary conditions are different. When to use this load condition and how to apply it on a model is vague.

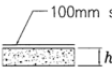
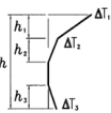
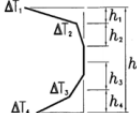
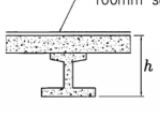
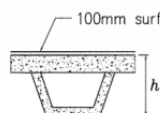
| Type of Construction | Temperature Difference (ΔT) | | | | | | | | | | | | | | | | | | | | | | | | | | | | | | | | | | | | | | | | | | | | | | | | | | | | | | | | | | | | | | | | | |
|--|---|---|--------------|--------------|--------------|--|----|--|--|------------|-----|-----|-----|-----|------|-----|-----|-----|------|-----|-----|------------|------|-----|-----|---|---------------|--------------|--------------|--------------|--------------|--|----|--|--|--|------------|------|------|------|------|-----|------|------|------|------|-----|------|------|------|------|-----|------|------|------|------|-----|------|------|------|------|------------|------|------|------|------|
| | (a) Heating | (b) Cooling | | | | | | | | | | | | | | | | | | | | | | | | | | | | | | | | | | | | | | | | | | | | | | | | | | | | | | | | | | | | | | | | |
|  3a. Concrete slab |  $h_1 = 0.3h$ but $\leq 0.15m$ $h_2 = 0.3h$ but $\geq 0.10m$ but $\leq 0.25m$ $h_3 = 0.3h$ but $\leq (0.10m + \text{surfacing depth in metres})$ (for thin slabs, h_3 is limited by $h - h_1 - h_2$) |  $h_1 = h_2 = 0.20h$ but $\leq 0.25m$ $h_2 = h_3 = 0.25h$ but $\leq 0.20m$ | | | | | | | | | | | | | | | | | | | | | | | | | | | | | | | | | | | | | | | | | | | | | | | | | | | | | | | | | | | | | | | | |
|  3b. Concrete beams | | | | | | | | | | | | | | | | | | | | | | | | | | | | | | | | | | | | | | | | | | | | | | | | | | | | | | | | | | | | | | | | | | |
|  3c. Concrete box girder | | | | | | | | | | | | | | | | | | | | | | | | | | | | | | | | | | | | | | | | | | | | | | | | | | | | | | | | | | | | | | | | | | |
| | <table border="1"> <thead> <tr> <th>$\frac{h}{m}$</th> <th>ΔT_1</th> <th>ΔT_2</th> <th>ΔT_3</th> </tr> <tr> <th></th> <th colspan="3">°C</th> </tr> </thead> <tbody> <tr> <td>≤ 0.2</td> <td>8.5</td> <td>3.5</td> <td>0.5</td> </tr> <tr> <td>0.4</td> <td>12.0</td> <td>3.0</td> <td>1.5</td> </tr> <tr> <td>0.6</td> <td>13.0</td> <td>3.0</td> <td>2.0</td> </tr> <tr> <td>≥ 0.8</td> <td>13.0</td> <td>3.0</td> <td>2.5</td> </tr> </tbody> </table> | $\frac{h}{m}$ | ΔT_1 | ΔT_2 | ΔT_3 | | °C | | | ≤ 0.2 | 8.5 | 3.5 | 0.5 | 0.4 | 12.0 | 3.0 | 1.5 | 0.6 | 13.0 | 3.0 | 2.0 | ≥ 0.8 | 13.0 | 3.0 | 2.5 | <table border="1"> <thead> <tr> <th>$\frac{h}{m}$</th> <th>ΔT_1</th> <th>ΔT_2</th> <th>ΔT_3</th> <th>ΔT_4</th> </tr> <tr> <th></th> <th colspan="4">°C</th> </tr> </thead> <tbody> <tr> <td>≤ 0.2</td> <td>-2.0</td> <td>-0.5</td> <td>-0.5</td> <td>-1.5</td> </tr> <tr> <td>0.4</td> <td>-4.5</td> <td>-1.4</td> <td>-1.0</td> <td>-3.5</td> </tr> <tr> <td>0.6</td> <td>-6.5</td> <td>-1.8</td> <td>-1.5</td> <td>-5.0</td> </tr> <tr> <td>0.8</td> <td>-7.6</td> <td>-1.7</td> <td>-1.5</td> <td>-6.0</td> </tr> <tr> <td>1.0</td> <td>-8.0</td> <td>-1.5</td> <td>-1.5</td> <td>-6.3</td> </tr> <tr> <td>≥ 1.5</td> <td>-8.4</td> <td>-0.5</td> <td>-1.0</td> <td>-6.5</td> </tr> </tbody> </table> | $\frac{h}{m}$ | ΔT_1 | ΔT_2 | ΔT_3 | ΔT_4 | | °C | | | | ≤ 0.2 | -2.0 | -0.5 | -0.5 | -1.5 | 0.4 | -4.5 | -1.4 | -1.0 | -3.5 | 0.6 | -6.5 | -1.8 | -1.5 | -5.0 | 0.8 | -7.6 | -1.7 | -1.5 | -6.0 | 1.0 | -8.0 | -1.5 | -1.5 | -6.3 | ≥ 1.5 | -8.4 | -0.5 | -1.0 | -6.5 |
| $\frac{h}{m}$ | ΔT_1 | ΔT_2 | ΔT_3 | | | | | | | | | | | | | | | | | | | | | | | | | | | | | | | | | | | | | | | | | | | | | | | | | | | | | | | | | | | | | | | |
| | °C | | | | | | | | | | | | | | | | | | | | | | | | | | | | | | | | | | | | | | | | | | | | | | | | | | | | | | | | | | | | | | | | | |
| ≤ 0.2 | 8.5 | 3.5 | 0.5 | | | | | | | | | | | | | | | | | | | | | | | | | | | | | | | | | | | | | | | | | | | | | | | | | | | | | | | | | | | | | | | |
| 0.4 | 12.0 | 3.0 | 1.5 | | | | | | | | | | | | | | | | | | | | | | | | | | | | | | | | | | | | | | | | | | | | | | | | | | | | | | | | | | | | | | | |
| 0.6 | 13.0 | 3.0 | 2.0 | | | | | | | | | | | | | | | | | | | | | | | | | | | | | | | | | | | | | | | | | | | | | | | | | | | | | | | | | | | | | | | |
| ≥ 0.8 | 13.0 | 3.0 | 2.5 | | | | | | | | | | | | | | | | | | | | | | | | | | | | | | | | | | | | | | | | | | | | | | | | | | | | | | | | | | | | | | | |
| $\frac{h}{m}$ | ΔT_1 | ΔT_2 | ΔT_3 | ΔT_4 | | | | | | | | | | | | | | | | | | | | | | | | | | | | | | | | | | | | | | | | | | | | | | | | | | | | | | | | | | | | | | |
| | °C | | | | | | | | | | | | | | | | | | | | | | | | | | | | | | | | | | | | | | | | | | | | | | | | | | | | | | | | | | | | | | | | | |
| ≤ 0.2 | -2.0 | -0.5 | -0.5 | -1.5 | | | | | | | | | | | | | | | | | | | | | | | | | | | | | | | | | | | | | | | | | | | | | | | | | | | | | | | | | | | | | | |
| 0.4 | -4.5 | -1.4 | -1.0 | -3.5 | | | | | | | | | | | | | | | | | | | | | | | | | | | | | | | | | | | | | | | | | | | | | | | | | | | | | | | | | | | | | | |
| 0.6 | -6.5 | -1.8 | -1.5 | -5.0 | | | | | | | | | | | | | | | | | | | | | | | | | | | | | | | | | | | | | | | | | | | | | | | | | | | | | | | | | | | | | | |
| 0.8 | -7.6 | -1.7 | -1.5 | -6.0 | | | | | | | | | | | | | | | | | | | | | | | | | | | | | | | | | | | | | | | | | | | | | | | | | | | | | | | | | | | | | | |
| 1.0 | -8.0 | -1.5 | -1.5 | -6.3 | | | | | | | | | | | | | | | | | | | | | | | | | | | | | | | | | | | | | | | | | | | | | | | | | | | | | | | | | | | | | | |
| ≥ 1.5 | -8.4 | -0.5 | -1.0 | -6.5 | | | | | | | | | | | | | | | | | | | | | | | | | | | | | | | | | | | | | | | | | | | | | | | | | | | | | | | | | | | | | | |

Figure 4.3: Eurocode 1991-1-5 [CEN, 2009] describes the temperature distribution that should be applied to bridge type 3 bridge according to approach 2

4.3 Crack widths

Calculation of crack width is regulated in Eurocode 1992-1-1, [CEN, 2005] . The characteristic value of the crack width is calculated by:

$$w_k = s_{r,max}(\varepsilon_{sm} - \varepsilon_{cm}) \quad [m] \quad (4.3)$$

The $s_{r,max}$ variable is the maximum allowed distance between cracks. It is calculated according to:

$$s_{r,max} = k_3c + k_1k_2k_4 \frac{\phi}{\rho_{p,eff}} \quad [m] \quad (4.4)$$

where the constants k_n regards the reinforcement attachment and the strain distribution. According to equation 4.5 $\rho_{p,eff}$ is calculated as the ratio of the reinforcement area and the effective area of the concrete for the section.

$$\rho_{p,eff} = \frac{A_s}{A_{eff}} \quad [-] \quad (4.5)$$

where

$$A_{c,eff} = b \cdot \min \left[2.5(h - d), \frac{h - x}{3}, \frac{h}{2} \right] \quad [m^2] \quad (4.6)$$

The strain ε_{sm} is the average strain in the reinforcement at the applied load combination. ε_{cm} is the average strain in the concrete between cracks. The difference between these are calculated as follows:

$$\varepsilon_{sm} - \varepsilon_{cm} = \frac{\sigma_s - k_t \frac{f_{ct,eff}}{\rho_{p,eff}} (1 + \alpha_e \rho_{p,eff})}{E_s} \geq 0.6 \frac{\sigma_s}{E_s} \quad [-] \quad (4.7)$$

The factor k_t depends on the duration of the loading, $f_{ct,eff}$ is the concrete tension capacity at the first crack. The stresses in the reinforcement σ_s , are derived from strain relations and moment equilibrium equations for the concrete and reinforcement.

4.4 Additional building codes

The additional regulating document during design of bridges in Sweden is the National Annex, TRVR Bro and TRVK Bro.

4.4.1 TRVR Bro

During FE analysis one of the main aspects is to model with realistic boundary conditions. Trafikverket states in TRVR bro [Trafikverket, 2011c] a method for calculating the boundary condition to the ground with springs at a certain stiffness.

The stiffness of the foundation can be calculated according to TRVR bro. The stiffness depends on the modulus of elasticity of the soil at the foundation and the geometry. The stiffness is calculated according to equation 4.8 and 4.9.

Spring rotation stiffness in the stiff direction:

$$k_{\theta k} = \frac{E_k B^2 L}{5} \quad [Nm/rad] \quad (4.8)$$

Spring rotation stiffness in the weak direction:

$$k_{\theta k} = \frac{E_k B L^2}{5} \quad [Nm/rad] \quad (4.9)$$

where E_k is the moduli elasticity of the soil according to TK Geo, B is the width of the abutment and L is the length of the abutment

The vertical spring stiffness of the foundation can be calculated according to ScanscotTechnology [2010]. It depends on the rotational stiffness and the moment of inertia of the abutment. Simplified the expression turns out as:

$$k_z = \frac{2.4 E_k}{B} \quad [N/m] \quad (4.10)$$

Since the vertical stiffness is a product of the geometry and the rotational stiffness this can be calculated from data used in equation 4.8 and 4.9.

Chapter 5

Climate simulation of bridge cross section

To investigate which temperature profiles that appear in a bridge, a simulation with measured climate data is performed. The objective is to investigate how real temperature modeling compares with the temperature profiles suggested in the current building codes presented in chapter 4. This could show which of the approaches that is more preferable if the aim is to emulate the real situation.

For this investigation, a simulation of a bridge deck subjected to external climate related loads is performed. This is done using data from SMHI in Stockholm during 1986. The temperature related loads and the theory of the analysis is described in chapter 2. A portal frame bridge in concrete, built in Katrineholm is investigated. Additional background theory of the material model used is described in chapter 3.

5.1 Portal frame bridge 829 in Katrineholm

A real bridge is subject to the calculations on thermal effects that are being conducted here. The bridge is one of many bridges that were designed in the project "Väg 55/56 Östra förbifarten Katrineholm" which was finished October 1st 2012 at a cost of totally 440 MSEK, and was one of the longer portal frame bridges in this project.

This type of bridge was chosen because restraining forces in a portal frame bridge has a significant effect. These effects are explained in chapter 2. It also happens to be one of the most common types of bridges in Sweden.

This particular bridge separates two roads and is a standard portal frame bridge built with reinforced concrete according to figure 5.1 and figure 5.2.

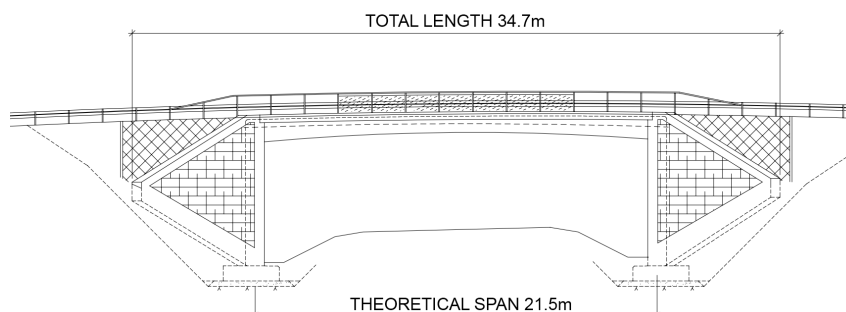


Figure 5.1: Elevation of bridge 829 in Katrineholm

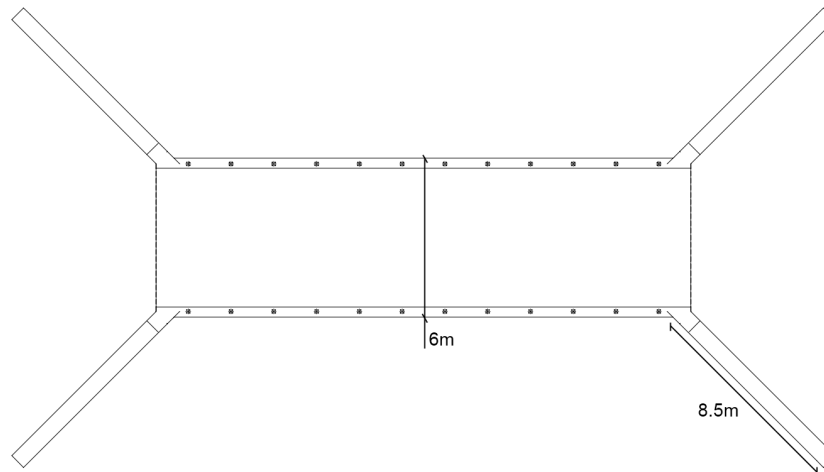


Figure 5.2: Floor plan of bridge 829 in Katrineholm

5.2 Climate simulation

To determine a realistic temperature distribution in a cross section of the portal frame bridge, a simulation is performed with measured climate data. For this analysis, a simple 2D model of the bridge deck is evaluated. The climate data is measured and collected by SMHI in Stockholm. This data was first used in Larsson [2012]. The quantities that have been measured are:

- Air temperature
- Solar radiation
- Wind speed
- Sky temperature

Larsson identified 1986 as a year when the climate effects are particularly unfavorable [Larsson, 2012]. Therefore this simulation has been conducted with data from 1986. One value of each quantity have been registered each hour during one year. Since four quantities are registered there have been a total of 35040 measured values used in this simulation. The air temperature and the wind speed can be used to calculate the effects from convection. Loads from solar radiation and long wave radiation are directly proportional to the measured values. This is further described in chapter 2. For the interested reader this climate data can be obtained directly through SMHI.

5.2.1 Finite element model

To simulate the temperature throughout the cross section Scanscot BrigadePlus is used. This commercial finite element software is based on the Simulia Abaqus and uses Simulia Abaqus FEA as solver. This software is chosen because it is used at both Skanska and in Larsson [2012]. To make the amount of data manageable a 2D model is created of the bridge deck using dimensions from bridge 829 in Katrineholm. One limitation with a simple 2D model of the bridge deck is the inability to see conditions close to boundaries (supports).

The cross section is modeled with heat transfer shell elements. The dimensions are defined from the bridge deck near the supports with a total width of 6m and a thickness of 1.1m. Since the model is a 2D model the results will be more representable far from support but the thickness of the section is not crucial for obtaining a correct distribution. On top of this a paving layer of 50mm or 100mm is modeled. In figure 5.3 the 2D model is shown where the darker top is asphalt and the lighter color is concrete.

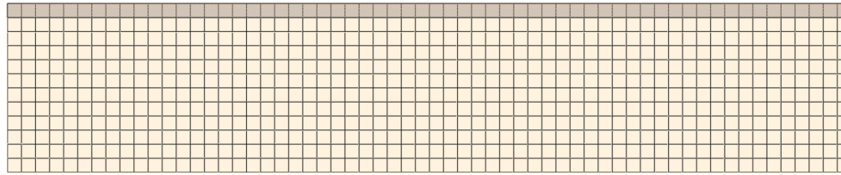


Figure 5.3: The 2D model used when simulating temperature distribution in the cross section

5.2.1.1 Material properties

The material properties for concrete, described in chapter 2 and in chapter 3, which are used in this model are listed in table 5.1.

| | Concrete | Asphalt |
|------------------------|--|---|
| Density | $\rho = 2500 \text{ kg/m}^3$ | $\rho = 2100 \text{ kg/m}^3$ |
| Specific heat capacity | $c = 900 \text{ J/(kg}^\circ\text{C)}$ | $c = 920 \text{ J/(kg}^\circ\text{C)}$ |
| Conductivity | $k = 2.5 \text{ W/(kg}^\circ\text{C)}$ | $k = 0.93 \text{ W/(kg}^\circ\text{C)}$ |
| Absorption | $\alpha = 0.5$ | $\alpha = 0.9$ |
| Emissivity | $\varepsilon = 0.9$ | $\varepsilon = 0.9$ |

Table 5.1: Material properties of concrete and asphalt

5.2.1.2 Loads

The climate loads will be applied at the surfaces. Each load step is one hour which corresponds to the meteorological data collected. This will simulate one temperature in each element each hour during one year, giving a total of 8760 temperatures in each element. Convection is equally applied on all surfaces of the cross section. Solar radiation is applied in three ways where the top surface have one value, the vertical south side one value and the northern vertical side one value. Ingoing and outgoing radiation is applied at the vertical and top horizontal surfaces. The ingoing and outgoing radiation at the horizontal bottom surface is assumed to be equal and therefore neglected. On the bottom surface there is in reality reflected light that will increase the temperature during sunny days. This have been neglected in this model which could result in larger temperature gradients than in reality. The reason for neglecting this part is lack of measured values on reflected light.

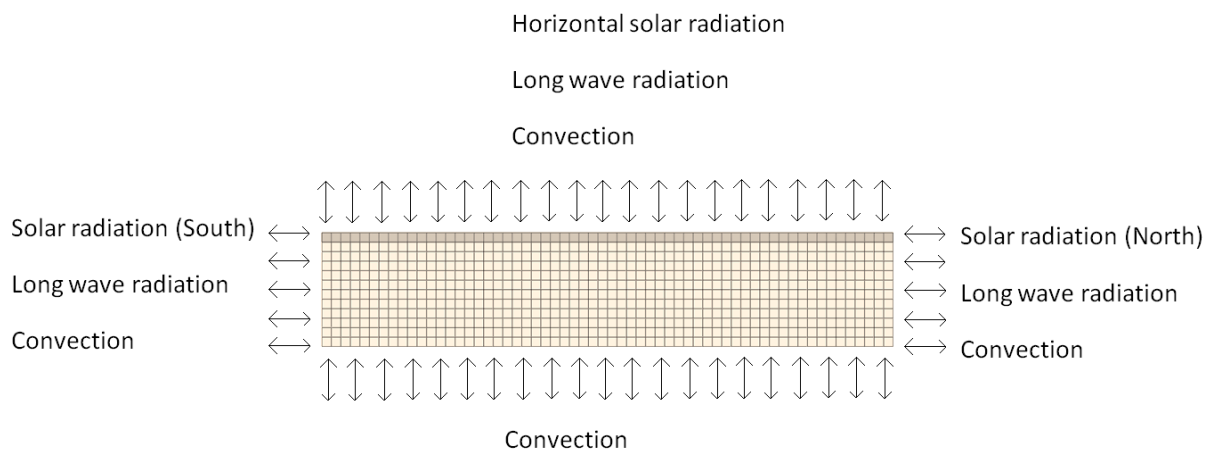


Figure 5.4: Climate effects applied at the different surfaces of the cross section

5.2.1.3 Initial conditions

The initial temperature of the model is set to -10°C . This is the air temperature when the simulation begins. This assumption could cause a small error the first hours. If any extreme situations appear

during these hours this initial condition should be investigated further.

5.2.1.4 Mesh

The model is meshed with heat transfer elements with the size 0.1 x 0.1m. This will give one temperature point each 0.1 meters through the section.

5.3 Results

The temperature simulation produces a large amount of data. From this data the worst cases are identified. The worst cases could be interpreted in different ways and therefore several approaches have been used and investigated. According to equations 2.10, 2.11 and 2.12 the temperature can be divided into three different parts, uniform part, linear gradient and non-linear gradient according to figure 2.2. Since the analysis is conducted on a 2D model no horizontal components will be obtained.

From these values the largest and smallest component of each type is identified. All 6 cases are presented in appendix A, but here the case with the largest linear gradient will be evaluated. This is chosen to get a good comparison with approach 1 and 2 according to Eurocode [CEN, 2009]. Results are presented for both 100mm and 50mm paving but the thickness of the concrete section is constant 1.1m. The results for 50mm paving can be found in appendix A. All of these gradients occurred during June in 1986.

Numerical values of the results is evaluated along a line in the middle of the section according to figure 5.5. This line is chosen to identify the largest temperature variations throughout the cross section. By choosing this line, boundary effects are avoided making this load the largest. By approaching any boundary the temperature difference will be reduced. Figure 5.5 visualizes an example of how the result is presented for a specific hour. The color distribution represents the temperature distribution of the simulation.

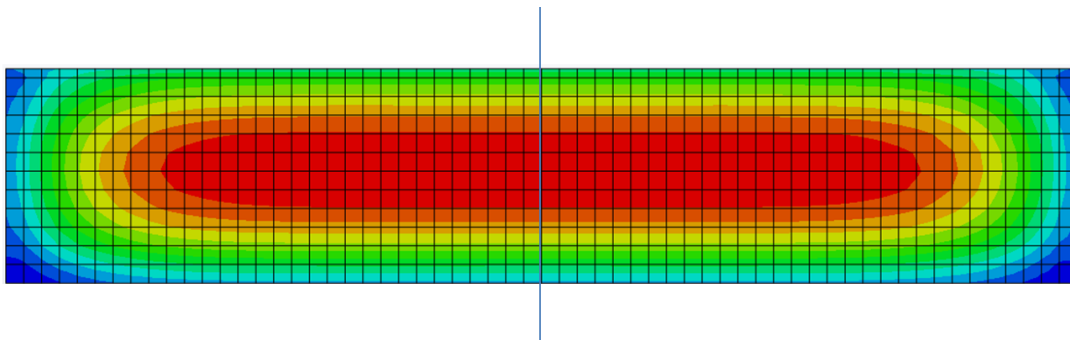


Figure 5.5: Simulated temperature distribution of the concrete deck at a specific hour where the color red stands for warmer elements and the color blue for cooler elements. It also visualizes the distribution line in the middle that further plots are based on.

5.3.1 100mm paving

5.3.1.1 Heating load case

Results presented origin from the simulation with 100mm paving of asphalt. In figure 5.6 the temperature distribution for the largest positive gradient is visualized. Positive gradient is defined as warm top and cold bottom.

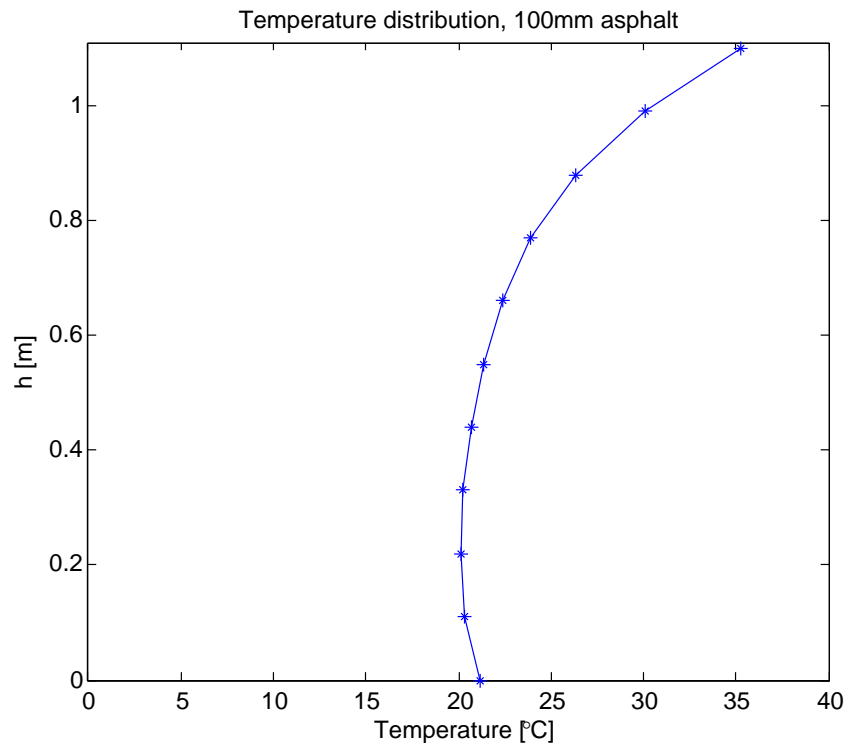


Figure 5.6: Temperature distribution for largest positive gradient with 100mm paving

The temperature distribution in figure 5.6 is divided into its uniform, linear and non-linear components and shown in figure 5.7.

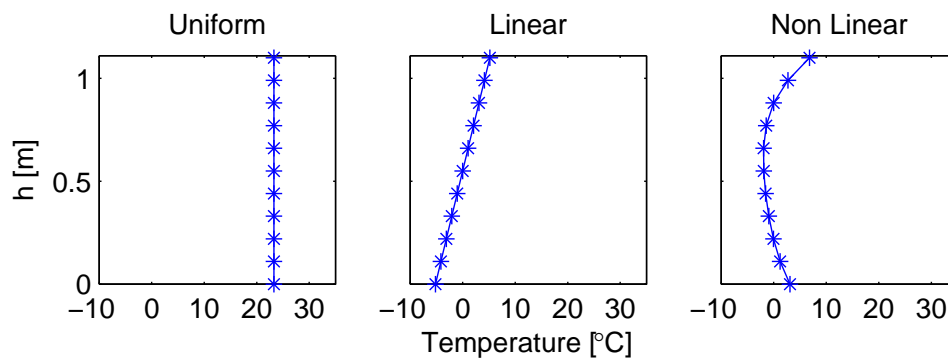


Figure 5.7: Temperature distribution divided into its components with 100mm paving.

Eurocode 1991-1-5 [CEN, 2009] provide temperature distributions for both the uniform and the non-uniform temperature distribution. The non-uniform part should include effects from both the linear and non-linear gradient. To compare the results from the simulation with the code the linear gradient have been added to non-linear distribution and plotted together with the distributions prescribed by approach 1 and approach 2 according to the code, this is visualized in figure 5.8.

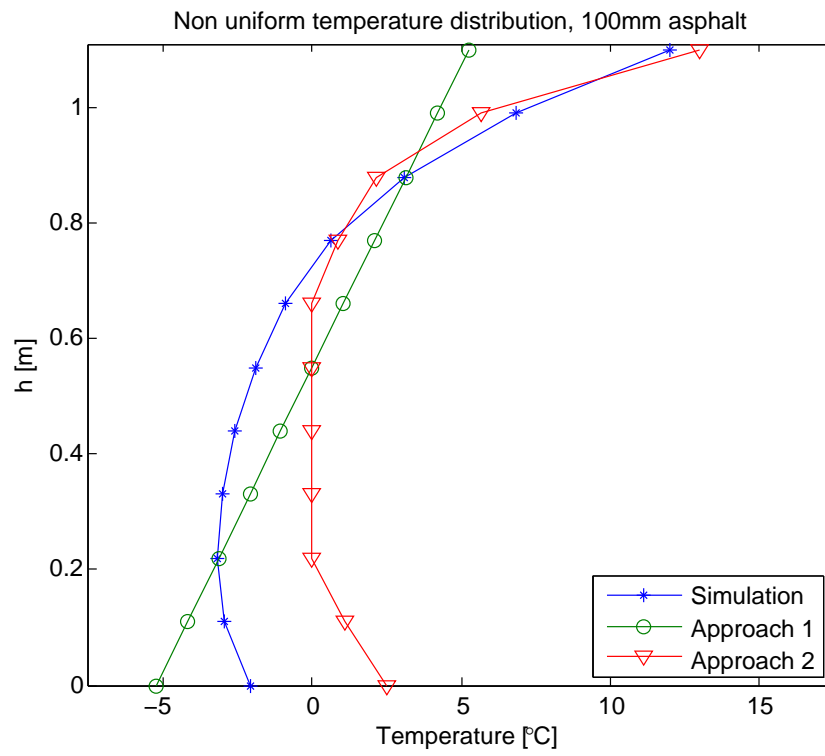


Figure 5.8: Linear and non-linear temperature components compared to values from Eurocode 1991-1-5 [CEN, 2009] with 100mm paving

5.3.1.2 Cooling load case

Results presented are from the simulation with 100mm paving of asphalt. In figure 5.9 the temperature distribution for the largest non-linear part is visualized. This is chosen because it is the case that gives the largest tension forces close to surface. The case with largest negative linear gradient were shown to be cooler in the middle than close to surface, this distribution is shown in appendix A.

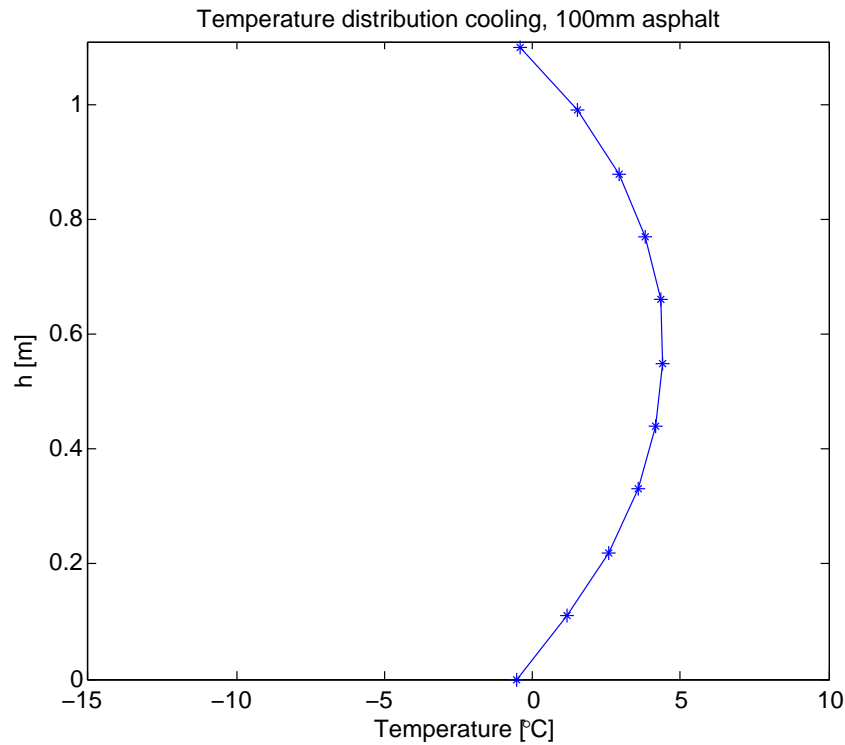


Figure 5.9: Temperature distribution for largest non-linear part with 100mm paving

The temperature distribution in figure 5.9 is divided into its uniform, linear and non-linear components and shown in figure 5.10.

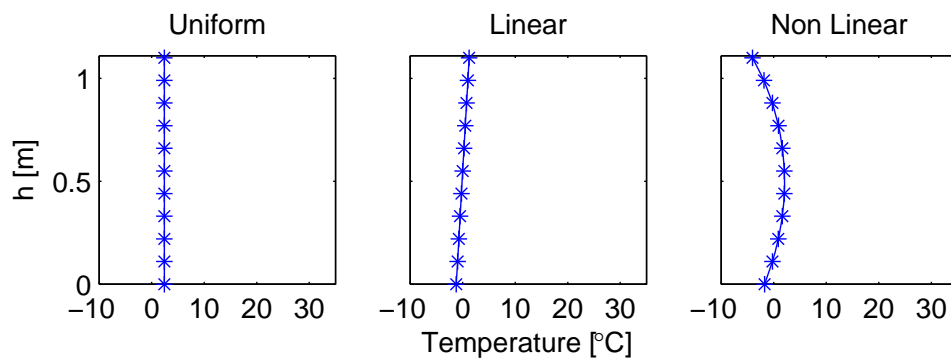


Figure 5.10: Temperature distribution divided into its components with 100mm paving.

Equal to the heating load case this distribution is compared with gradients suggested by Eurocode. This is visualized in figure 5.11

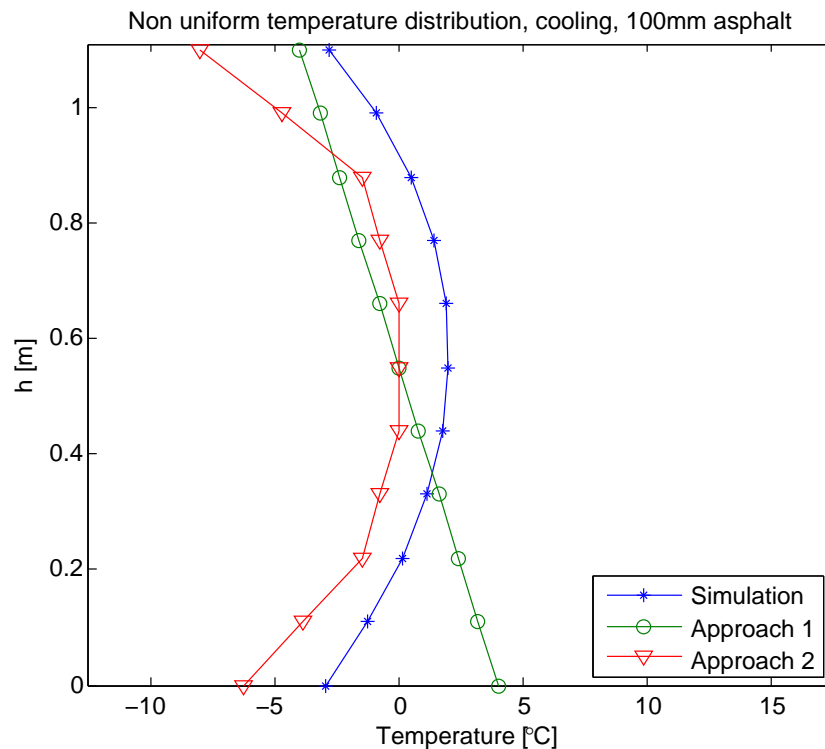


Figure 5.11: Linear and non-linear temperature components compared to values from Eurocode 1991-1-5 [CEN, 2009] with 100mm paving

5.3.1.3 Comments

Figure 5.8 visualizes certain similarities between the FE simulation and the approach 2 according to Eurocode 1991-1-5 [CEN, 2009]. At top, the temperature distributions are equal, however at the bottom of the concrete deck the difference in temperature is about 5°C . According to the FE simulation, approach 2 according to Eurocode is a more realistic choice of modeling than approach 1. The temperature distribution investigated is taken at the middle of the cross section. By taking distributions closer to the edge beam or a support the load would be reduced, making the section investigated as the worst case. In other words, this load might not be adapted for applying at the whole bridge deck alone, some kind of average value of the load could be a better approximation.

5.3.2 Comparison between paving thickness

A comparison of how the paving thickness affects the temperature distribution in the simulation is visualized in figure 5.12. This figure illustrates the difference between figure 5.6 and figure A.1. These distributions are taken the same hour with the same simulation where the paving thickness is the only parameter that has been changed.

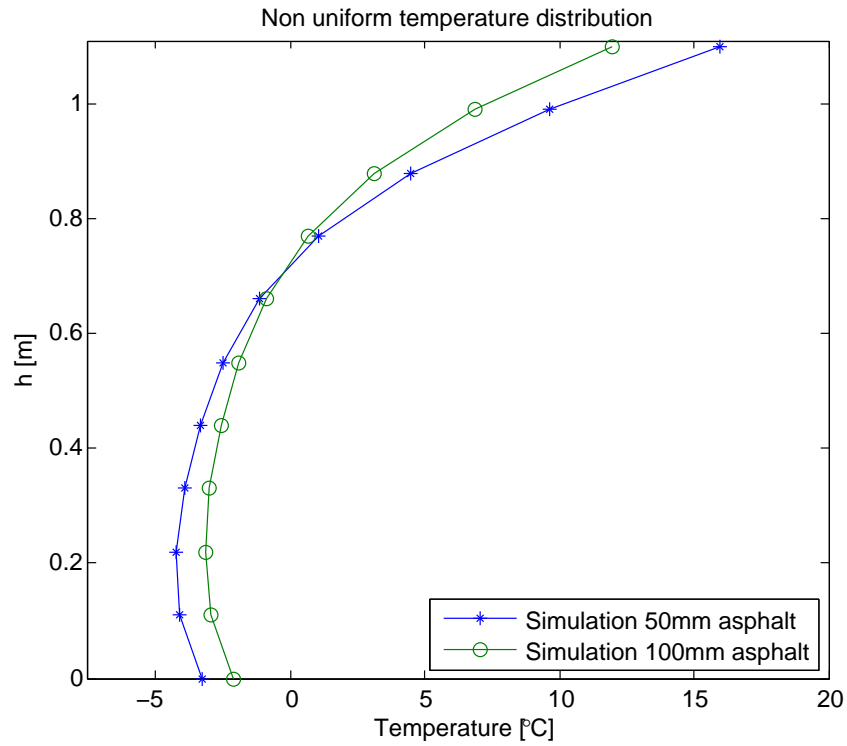


Figure 5.12: Total temperature distribution compared between 100mm and 50mm paving thickness for heating loadcase

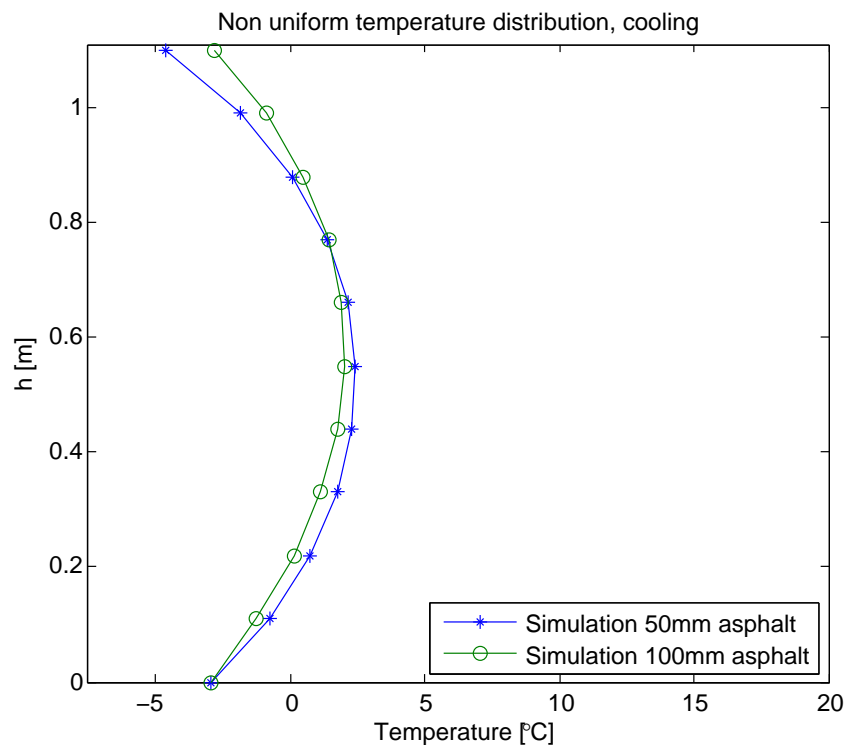


Figure 5.13: Total temperature distribution compared between 100mm and 50mm paving thickness for cooling load case

5.3.2.1 Comments

Figure 5.12 and 5.13 shows that the paving thickness has an impact on the temperature distribution. This validates the Eurocode 1991-1-5 [CEN, 2009] which states different temperature distributions for different thicknesses on the paving layer. A thinner paving will give a larger difference between bottom and top and therefore a larger design load.

Chapter 6

Temperature effects during bridge design

In chapter 5, the distribution of a realistic temperature profile for a concrete bridge deck was investigated. This chapter will evaluate how these temperature profiles affect load effects during bridge design using both the building codes in chapter 4 and the result of the simulation in chapter 5.

The analysis in this chapter will use the same bridge as an example as in the previous chapter, the portal frame bridge in Katrineholm. The material properties used for the analysis are stated in chapter 5. The investigated load case is described in chapter 4.

6.1 Temperature load analysis

The geometry, material properties, boundary conditions and loads used in the FE-model of bridge 829 in Katrineholm are described in this section.

6.1.1 Finite element model

The bridge is modeled in 3D using Scanscot BrigadePlus, the same software used in chapter 5. However in chapter 5 a heat flux analysis was performed. This chapter will perform a statical stress and load effect analysis.

6.1.1.1 Geometry and material

This model consists of the following parts; abutments, wing walls, bridge deck and edge beams with dimensions according to table 6.1. The bridge deck is thicker at the supports and thinner at midspan. For more information regarding the geometry, see figure 5.1 and 5.2

| Part | Dimensions [m] |
|------------------|------------------------------------|
| Bridge deck | 21.5 x 6.0 x [1.20 - 0.865] |
| Abutments | 6 x 7.97 x 1 |
| Wing walls | According to figure 5.2 with t=0.7 |
| Edge beams | 21.5 x 0.4 x 0.4 |
| Paving thickness | 0.1 |

Table 6.1: Dimensions of bridge 829 in Katrineholm

Shell elements are used for the abutments, wing walls and bridge deck. The edge beam is modeled as a beam element. A rough mesh with quadratic element and an approximate size of 0.4m is created according to figure 6.1. Each element has 9 integration points throughout the thickness of the bridge deck to acquire accurate results for the stress distribution in the bridge deck.

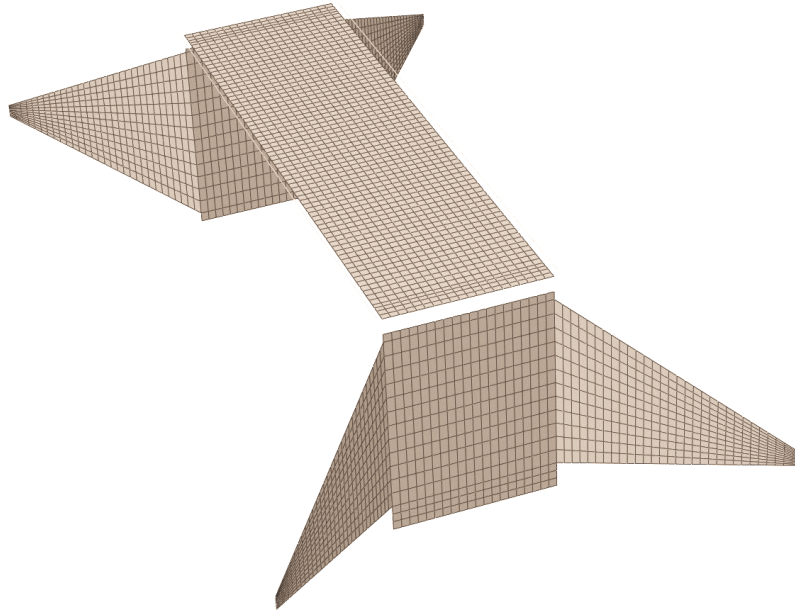


Figure 6.1: FE-model with a quad mesh using shell elements

The material properties for concrete, described in chapter 3, used in the model are listed in table 6.2. When modeling, a simple isotropic constitutive model is used.

| | |
|-------------------------------|----------------------------|
| Young's modulus | $E = 34GPa$ |
| Density | $\rho = 2500kg/m^3$ |
| Poisson's ratio | $\nu = 0.2$ |
| Thermal expansion coefficient | $\alpha = 1 \cdot 10^{-5}$ |

Table 6.2: Material properties of the concrete used in the model

6.1.1.2 Constraints and boundary conditions

The constraints between the different structural parts are all modeled as tie contact constraints. These constraints are defined by master and slave nodes. The slave nodes displacements and rotations are prescribed by the master nodes. For this model the bridge deck was defined as master surface.

The boundary conditions between the abutments and the ground were modeled as a stiff spring support. A spring will simulate real boundary condition more realistic, where the soil has some elasticity better than a rigid condition. Due to the large impact the boundary condition has on the results from the model it is of interest to model these accurate. The stiffness of the boundary spring supports are calculated according to equation 4.8, 4.9 and 4.10.

The calculated stiffness of the foundation is shown in table 6.3

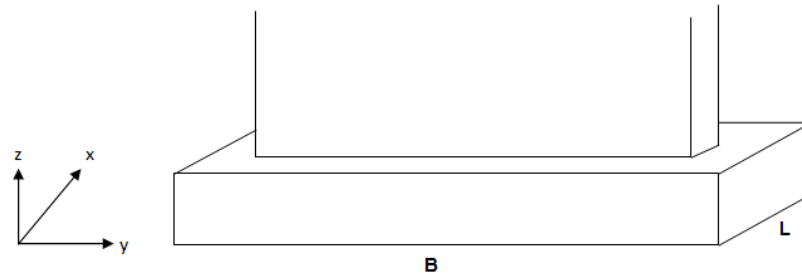


Figure 6.2: Coordinate directions when calculating spring stiffnesses

| | |
|------------------------|----------------|
| Rotation around x-axis | 5070 MNm/rad |
| Rotation around y-axis | 2340 MNm/rad |
| Vertical translation | 1921,59 MN/m |

Table 6.3: Stiffness of foundation according to equations 4.8, 4.9 and 4.10

6.1.1.3 Loads

The main load investigated in this thesis is the temperature load. However, to achieve a relevant model and compare results with the actual model used while designing bridge 829 in Katrineholm, each load is included separately such as:

- Self weight
- Earth pressure
- Support yielding
- Shrinkage
- Surface load
- Traffic load
- Surcharge load
- Temperature load
- Wind load

These loads are modeled in the same way as in the origin model and a comparison between the models is done in section 6.1.2. The aim is to get the same results from the reference model and the new model under the same loading conditions for validation purposes. The bridge deck is designed in safety class 3.

6.1.2 Validation of FE-model

The advanced model, modeled in Scanscot BrigadePlus is compared with the actual model that was used during the bridge design and produced in Scanscot BrigadeStandard by Joel Bjerstedt for Skanska Teknik. In this initial state, the main objective is to validate the advanced model by comparing the moment distribution. This moment distribution will be validated along line 2 according to figure 6.6. The load combination is ULS Transient according to table 4.3. Figure 6.3 visualizes this comparison between the Scanscot BrigadePlus and the Scanscot BrigadeStandard models for the maximum bending moment M_x . For all results M_x is the bending moment giving stresses in the x-direction (along the bridge deck).

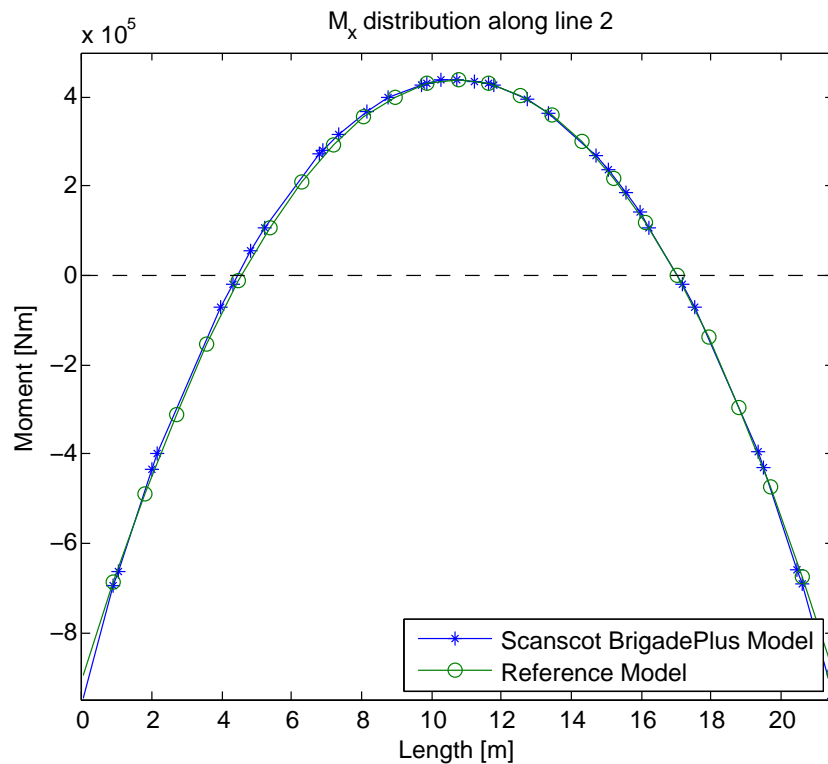


Figure 6.3: Comparison between M_x along line 2 with FE-analysis of bridge 829 done with Scanscot BrigadePlus and the reference model modeled in Scanscot BrigadeStandard

In Appendix B other plots are presented to visualize results from the validation in regard to section forces and section moments.

6.1.3 Temperature modeling

With a validated advanced finite element model the temperature difference is modeled with approach 1 and approach 2 according to Eurocode 1991-1-5 [CEN, 2009]. The models are identical apart from the temperature distribution due to climate effects.

In Scanscot BrigadePlus a temperature distribution is created through specifying a specific temperature at a number of temperature points. The points are placed equidistant throughout the cross section. For this analysis 10 temperature points are stated for the bridge deck section. Figure 6.5 and 6.4 visualizes the temperature distribution for approach 1 and approach 2 according to Eurocode 1991-1-5 CEN [2009]. Section 4.2.2.1 introduces approach 1 and section 4.2.2.2 introduces approach 2. These distributions are also used during the modeling presented in this chapter. In addition to the approaches stated in Eurocode, the temperature distribution from results in chapter 5 is used during modeling.

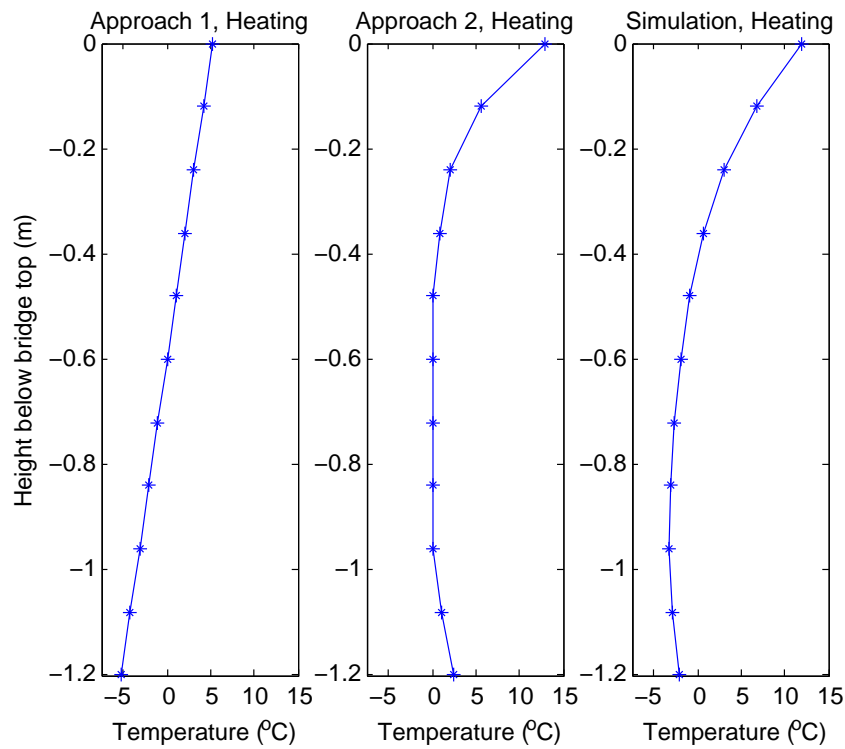


Figure 6.4: Temperature distribution at heating for approach 1, approach 2 and results of simulation

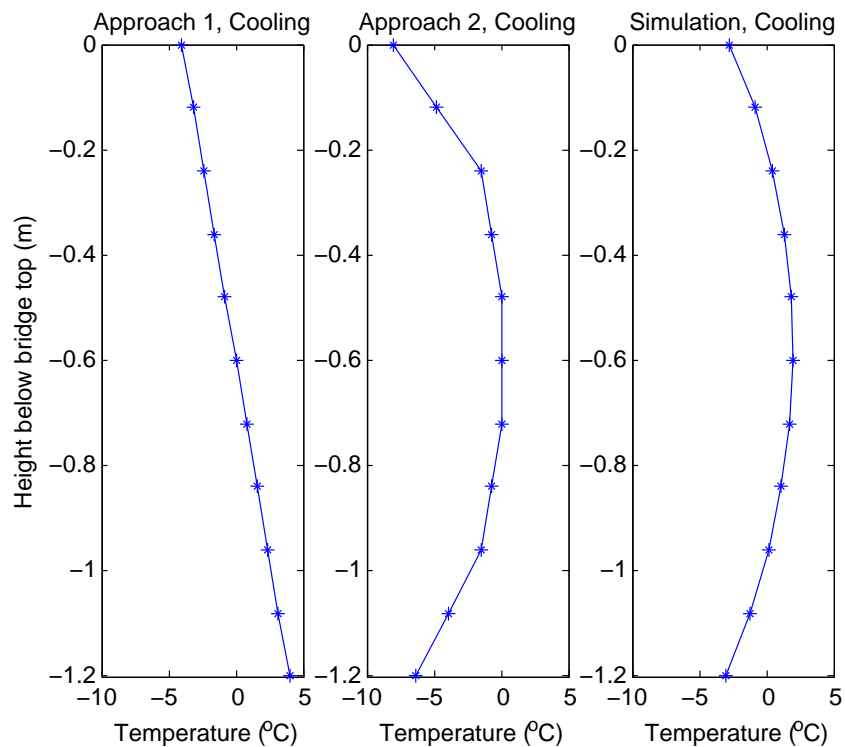


Figure 6.5: Temperature distribution at cooling for approach 1, approach 2 and results of simulation

By choosing 10 temperature points throughout the cross section, a good accuracy for the temperature distribution behavior is acquired. These temperature points however, are not to be mistaken for integration points displayed previous in figure 3.4. In section 6.1.1, a value of 9 integration points was selected for accurate results of the stress distribution in the concrete bridge deck during analysis.

6.2 Results

The final results of the model described in section 6.1.1 and validated in section 6.1.2 are presented in this section. The temperature difference loads for the model are modeled according to Eurocode 1991-1-5 [CEN, 2009]. Moments, normal forces, shear forces and local stresses have been evaluated for the different load cases.

A comparison between the models using approach 1 and approach 2 according to Eurocode is performed for bridge 829 in Katrineholm. The loads are described closer in chapter 4. By using approach 2 instead of approach 1 the maximum bending moment caused by temperature difference is significantly reduced. This difference is given at midspan where the difference is greatest. However, it shows that the bending moment overall can be reduced using this method. Using approach 2 will cause higher compressive normal forces.

During analysis of the bridge using temperature distribution from the simulation in chapter 5, unfavorable load effects are found. This is further discussed in section 6.2.3 and in chapter 8.

Moments, normal forces and shear forces are evaluated along the three lines visualized in figure 6.6. Two of the lines are located along the bridge deck, one in the middle and one close to the edge. The third line is located across the bridge deck close to a support. When referring to line 1, line 2 and line 3, these references are made to figure 6.6.

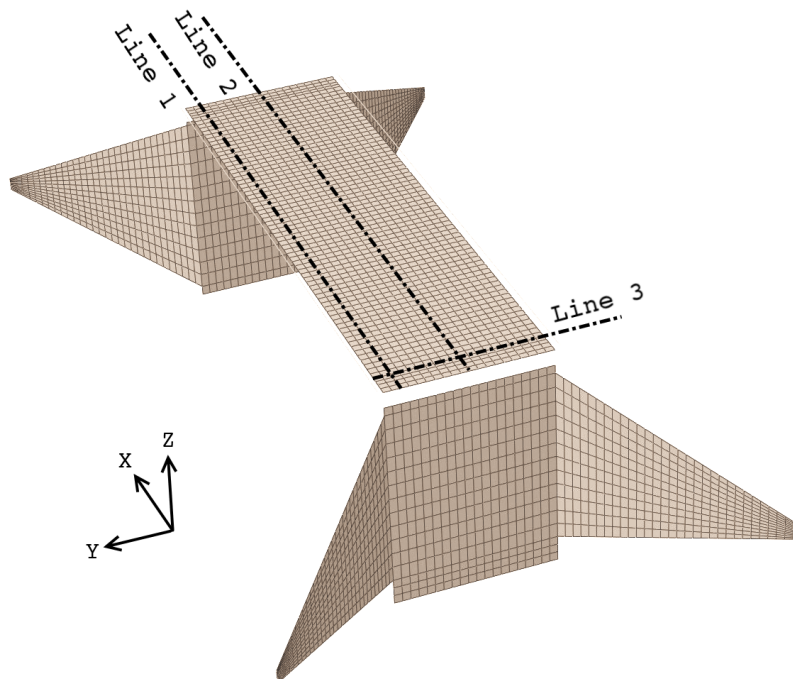


Figure 6.6: Visualization of distribution lines where section moments and forces are investigated

Stresses are evaluated in two elements according to figure 6.11 to identify if local stresses throughout the cross section could cause further problems. This is evaluated and are shown for both approaches.

When the load effects from temperature difference are presented they are divided into the load cases heating and cooling. Heating refers to the case where the top surface is warmer than the initial temperature T_0 whereas cooling refers to top surface being cooler than the initial temperature T_0 .

6.2.1 Section moments

A large share of the reinforcement in a concrete bridge is designed to resist bending moment. Therefore it is vital to investigate the section moments the temperature load model give rise to. In this model, the section moment is plotted for line 2 over the bridge deck according to figure 6.6. Additional results of line 1 and line 3 is given in appendix B.

6.2.1.1 Heating of bridge deck

Figure 6.7 visualizes the moment distribution along line 2 in figure 6.6 when the concrete bridge deck is heated. A direct conclusion is that when using approach 2, the section moments is significantly reduced compared to approach 1. The reduced moments depend upon the stress distribution in the concrete deck, stated in section 6.2.4. Note that these moment distributions apply for one isolated load only, the temperature difference.

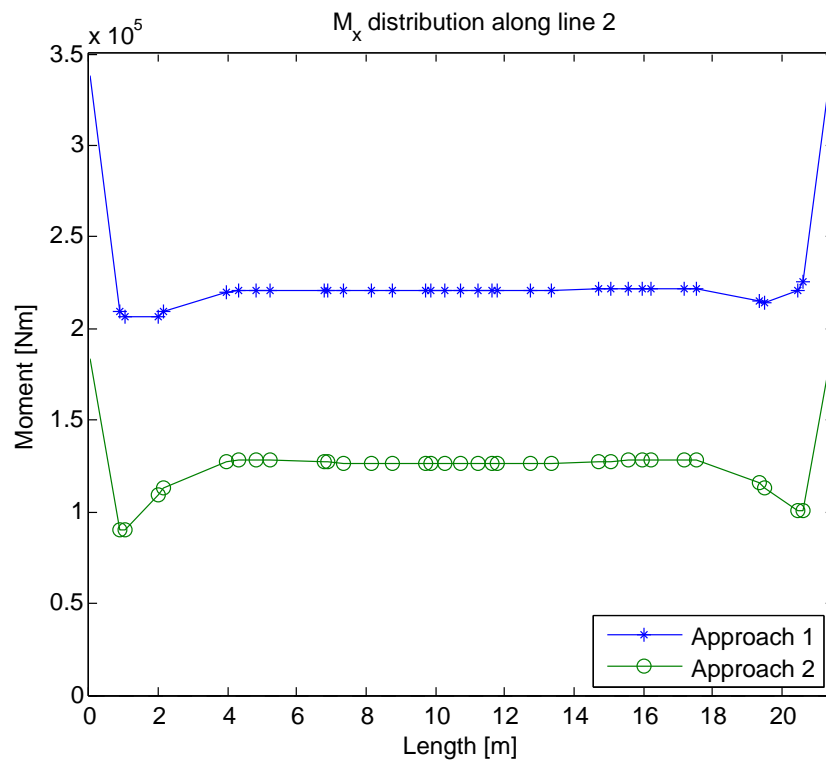


Figure 6.7: Moment distribution along line 2 with heating of the concrete bridge deck

In appendix B, figures B.7 and B.9 show similar results for line 1 and line 3 using approach 2 according to Eurocode 1991-1-5 [CEN, 2009]. The appendix also shows result of M_y in these 3 lines.

6.2.1.2 Cooling of bridge deck

Figure 6.8 shows the moment distribution along line 2 in figure 6.6 when the concrete bridge deck is cooled. As in the case of heating, approach 2 gives more favorable section moments. Note that these moment distributions apply for one isolated load only, the temperature difference.

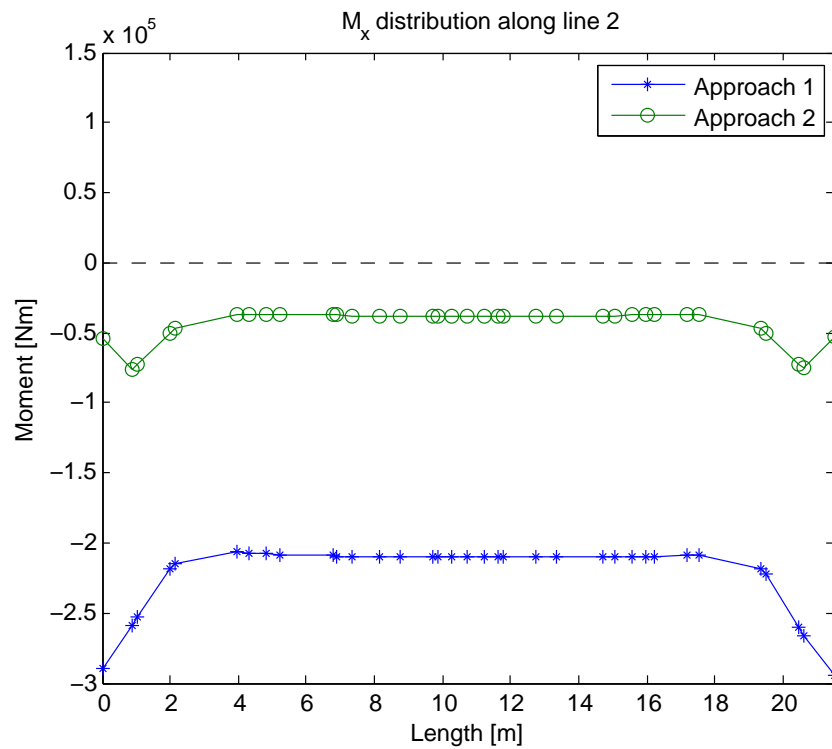


Figure 6.8: Moment distribution along line 1 with cooling of the concrete bridge deck

In appendix B, figure B.13 and B.15 shows similar results for line 1 and line 3 using approach 2 according to Eurocode 1991-1-5 [CEN, 2009]. The appendix also shows results for M_y in these 3 lines.

6.2.2 Section forces

Section forces are primarily investigated in case of any unfavorable tension force arises. These forces affect the reinforcement area, but not of the same magnitude that sectional moments do in this case. For the case of heating of the bridge deck, figure 6.9 shows the section force distribution N_x for line 2 in figure 6.6.

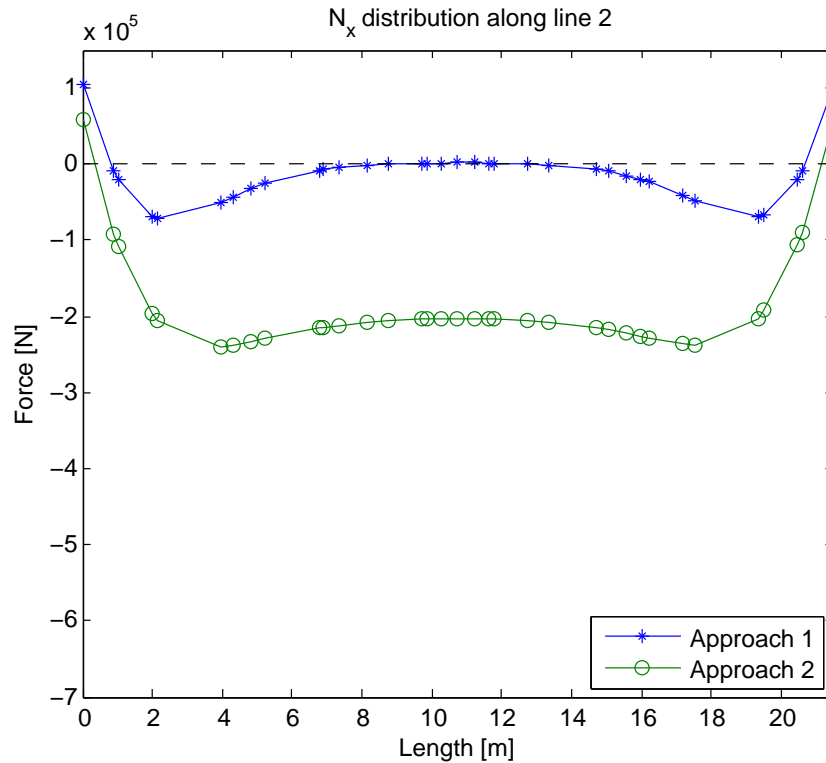


Figure 6.9: Section forces N_x along line 2 with heating of the concrete bridge deck

Figure 6.9 shows that when using approach 2 the resulting compressive normal forces is significantly larger than when using approach 1. This behavior is similar with the behavior along the other lines stated in appendix B. This increase in compressive forces using approach 2 might be seen as unfavorable at a first sight, however, concrete as a material is much more capable of handling this type of forces in comparison to tensile forces.

In the appendix B, additional plots showing N_x and N_y for the additional lines are presented. In appendix, results from the analysis of the bridge using the load case of the bridge deck being cooled are also displayed.

6.2.3 Results from climate simulation

As for the analysis using temperature distribution data from the simulation in chapter 5, figure 6.10 shows the result of the case with heating of the concrete bridge deck.

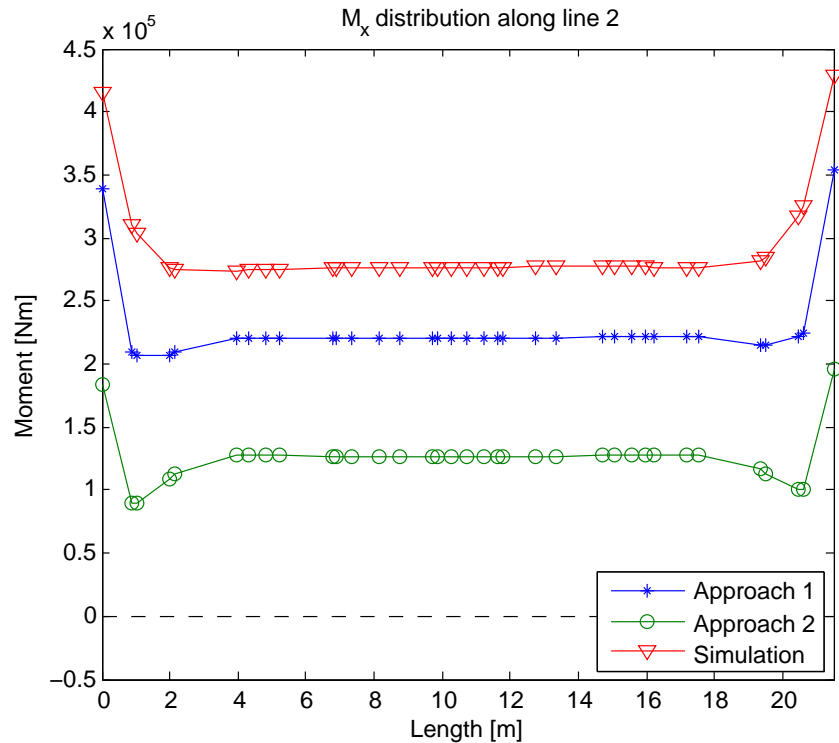


Figure 6.10: Section forces M_x along line 2 with heating of the concrete bridge deck

The result shows that when using temperature profiles from the simulation and evaluating these in a full 3D model the results may be misleading. This because the temperature distribution from the result in chapter 5 is taken for the worst possible element for the bridge deck. Using this distribution is only accurate in the element where it was investigated. For all other elements different temperature distribution from the simulation has to be used for accurate results.

This behavior implies the difficulties when choosing a characteristic temperature distribution from a large amount of data. As figure 6.10 shows, using the temperature profile from the simulation give the most unfavorable load effects. For a more realistic temperature distribution that is applicable for the whole bridge deck in a 3D model, different types of statistical analysis for the output of the simulation can be used. Another approach may be to divide the bridge deck in different temperature distribution zones. However, this type of analysis is outside the scope of work in this thesis.

To avoid misleading the reader these results are not shown in section 6.2.1 and 6.2.2, however in appendix B additional plots of load effects are shown and compared with approach 1 and approach 2.

6.2.4 Stresses in cross section

The stresses in the bridge deck are investigated to identify if approach 2 give rise to any additional unfavorable stresses in the concrete cross section compared with approach 1. The stresses are compared in two different elements of the bridge concrete deck. The first is placed at the middle of the deck and the second near a corner of the deck according to figure 6.11. These elements were chosen to compare if elements close to the supports would differ in stress distribution compared to elements far from any boundary. The stress is measured over the thickness of the cross section.

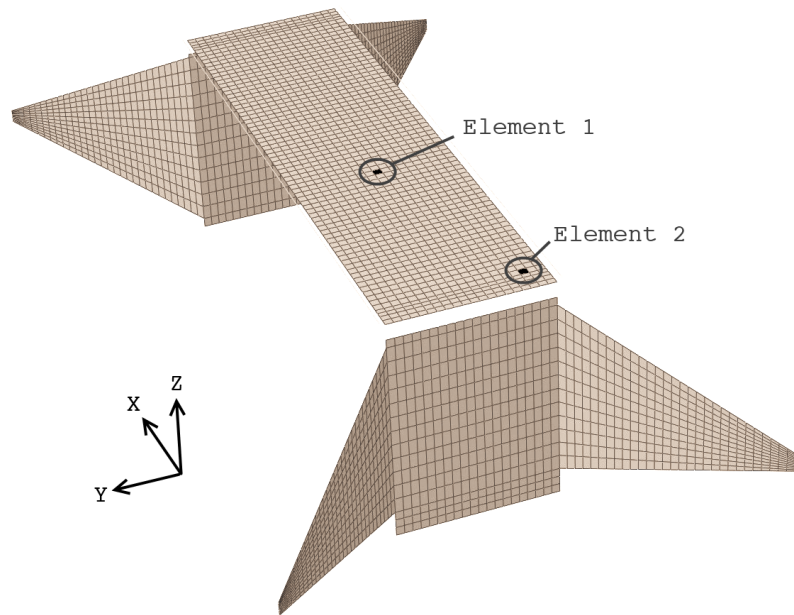


Figure 6.11: Visualization of elements where stresses are evaluated throughout the thickness of the cross section

In this chapter, figures showing the results of element 1 are presented, additional results for element 2 are given in appendix B.

6.2.4.1 Stresses from heating of bridge deck

Figure 6.12 shows the stress distribution of σ_x in element 1 according to figure 6.11 with the heating temperature difference. The plot clearly visualizes the difference between approach 1 and approach 2 according to the Eurocode 1991-1-5 [CEN, 2009]. Figure 6.12 shows that the stress distribution of σ_x has the same shape as the temperature distribution stated by the Eurocode even if the temperature values differ. These results can be derived from equation 2.13 which state that the stresses are directly related to the temperature distribution ΔT . Note that these stresses are only from one load; temperature difference where the deck is heated.

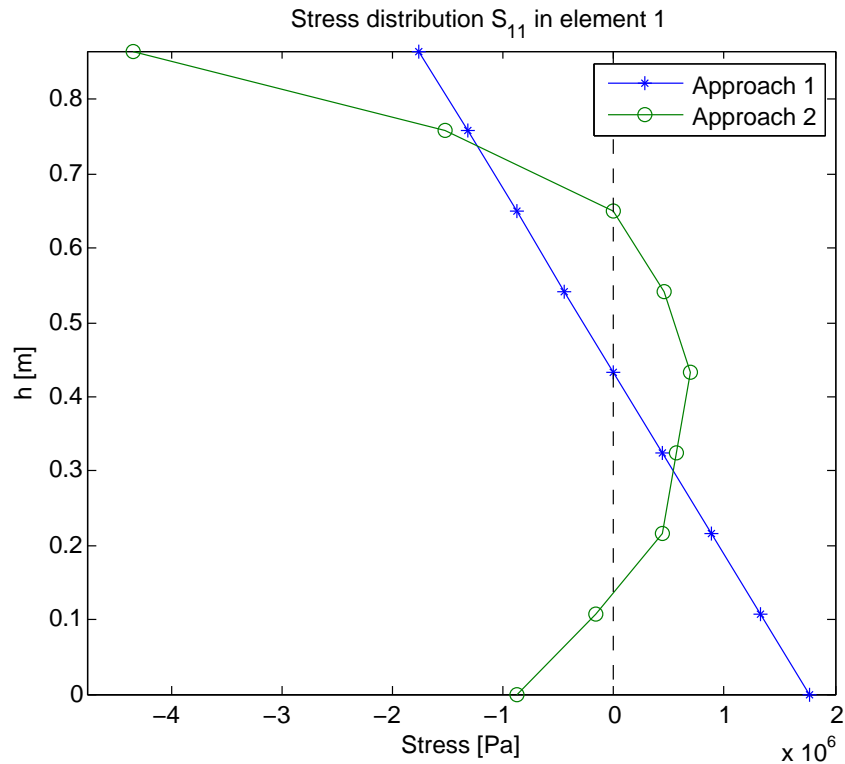


Figure 6.12: Stress distribution σ_x in element 1, heating of bridge deck

Figure 6.12 shows that approach 2 gives compressive stresses at the top and bottom of the bridge deck. In the middle tensile stresses occurs with a magnitude of 1 MPa. As for this load case, no unfavorable tensile stresses is present close to the surface in the concrete cross section using approach 2 in comparison to approach 1.

6.2.4.2 Stresses from cooling of bridge deck

Figure 6.13 shows the stress distributions with the cooling temperature difference. The figure shows that the stress distribution share the same shape as the temperature distribution. However, the compressive stresses that occurred in the heating load case, has been replaced by tensile stresses at the top and bottom of the bridge deck with approach 2. At the middle of the cross section compressive stresses occur. The stress distribution using approach 1 is linear with tensile stresses at top and compressive at bottom. Note that these are only stresses from one load, temperature difference where the deck is cooled.

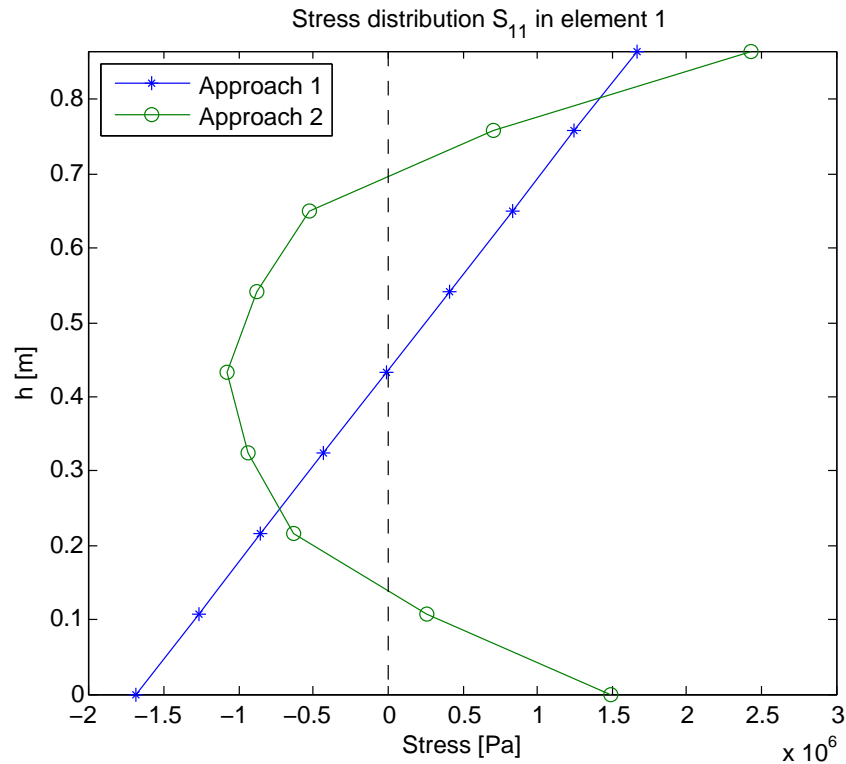


Figure 6.13: Stress distribution σ_x in element 1, cooling of bridge deck

For this load case, tensile stress peaks arises at the top and bottom of the concrete section. This will further be treated in chapter 7.

6.2.4.3 Stresses from self weight

All stresses presented in this chapter are only load effects from one load, a temperature difference load. To put the load effects from temperature in a larger perspective, stresses from an analysis using only self weight is presented. In appendix B, figure B.37 and B.38 shows the stress distribution when self weight is the only load for element 1 and 2 according to figure 6.11.

These figures shows stresses in the range from -3 MPa to 3 Mpa. The stresses from the temperature loads are smaller, but are still quite large in comparison with stresses from the self weight simulation. This implies that temperature effects is of such magnitude that it cannot be neglected and a realistic temperature modeling is important for a valid bridge design.

Chapter 7

Crack width limitations

During nights when the sky is clear the surface of the bridge can be significantly cooler than the temperature inside the structure. This difference in temperature will create tensile stresses close to the surface, shown in chapter 6. The results in chapter 6 show that unfavorable stresses develop when modeling with approach 2 [CEN, 2009], especially during cooling of the bridge deck.

As investigated in chapter 6, results indicate stresses above the tensile strength of concrete. In the serviceability limit state such stress levels will cause cracks in the concrete cross section and therefore it could be appropriate to take these stresses into account during design. This chapter will investigate the risk of cracking during this load case and suggest a method to manage these stresses during bridge design. The methods presented in this chapter are based on concrete material theory presented in chapter 3 and the current building code stated in chapter 4.

7.1 Method for calculating crack widths

As mentioned in chapter 3, equations 4.3 to 4.7 describe the calculation procedure of limiting crack widths in bridge design. However, to use these equations, assumptions need to be made to determine the stress in the reinforcement steel, σ_s .

Two different methods of calculating σ_s are developed in this thesis. Both methods are based on the following main assumptions:

- σ_s is calculated by a linear strain distribution of the concrete cross section.
- The linear stress distribution consists of stresses that originate from moments in the Serviceability limit state load combination.

Both of the methods described below use element 1 in figure 6.11. In this element, the combined load effects result in compression at the top and tension at the bottom of the cross section. For crack width analysis in element 1, only the tensile stresses at the bottom of the cross section are of interest. The maximum allowed crack width for the investigated bridge is $w_k \leq 0.2mm$.

7.1.1 Method A - Force added manually

The non-linear tensile stress is manually added using the force that the stress distribution of the temperature load case causes. This force F_{temp} is visualized in figure 7.1 and can be simplified to the following equation:

$$F_{temp} = \sigma_{ct} \frac{h_{peak}}{2} b \quad [N] \quad (7.1)$$

where b is the width of the section being investigated. F_{temp} is taken at either the top or the bottom of the cross section depending on where the resulting tensile stresses arise. Choosing top or bottom depends on where cracking is evaluated. Figure 7.1 displays the force used for the case in element 1 with the cooling temperature load case. This method will give the demand of reinforcement for all summed tensile

stresses appearing from the non-linear temperature stress distribution. This should be an assumption on the safe side, assuming that the concrete is not taking any tensile stresses. Since all stresses are added to the reinforcement the traditionally integrated section moments are removed from this load and replaced by this method.

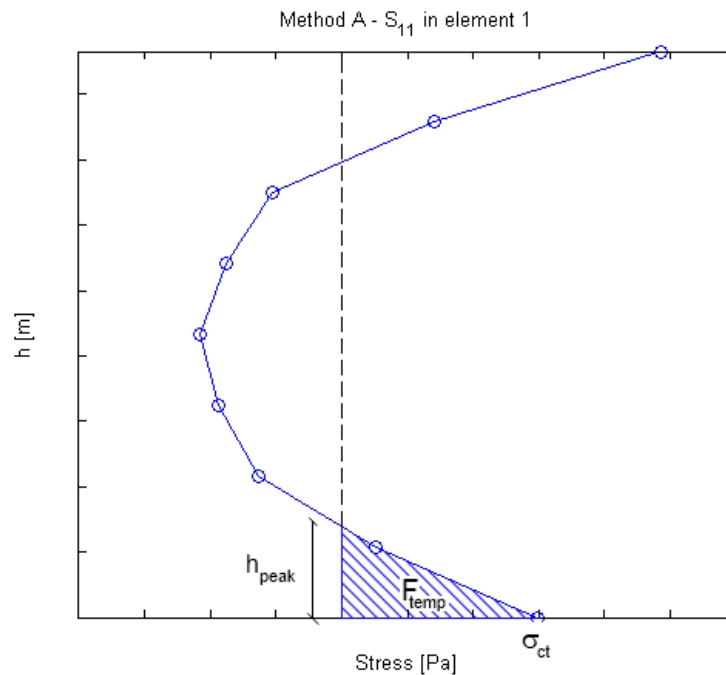


Figure 7.1: Visualization of the force F_{temp} used in method A for stress distribution in element 1, cooling of bridge deck.

For method A the first expression is stated in equation 7.2 where the non-linear stress is manually added using the force, F_{temp} , and a value of the reinforcement area, A_s , which is iterated. The variable x is the height of the compressive zone, H is the total height and d is the effective height of the cross section.

$$\sigma_s = \alpha \sigma_c \left(\frac{d-x}{x} \right) + \frac{F_{temp}}{A_s} \quad [Pa] \quad (7.2)$$

The variable σ_c is the maximum compressive stress in the concrete at either top or bottom of the concrete section. A linear elastic relationship between stress and strain is assumed in these calculations. The linear stress distribution is written as:

$$\sigma_c = \frac{M}{\frac{bx}{2} \left(\frac{H}{2} - \frac{x}{3} \right) + \alpha \frac{d-x}{x} A_s \left(d - \frac{H}{2} \right)} \quad [Pa] \quad (7.3)$$

where the moment M is the load effect in quasi-permanent load combination without the non-linear temperature effects. α is the ratio of the long-term E-modulus of the concrete and the reinforcement. This is described by:

$$\alpha = \frac{E_s(1 + \varphi_{eff})}{E_{cm}} \quad [-]$$

In equation 7.3 there are two unknowns, the amount of reinforcement A_s and the height of the pressure zone, x in the concrete cross section. To solve this, a value of x is estimated through an iteration process. An initial estimation of x is given by:

$$x_0 = \frac{h}{3} \quad [m]$$

and for the following iterations x is given as:

$$x_i = x_0 + \frac{h}{6} \frac{N_i - N_0}{\text{abs}(N_i - N_0)} \quad [m]$$

$$x_{i+1} = x_i + (x_0 - x_i) \frac{N_{i+1} - N_0}{N_{i+1} - N_i} \quad [m]$$

The iteration scheme that is used is presented in table 7.1.

| | |
|--------------------------------------|---|
| 1. Define variables | Load effects M_{ref} , N_{ref} and F_{temp} Determine maximum allowed crack width w_k Geometry including the height h_{peak} for the stress peak Material parameters and coefficients |
| 2. Assume $x = \frac{h}{3}$ | |
| 3. Loop until $residual < tolerance$ | Calculate $A_{c,eff}$ (4.6) Calculate $\rho_{p,eff}$ (4.5) and $s_{r,max}$ (4.4) with A_s as unknown Calculate σ_c (7.3) and σ_s (7.2) with A_s as unknown Solve A_s from equation 4.3 Calculate M_i and N_i with the solved value of A_s Predict x for next step Calculate residual of M_i and N_i in reference to M_{ref} and N_{ref} |

Table 7.1: Method A: Iteration scheme of calculating A_s and x

7.1.2 Method B - Moment added manually

Instead of adding a force as in method A a moment is added in this method. The total force added to the reinforcement is equal for method A and B, but in method B a fictitious compressive force in the concrete will be added. The compressive force is considered to have a limited effect. The method is less precise but is easier to use in a design process where section moments are used to calculate the amount of reinforcement. Similar to method A, the traditionally integrated section moments are removed and replaced by this (larger) moment. Using the stress distribution from a specific element, an additional moment ΔM_{temp} is calculated according to equation 7.4.

$$\Delta M_{temp} = \sigma_{ct} \frac{h_{peak}}{2} b \cdot z \quad [Nm] \quad (7.4)$$

The variable σ_{ct} is the stress at the top or bottom of the section being investigated. Choosing top or bottom depends on where cracking is evaluated. h_{peak} is the height of the stress peak investigated and z is the lever arm, both according to figure 7.2. b is the width of the section.

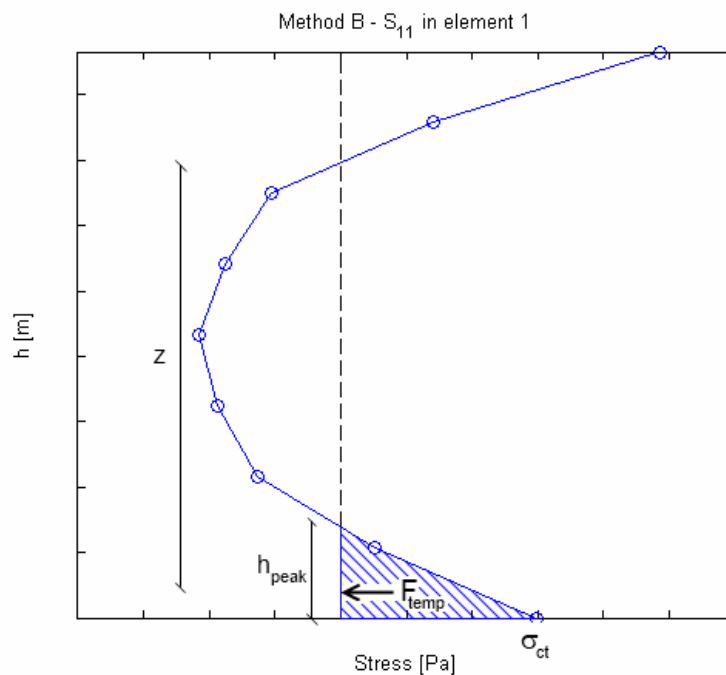


Figure 7.2: Visualization of the height h_{peak} of the stress peak and the lever arm z used in method B for stress distribution in element 1, negative temperature gradient.

From the additional moment, ΔM_{temp} , the maximum compressive stress in the concrete is calculated according to equation 7.5

$$\sigma_c = \frac{M + \Delta M_{temp}}{\frac{bx}{2} \left(\frac{H}{2} - \frac{x}{3} \right) + \alpha \frac{d-x}{x} A_s \left(d - \frac{H}{2} \right)} \quad [Pa] \quad (7.5)$$

The maximum compressive stress in the concrete is proportional to the stress in the reinforcement according to equation 7.6. Here a linear elastic relationship between stress and strain is assumed.

$$\sigma_s = \alpha \sigma_c \left(\frac{d-x}{x} \right) \quad [Pa] \quad (7.6)$$

All other equations are according to method A. The iteration scheme that is used in method B is presented in table 7.2.

| | |
|--|---|
| <p>1. Define variables</p> <p>2. Assume $x = \frac{h}{3}$</p> <p>3. Loop until $residual < tolerance$</p> | <p>Load effects M_{ref}, N_{ref} and σ_{temp}</p> <p>Determine maximum allowed crack width w_k</p> <p>Geometry including the height h_{peak} for the stress peak</p> <p>Material parameters and coefficients</p> <p>Calculate $A_{c,eff}$ (4.6)</p> <p>Calculate $\rho_{p,eff}$ (4.5) and $s_{r,max}$ (4.4) with A_s as unknown</p> <p>Calculate σ_c (7.3) and σ_s (7.2) with A_s as unknown</p> <p>Solve A_s from equation 4.3</p> <p>Calculate M_i and N_i according to the solution of A_s</p> <p>Predict x for next step</p> <p>Calculate residual of M_i and N_i in reference to M_{ref} and N_{ref}</p> |
|--|---|

Table 7.2: Method B: Iteration scheme of calculating A_s and x

7.1.3 Graphical comparison of Method A and Method B

A graphical comparison of method A and method B is visualized in figures 7.3 and 7.4.

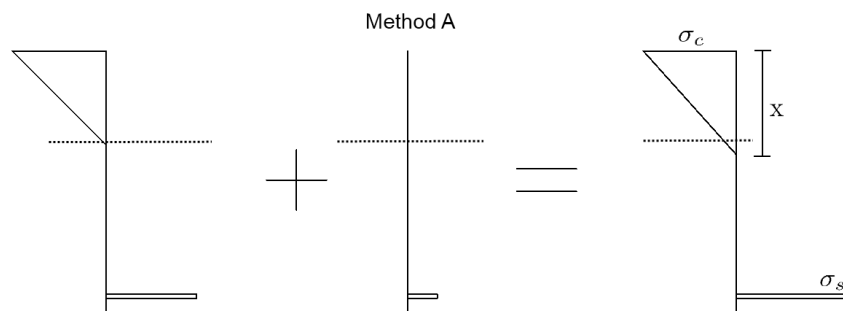


Figure 7.3: Visualization of equilibrium forces in the concrete section according to method A

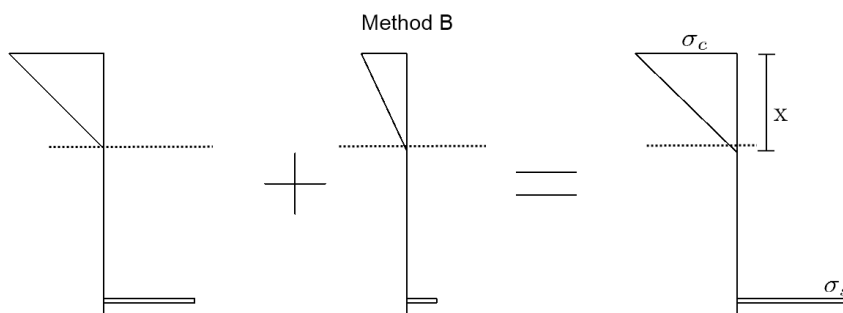


Figure 7.4: Visualization of equilibrium forces in the concrete section according to method B

For method A, figure 7.3 shows how the force F_{temp} is added. Using this approach, the compressive height x in the concrete section will increase due to a self equilibrated concrete section. This will result of reduced stress in the concrete, σ_c . However, for method B, the compressive height x in the concrete section is relatively uninfluenced in comparison to method A. With this method, the extra moment added will affect the stress in the concrete, σ_c , shown in figure 7.4.

7.2 Results

The final results of the evaluation of method A and method B described in this chapter is presented in this section. The results will state the total demand of reinforcement for a specific element in the bridge deck. The elements evaluated are element 1 and element 2 according to figure 6.11. The first element represent a section in the midspan of the bridge where cracks in the bottom of the bridge deck section may cause problems. The second element represent a section near the support where cracks at the top of the bridge deck could cause problems.

During comparison of these two methods regarding crack widths in bridge design, similar results are shown. Using both methods, the demand of reinforcement in the bridge cross section is higher than using traditional calculations without the extra care of the stress peaks using approach 2 according to Eurocode 1991-1-5 [CEN, 2009]. For element 1, the demand of reinforcement is similar between using load effects from approach 1 and using approach 2 with the extra care for the stress peak. In element 2, the demand of reinforcement is significantly larger using the two methods described in this chapter.

7.2.1 Element 1

When using method A and method B according to the iteration schemes suggested in table 7.1 and 7.2, input variables from the FE analysis performed in chapter 6 are used. Three different load cases are represented, Ultimate Limit State (table 4.3), SLS Quasi-permanent (table 4.4) and SLS Characteristic (table 4.5). The load cases are evaluated using approach 1 and approach 2 according to Eurocode 1991-1-5 [CEN, 2009] and one case with the temperature gradient load case inactive. The input parameters are presented in table 7.3.

| | Approach 1 | | Approach 2 | | Without tempdiff | |
|-----------|-------------------|----------------|-------------------|----------------|-------------------------|----------------|
| | M(<i>kNm</i>) | N(<i>kN</i>) | M(<i>kNm</i>) | N(<i>kN</i>) | M(<i>kNm</i>) | N(<i>kN</i>) |
| ULS | 1402 | -397 | 1337 | -397 | 1268 | -397 |
| SLS Char | 1011 | -406 | 968 | -406 | 922 | -406 |
| SLS Quasi | 564 | -415 | 527 | -415 | 489 | -415 |

Table 7.3: Section forces at element 1 in midspan used for reinforcement calculations

Table 7.4 displays the necessary reinforcement calculated using method A and method B with input variables from the SLS Quasi-permanent load combination. In addition, a comparison using ordinary crack width calculations without the extra attention to the stress peaks are displayed. These calculations use the design load effects directly from the FE analysis, using both approach 1 and approach 2 according to Eurocode and a simulation without the temperature load case.

| | Approach 1 | Approach 2 | No TempDiff | Method A | Method B |
|---|------------|------------|-------------|----------|----------|
| Reinforcement(<i>mm</i> ²) | 3498 | 3188 | 2890 | 3510 | 3485 |
| x(<i>mm</i>) | 318 | 312 | 306 | 328 | 318 |
| σ_c (<i>MPa</i>) | -6.4 | -6.2 | -6.0 | -5.6 | -6.4 |
| σ_s (<i>MPa</i>) | 174.5 | 174.3 | 172.5 | 174.5 | 174.5 |

Table 7.4: Reinforcement at element 1 in midspan from crack width calculations with different methods

7.2.1.1 Comments

As table 7.4 shows, the two methods used to compensate the stress peaks gives a larger amount of reinforcement in comparison to using the load effects from approach 2 directly. Both of these methods handling the stress peaks results in a nearly identical demand of reinforcement, implying that the two methods shown in figures 7.3 and 7.4 has the same effect. As for a bridge designer, there is benefits of handling moment with method B instead of forces for easier integration in standard crack width calculations.

For element 1, the results of the reinforcement demand states that using approach 1 gives similar demand as when using both method A and method B to handle the extra stress peak. These similarities

is only valid for element 1 and should not be interpreted as approach 1 generally would give results equal to method A or B.

The results in table 7.4 shows that the demand of reinforcement with approach 1 and approach 2 is, as described in chapter 6, a result of the magnitude of the bending moments (normal forces are constant).

An interesting result shown in table 7.4 is that the demand of reinforcement is significantly lower for the load case using no temperature differential load. This result confirms that thermal effects has a large impact during bridge design in a serviceability load case. Table 7.3 shows that temperature differential load also has a large impact for the ULS and SLS Characteristic load case.

7.2.2 Element 2

As for the case with element 1 at the midspan, the same procedure is done for element 2 near the support. Input variables from previous FE analysis is presented in table 7.5.

| | Approach 1 | | Approach 2 | | Without tempdiff | |
|-----------|------------|-------|------------|-------|------------------|-------|
| | M(kNm) | N(kN) | M(kNm) | N(kN) | M(kNm) | N(kN) |
| ULS | -2065 | -411 | -1963 | -597 | -1960 | -597 |
| SLS Char | -1597 | -507 | -1528 | -631 | -1526 | -631 |
| SLS Quasi | -1106 | -624 | -1049 | -688 | -1047 | -688 |

Table 7.5: Section forces at support used for reinforcement calculations

In a similar way as for element 1, table 7.6 displays the demand of reinforcement for comparison between the different methods for element 2.

| | Approach 1 | Approach 2 | No TempDiff | Method A | Method B |
|---------------------------------|------------|------------|-------------|----------|----------|
| Reinforcement(mm ²) | 4860 | 4399 | 4391 | 5479 | 5434 |
| x(mm) | 443 | 442 | 442 | 477 | 460 |
| σ_c (MPa) | -6.7 | -6.6 | -6.6 | -6.2 | -7.2 |
| σ_s (MPa) | 178.4 | 176.8 | 176.8 | 180.7 | 180.5 |

Table 7.6: Demand of reinforcement at support from crack width calculations with different methods

7.2.2.1 Comments

Similar to element 1 at midspan, element 2 near the support shows similar behavior when treating differences between method A and method B. Comparing approach 2 with the case with no uneven temperature load, the results from approach 2 shows almost no increase in demand of reinforcement.

Because of these results, the use of method A and method B will give a significantly greater demand of reinforcement, which can be seen in table 7.6. These results are somehow troublesome and could either be interpreted as if approach 1 underestimates the demand of reinforcement. The other interpretation would be that method A and method B is invalid close to the support. This could be connected to results from the simulation in chapter 5 where it was concluded that the temperature profiles should be more beneficial closer to supports than in midspan.

Chapter 8

Conclusion

8.1 Summary of Results

The concluded results from this thesis are shortly summarized in this section:

- Approach 2 in Eurocode [CEN, 2009] gives a more realistic temperature profile than approach 1.
- Using approach 2 will give a lower demand of reinforcement than approach 1.
- Thermal effects from temperature difference could in portal frame bridges alone account for 20% of the reinforcement at midspan.
- The non linear temperature distribution could cause problems with cracks close to the surface.
- If approach 2 is used, additional analysis regarding crack width limitations in serviceability limit state might be necessary, two suggestions how to do this have been presented.

8.2 Discussion

This thesis has processed the basis of temperature loads, concrete as a material, the current building codes and then performed analysis in this subject. The first analysis is a climate simulation where a 2D section of bridge 829 in Katrineholm was subjected to climate data from Stockholm during 1986. In the second analysis on the same bridge all loads were applied together with thermal effects to evaluate section forces and stresses. The third part is suggestions how to handle stress peaks from a non linear temperature distribution in the serviceability limit state.

The climate simulation implies that approach 2 in Eurocode [CEN, 2009] is closer to the simulated situation than approach 1, which was expected. The distribution in figure 5.8 shows that even when the largest positive gradient is chosen approach 2 is more similar to the simulation. This indicates that approach 2 would be more appropriate for a realistic model compared with approach 1. Both approach 1 and approach 2 are recommended by Trafikverket for concrete, steel or composite bridges and thereby valid for use in bridge design in Sweden.

When section forces and stresses are evaluated from the 3D model it shows that the bending moment is significantly lower with approach 2 compared with approach 1. Reducing the bending moment will directly affect the amount of reinforcement needed. The lower section moments originates from the stress distribution from approach 2 being partially self equilibrated. This is a result from having included the non linear stress distribution, directly proportional to the non linear temperature distribution. Comparing the magnitude of the stresses from temperature difference and self weight shows that the magnitude of the temperature stresses is a significant part of the total load. The normal force from approach 2 has a higher compressive value. Compressive normal forces is usually not an issue, often it is beneficial because it reduces tensile stresses in the section.

The tensile stresses from the more non-linear distribution in approach 2 are worrying and are therefore investigated further. This tensile stress could cause cracks in the serviceability limit state and reduce the durability of the structure. If the structure is designed in the ultimate limit state we believe that

section forces from approach 1 and 2 could be evaluated through integrating the stresses in a traditional way. This is because the stresses will be significantly reduced when the concrete deck is heavily cracked. Something worth to discuss is the fact that the non-linear stresses occur even if approach 1 is used, but not treated there. With this in mind approach 2 may as well be applicable without extra considerations also in serviceability limit state. This would mean that both method A and B suggested in chapter 7 are redundant.

The phenomenon of cracked concrete in different zones makes the FE analysis complicated and difficult to handle for a complex structure as a bridge. A major assumption done in this thesis is to treat concrete as an isotropic material with a specific stiffness. Close to surface phenomena as cracking from thermal effects is probably heavily overestimated when modeling the concrete with its full Young's modulus. This could argue towards only considering section forces integrated the traditional way rather than applying the full tensile force from thermal effects in the reinforcement.

If the extra tensile force is to be added to the reinforcement two methods were suggested. They both add the full tension force that the temperature distribution gives rise to into the reinforcement. The reason for adding it as a moment rather than a force is better compatibility with traditional methods of designing a bridge structure. The normal procedure is to treat section forces and not stresses in different elements. When adding a bending moment a compressive force is also added in the concrete that is fictitious.

If the extra tensile force is added to the reinforcement according to suggested method A or B they both gives similar results. They both give an amount of reinforcement similar or higher than approach 1, see table 7.4 and 7.6 . The same table shows that temperature difference is a considerable part of the total reinforcement required in a bridge, making it important to investigate properly. In other words, a realistic temperature model could remove parts of redundant reinforcement or in other cases reinforce correctly where it is needed.

A reduced amount of reinforcement is favorable for many reasons. Not only the high price of reinforcement steel in comparison to concrete, but even more practical reason during construction at the building site.

It is shown that it is beneficial from a design perspective that the total amount of reinforcement could be reduced in bridges. However, to evaluate stresses and a model with a more non-linear temperature profile is additional work with the methods we have used compared with the standard designing methods of today. If the more non linear temperature profile is implemented in softwares like Scanscot Brigade-Standard this would probably not be any additional work. This extra work should be weighed against the lower material and labuor cost in production.

In all analysis in this thesis the non-uniform temperature effects have been reduced with the factor 0.769 to consider long term creep in the concrete. This is not allowed in the new Swedish building code and changing this coefficient to 1.0 would increase the effect of a more realistic model even further.

Implementing simulated temperature distributions into stress and reinforcement design implies unfavorable results. This could be an effect from taking the worst position on the bridge. To get a more representative value some kind of average value on the bridge might be more applicable.

What is clear is that temperature effects are complicated loads. It is unsure how to model it correctly and how it effects the bridge during different events. It is also hard to predict the size of the load in a cracked cross section. Combining this with the significant size of the load makes it interesting to investigate further. During a lifetime of a structure it will be subject to all kinds of temperature distributions, most of them rather harmless. The extreme events that have been evaluated here are infrequent, but still important. The resulting load effects from a temperature analysis is highly dependent on the expansion coefficient of the concrete and the boundary conditions. This is makes the model sensitive to changes in these parameters.

8.3 Further research

During investigating thermal effects on concrete bridges several questions have been raised that have been unable to answer within the frames of this project. These thoughts could be used as starting points for future projects.

This thesis only treats temperature profiles in portal frame bridges built in concrete. Interesting topics to follow for further analysis could be:

- How would a different temperature profile effect other types of bridges?
- Is temperature loads as significant on other bridge types?

When non-linear temperature profiles are applied, this thesis has shown that during cooling of the bridge deck, tensile stresses appear at top and bottom of the bridge cross section. This makes the topic of how large part of the tensile stresses will be taken by the reinforcement interesting.

- How large part of the tensile stresses from non-linear temperature should be taken by the reinforcement?

The topic of how large part of the tensile stresses the reinforcement will handle is strongly connected to the problem with cracks in concrete. Cracked concrete would probably induce lower stresses than a homogeneous concrete section. By how much can the stresses be reduced when cracking is allowed?

- The model is done with isotropic material, how would a close to surface behavior be described when cracks are allowed?

Chapter 5 shows a temperature simulation of the 2D case. A problem with this method is that the largest temperature effects occur far from boundaries and the temperature difference there is not representable for the full bridge. If a 3D simulation was done, a good average value could be computed and compared with the current building codes. The aim of this average value is to establish a simplified method that gives similar load effects as if the different temperature profiles from a 3D simulation is applied.

- Could temperature be simulated on a full 3D model and implemented to find a good average value of the temperature load effects?

Bibliography

- Banverket and Vägverket. *TK bro 2009*. Tomas Ramstedt, Mats Karlsson, 2009a.
- Banverket and Vägverket. *TR bro 2009*. Tomas Ramstedt, Mats Karlsson, 2009b.
- Boverket. *Boverkets författningssamling, EKS 1*. Lars Brask, 2008.
- F.A. Branco and P.A. Mendes. Thermal actions for concrete bridge design. *Journal of Structural Engineering*, 119(8):2313–2331, 1993.
- P-G. Burström. *Byggnadsmaterial - Uppbyggnad, tillverkning och egenskaper*. Studentlitteratur, 2007.
- Cementa. *Betonghandbok Material, utgåva 2*. Svensk Byggtjänst, 1997.
- CEN. *Eurocode SS-EN 1992-1-1*. European Committee for Standardization, Swedish Standards Institute, 2005.
- CEN. *Eurocode SS-EN 1991-1-5*. European Committee for Standardization, Swedish Standards Institute, 2009.
- CEN. *Eurocode SS-EN 1990*. European Committee for Standardization, Swedish Standards Institute, 2010.
- M. Emerson. *The Calculation of the Distribution of Temperature in Bridges*. Structures Department, Transport and Road Research Laboratory Crowthorne, Berkshire, 1973.
- F.P. Incropera, D.P. Dewitt, T.L. Bergman, and A.S. Lavine. *Fundamentals of Heat and Mass Transfer, (6nd edition)*. Wiley, Hoboken, 2007.
- H.G. Kwak and Filip C. Filippou. *Finite element analysis of reinforced concrete structures under monotonic loads*. University of California, Berkeley, 1990.
- O. Larsson. *Climate Related Thermal Actions for Reliable Design of Concrete Structures*. Lund University, Division of Structural Engineering, 2012.
- F. Leonhardt, G. Kolbe, and J. Peter. Temperaturunterschiede gefährden spannbetonbrücke. *Beton- und Stahlbetonbau*, (7):157–163, 1965.
- Gui-Rong Liu. *Finite element method : A practical course*. Butterworth-Heinemann, 2003.
- L.E. Nevander and B. Elmarsson. *Fukthandbok*. Svensk Byggtjänst, 2001.
- N. Saabye Ottosen and H. Petersson. *Introduction to the Finite Element Method*. Pearson Prentice Hall, 1992.
- N. Saabye Ottosen and Matti Ristinmaa. *The mechanics of constitutive modeling*. Elsevier, 2005.
- ScanscotTechnology. *Brigade Standard Theory manual v4.2*. ScanscotTechnology, 2010.
- Dassault Systèmes. *Abaqus 6.11 Documentation*. Dassault Systèmes, 2011.
- J.L Threlkeld. *Thermal Environmental Engineering (2nd edition)*. Prentice Hall Inc, Engelwood Cliffs, United States, 1970.
- Trafikverket. *Trafikverkets författningssamling*. Trafikverket, 2011a.

Trafikverket. *TRVK Bro 11*. Trafikverket, 2011b.

Trafikverket. *TRVR Bro 11*. Trafikverket, 2011c.

Vägverket. *Bro 2004*. Robert Ronnebrant, 2004.

Index

- Absorption, 31
- Absorptivity, 8
- Admixtures, 14
- Aggregate, 14
- Approach 1, 25, 43–47, 49, 50
- Approach 2, 25, 43–47, 49, 50

- Bridge 829 Katrineholm, 29, 39

- Cement, 14
- Concrete, 17
- Conductivity, 31
- Constitutive relationship, 17, 40
- Convection, 9
- Convection heat transfer coefficient, 9
- Crack width, 16, 26, 53, 56
- Cracks, 16, 53

- Dehydration, 16
- Density, 11, 14, 31, 40

- Effective bridge temperature, 23
- Emissivity, 9, 31
- Eurocode, 21, 23, 25, 26, 32, 34, 36, 38, 43–47, 49, 50

- FE analysis, 17, 30, 39
- Fourier's law, 11

- Hooke's law, 17

- Integration points, 19, 39
- Iteration scheme, 55, 57

- Linear temperature difference, 10, 23, 24, 33, 35
- Load combination, 22, 58, 59
- Long wave heat radiation, 8, 31

- Method A, 53
- Method B, 56
- Micro cracks, 16

- Non-linear temperature component, 10, 23, 24, 33, 35

- Partial coefficients, 21
- Poisson's ratio, 40
- Portal frame bridge, 29

- Reinforcement bars, 14, 54, 58, 59

- Safety class, 21

- Scanscot BrigadePlus, 30, 39, 42
- Scanscot BrigadeStandard, 42
- Serviceability Limit State - Characteristic, 23, 58, 59
- Serviceability Limit State - Quasi-permanent, 23, 58, 59
- Shell elements, 18, 30, 39
- Solar radiation, 7, 31
- Specific heat capacity, 11, 14, 31
- Strong formulation, 11
- Surface cracks, 16

- Temperature points, 19, 43
- Tensile, 17, 50, 53
- Thermal conductivity, 11, 14
- Thermal expansion coefficient, 11, 15, 40
- TRVK Bro, 22, 26
- TRVR Bro, 27

- Ultimate Limit State, 22, 58, 59
- Uniform temperature, 10, 23, 33, 35

- Water, 14

- Young's modulus, 18, 40

Appendix A

Climate Model

A.1 Climate model

A.1.1 50mm paving

A.1.1.1 Heating load case

Results are from the simulation with 50mm paving of asphalt. In figure A.1 the temperature distribution for the largest positive gradient is shown.

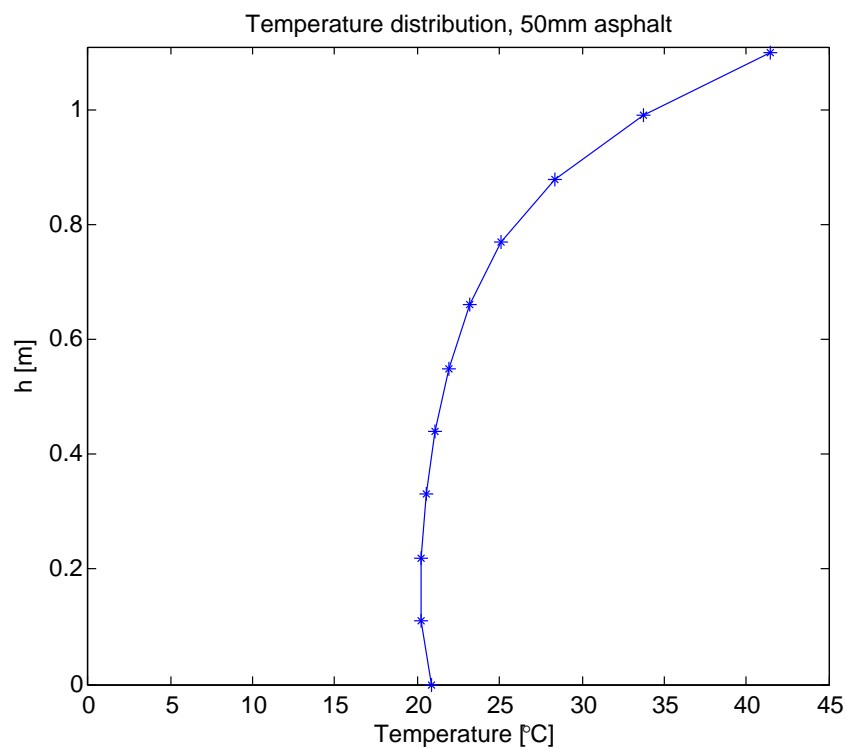


Figure A.1: Temperature distribution for largest positive gradient with 50mm paving, heating load case

The temperature distribution in figure A.1 is divided into its uniform, linear and non linear components and shown in figure A.2.

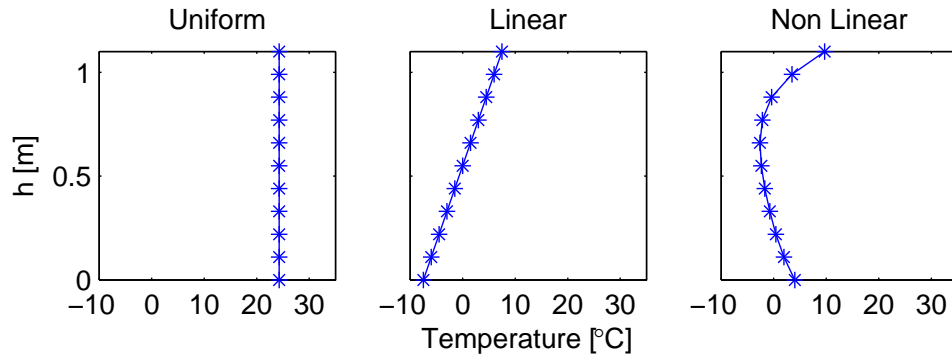


Figure A.2: Temperature distribution divided into its components with 50mm paving, heating load case

The annex in Eurocode 1991-1-5 [CEN, 2009] provide temperature distributions for different thickness of paving. The uniform component is not affected by paving thickness but only the non-uniform. As for the case with 100mm paving, figure A.3 compares the results from our simulation with the distribution according to Eurocode.

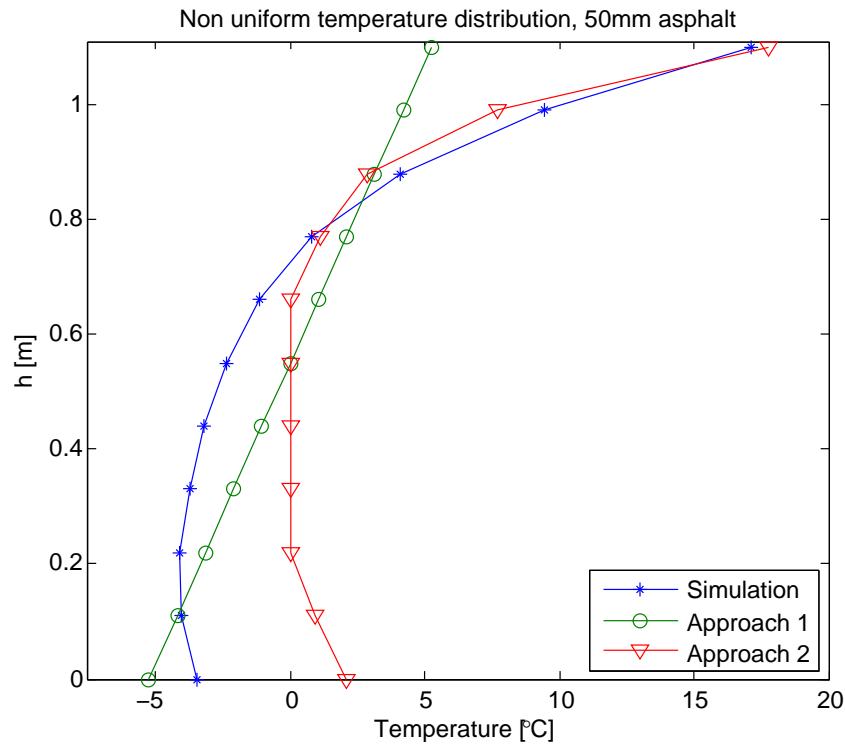


Figure A.3: Linear and non linear temperature components compared to values from Eurocode 1991-1-5 [CEN, 2009] with 50mm paving, heating load case

A.1.1.2 Cooling load case

Results are from the simulation with 50mm paving of asphalt. In figure A.4 the temperature distribution for the largest negative gradient is shown.

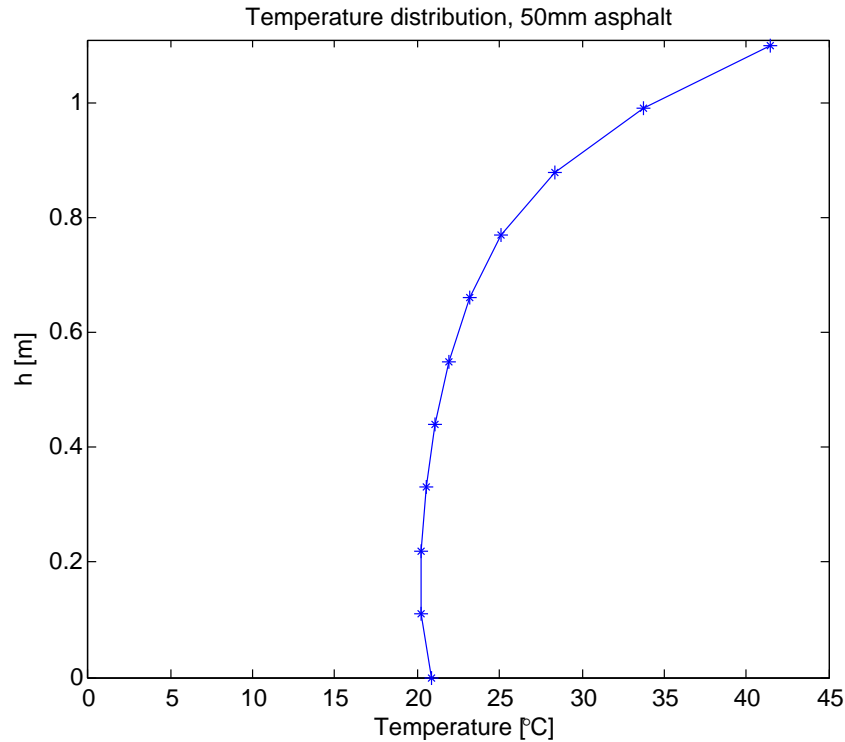


Figure A.4: Temperature distribution for largest positive gradient with 50mm paving, cooling load case

The temperature distribution in figure A.4 is divided into its uniform, linear and non linear components and shown in figure A.5.

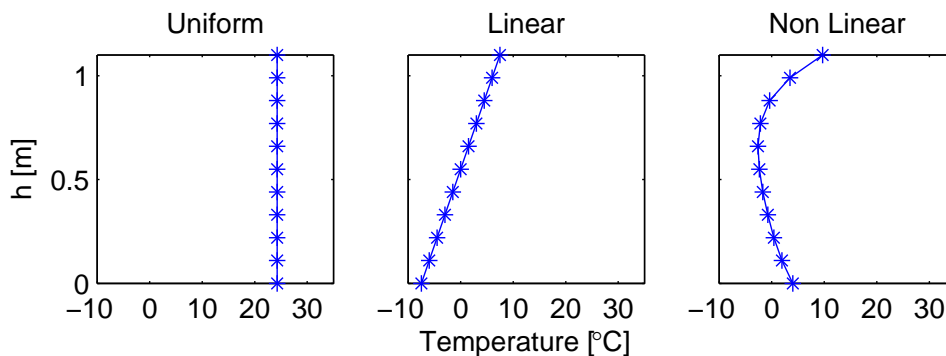


Figure A.5: Temperature distribution divided into its components with 50mm paving, cooling load case

The annex in Eurocode 1991-1-5 [CEN, 2009] provides temperature distributions for different thickness of paving. The uniform component is not affected by paving thickness but only the non uniform. As for the case with 100mm paving, figure A.6 compares the results from our simulation with the distribution according to Eurocode.

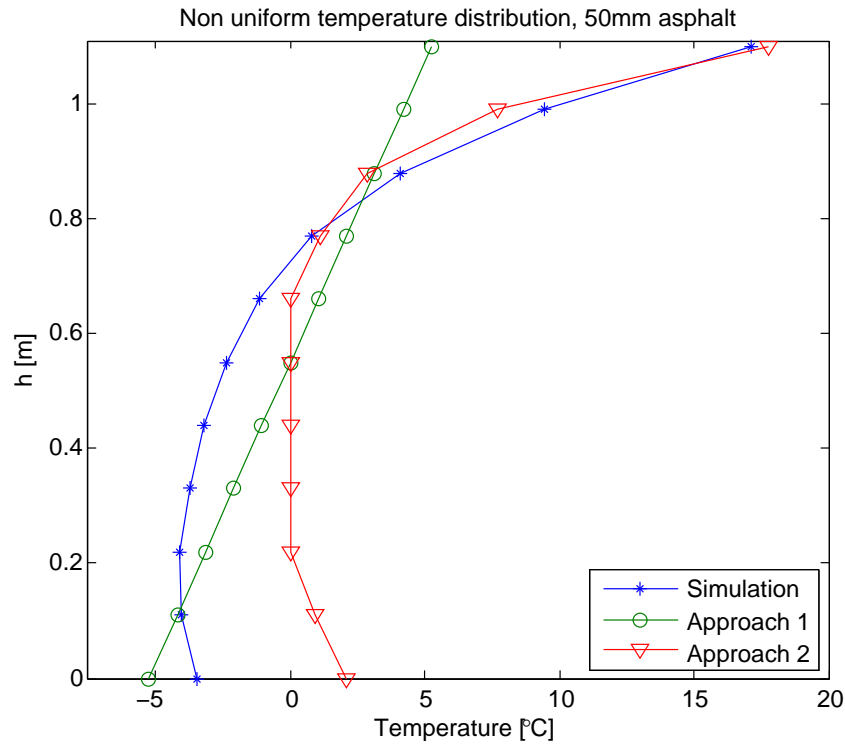


Figure A.6: Linear and non linear temperature components compared to values from Eurocode 1991-1-5 [CEN, 2009] with 50mm paving, cooling load case

A.1.1.3 Comments

As for the case with 100mm paving, figure A.6 visualizes certain similarities between the FE simulation and the approach 2 according to Eurocode 1991-1-5 [CEN, 2009]. In this case with 50mm paving, approach 2 is a more realistic choice of modeling than approach 1 according to the FE simulation. The gradient is as expected larger with thinner paving, other than that results are comparable with the case of 100mm paving.

A.1.2 100mm paving

As described in chapter 5 the largest non linear part is presented at the cooling load case. The results from the largest negative gradient is presented here.

The distribution for the largest negative gradient is shown in figure A.7.

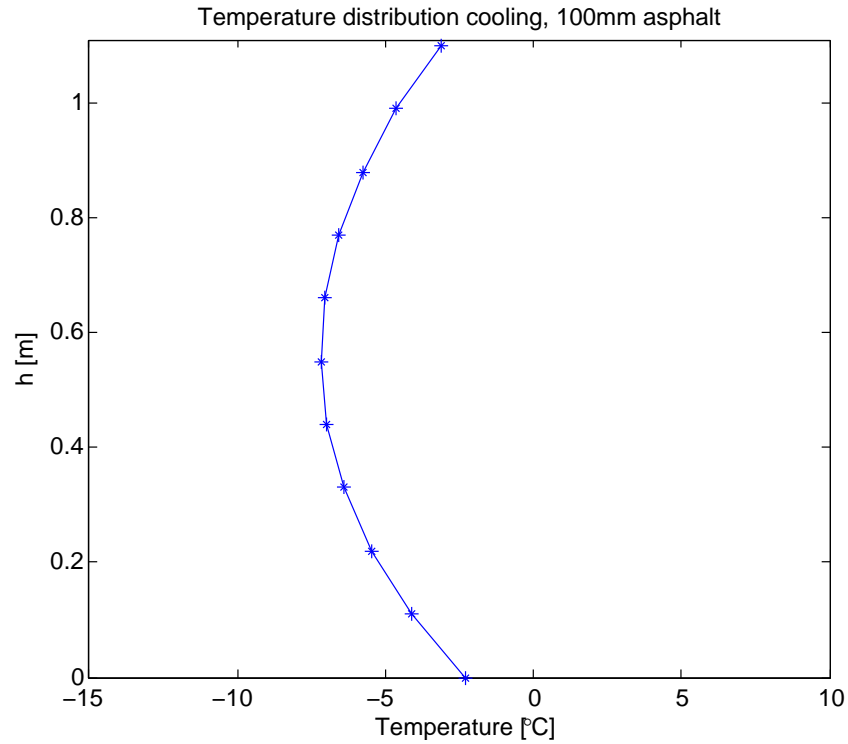


Figure A.7: Largest negative gradient for cooling load case

Appendix B

Case Study

B.1 Validation of model

Section 6.1.2 refers to this appendix for additional plots showing the comparison of two different models for comparison. Following plots shows this validation and the investigated lines 1,2 and 3 is according to figure 6.6.

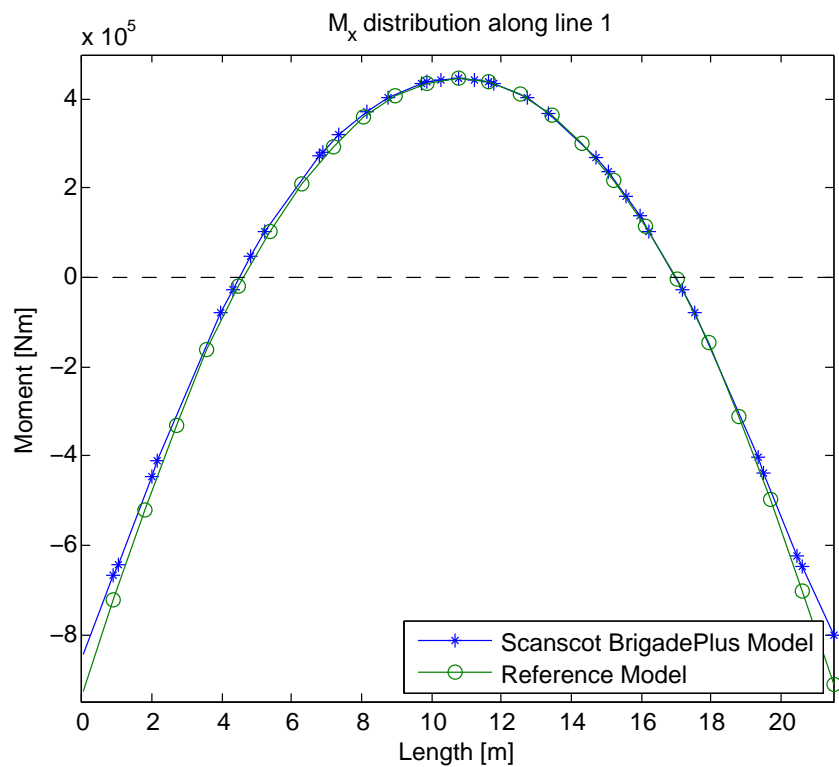


Figure B.1: Comparison between M_x along line 1 with FE-analysis of bridge 829 done with Scanscot BrigadePlus and the reference model modeled in Scanscot BrigadeStandard

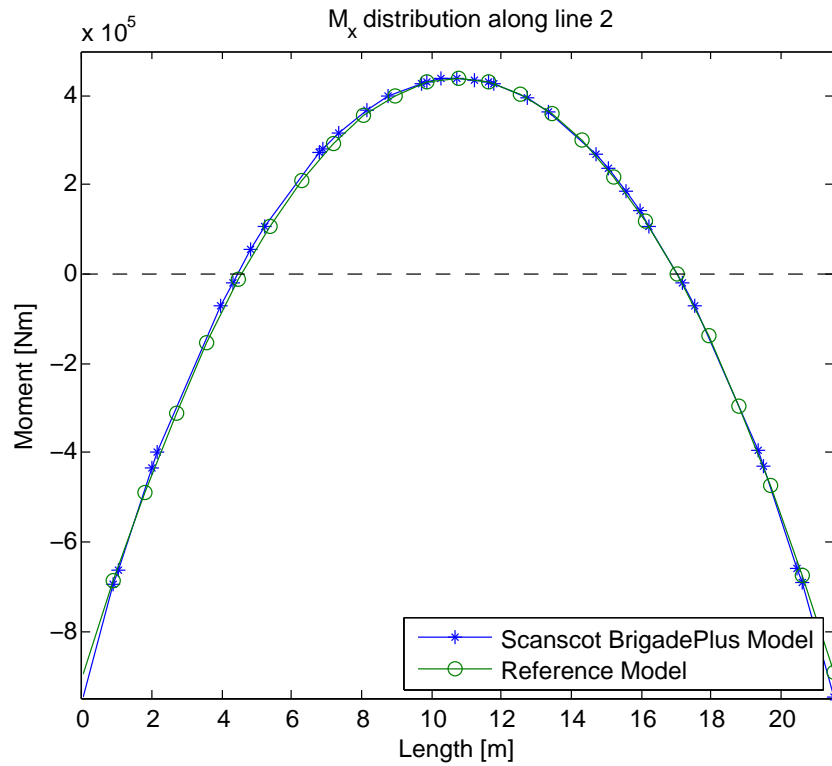


Figure B.2: Comparison between M_x along line 2 with FE-analysis of bridge 829 done with Scanscot BrigadePlus and the reference model modeled in Scanscot BrigadeStandard

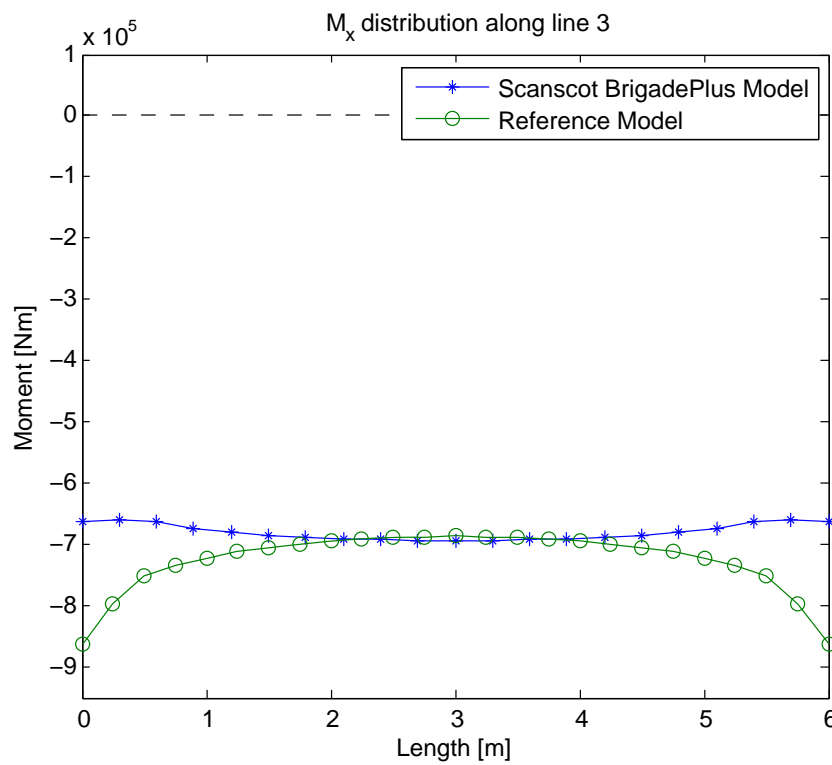


Figure B.3: Comparison between M_x along line 3 with FE-analysis of bridge 829 done with Scanscot BrigadePlus and the reference model modeled in Scanscot BrigadeStandard

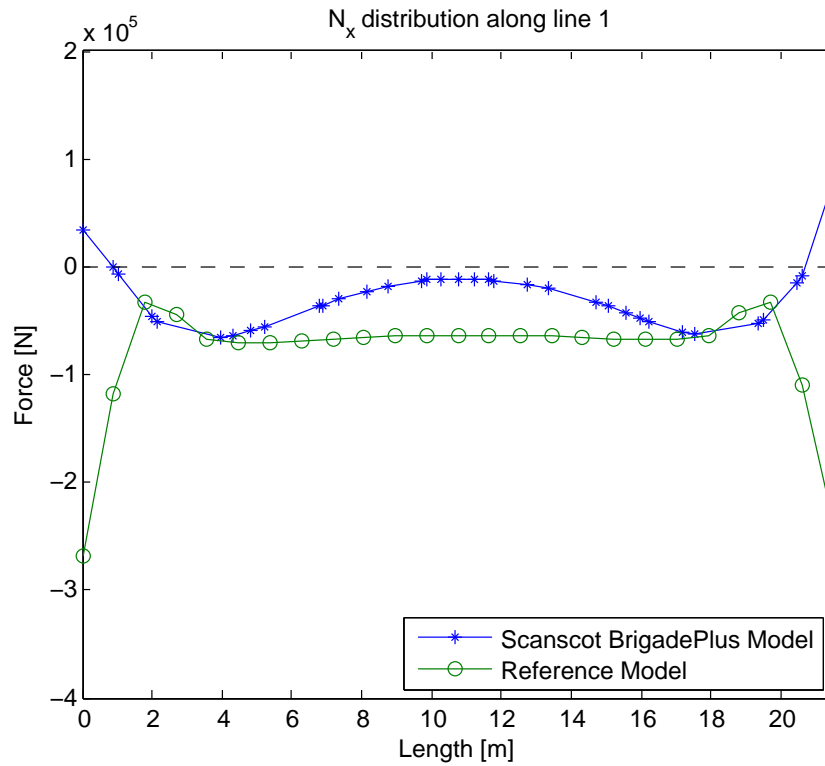


Figure B.4: Comparison between N_x along line 1 with FE-analysis of bridge 829 done with Scanscot BrigadePlus and the reference model modeled in Scanscot BrigadeStandard

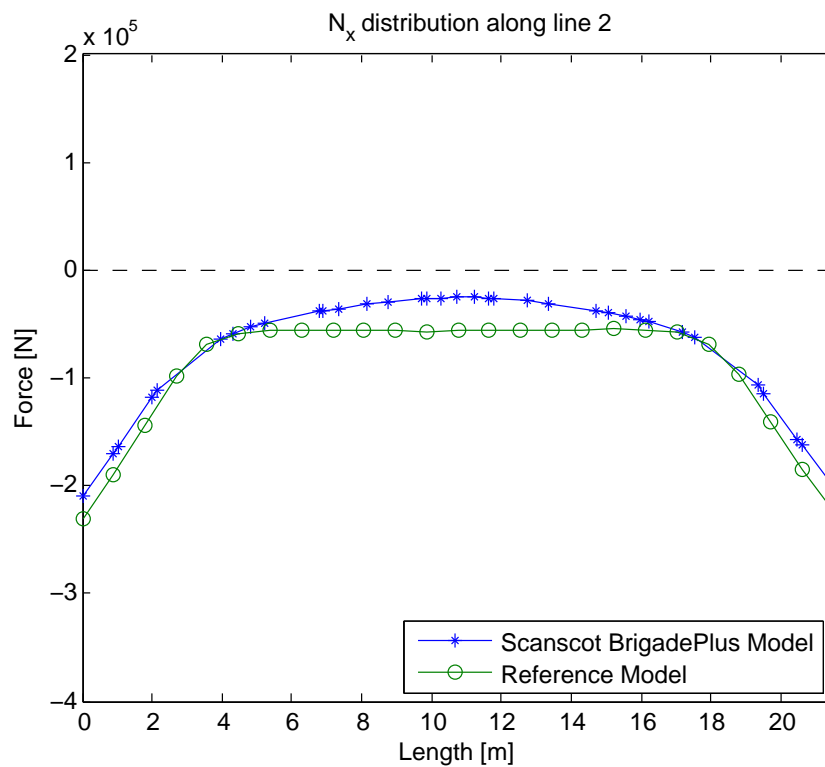


Figure B.5: Comparison between N_x along line 2 with FE-analysis of bridge 829 done with Scanscot BrigadePlus and the reference model modeled in Scanscot BrigadeStandard

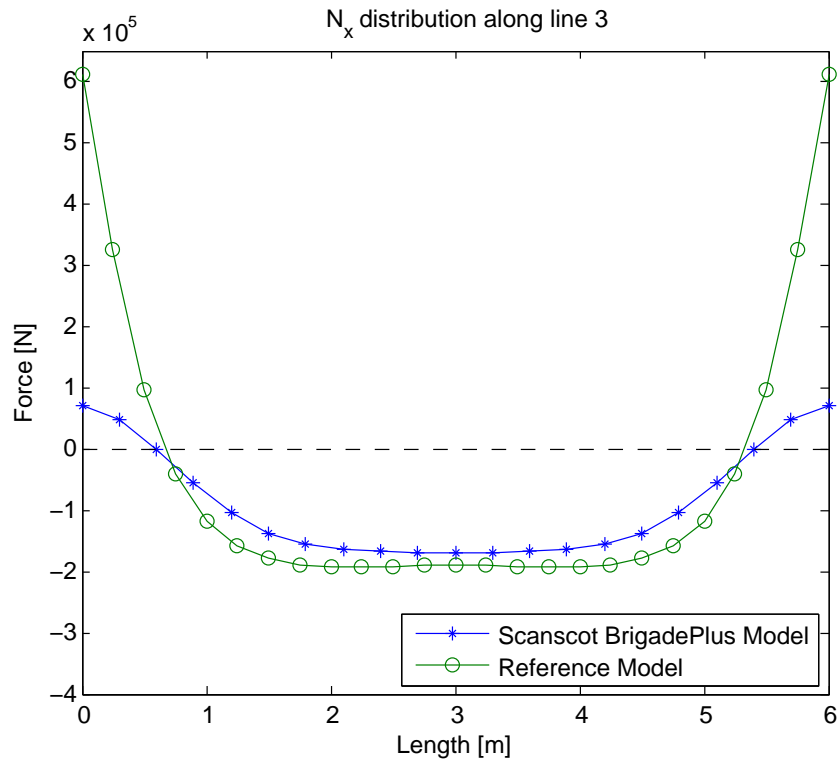


Figure B.6: Comparison between N_x along line 3 with FE-analysis of bridge 829 done with Scanscot BrigadePlus and the reference model modeled in Scanscot BrigadeStandard

B.2 Load effects from FE analysis

Additional plot showing section moments and section forces in addition to the plots in chapter 6.2.1 and 6.2.2

B.2.1 Section Moments

Additional plots referred from chapter 6.2.1. The investigated lines 1,2 and 3 is according to figure 6.6.

B.2.1.1 Heating of bridge deck

Following plots represents the section forces M_x and M_y as for the case of heating of the bridge deck.

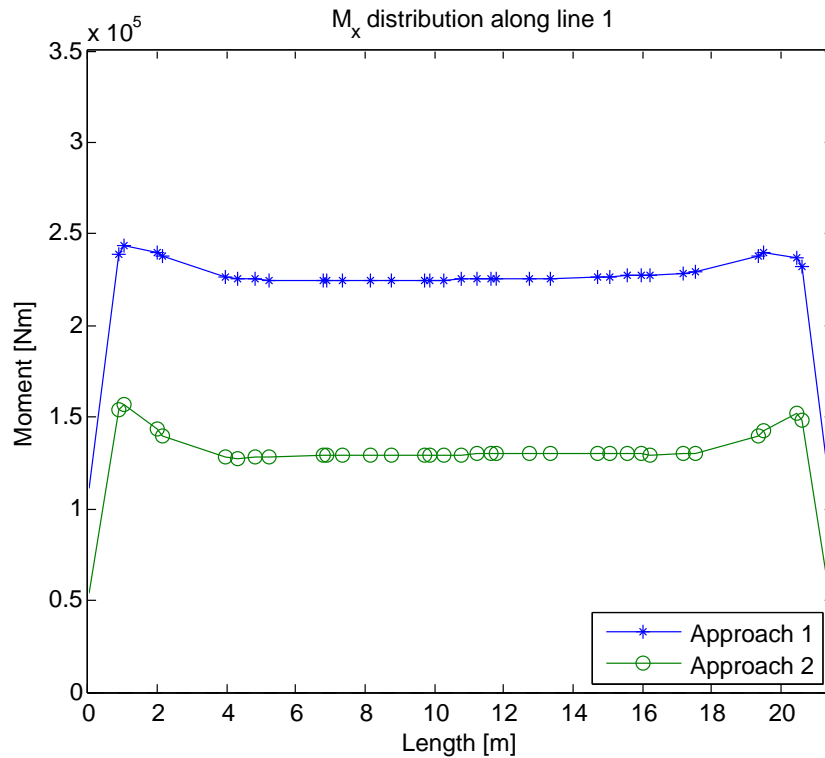


Figure B.7: Moment distribution along line 1 with heating of the concrete bridge deck

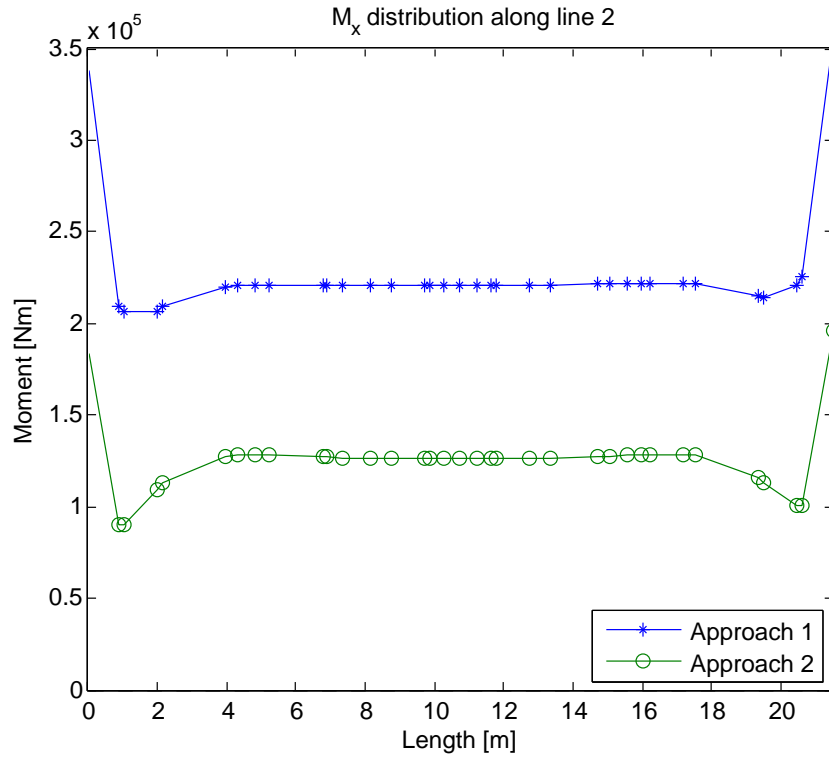


Figure B.8: Moment distribution along line 2 with heating of the concrete bridge deck

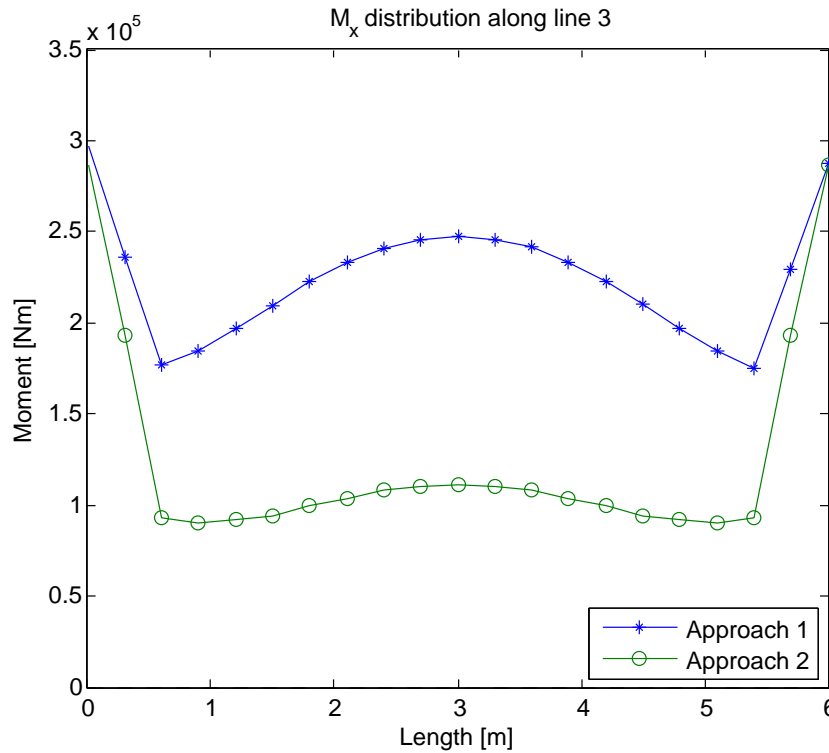


Figure B.9: Moment distribution along line 3 with heating of the concrete bridge deck

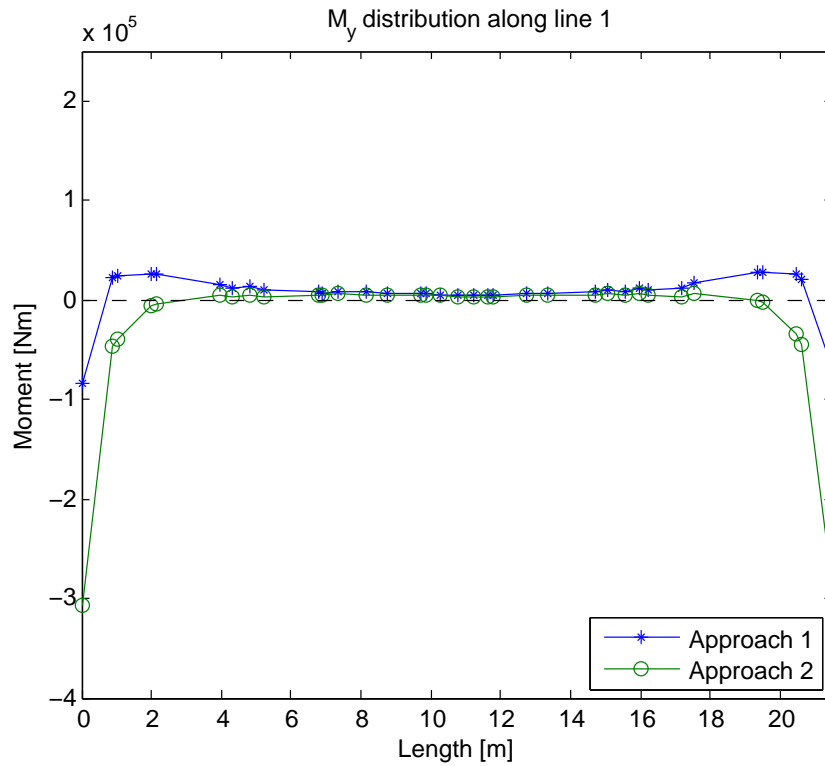


Figure B.10: Moment M_y distribution along line 1 with heating of the concrete bridge deck

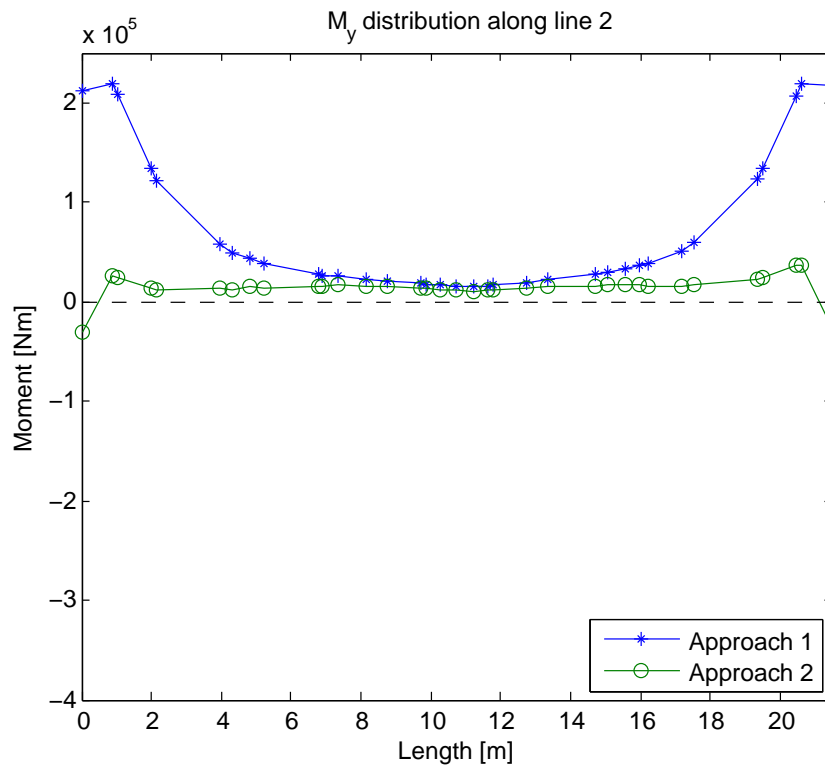


Figure B.11: Moment M_y distribution along line 2 with heating of the concrete bridge deck

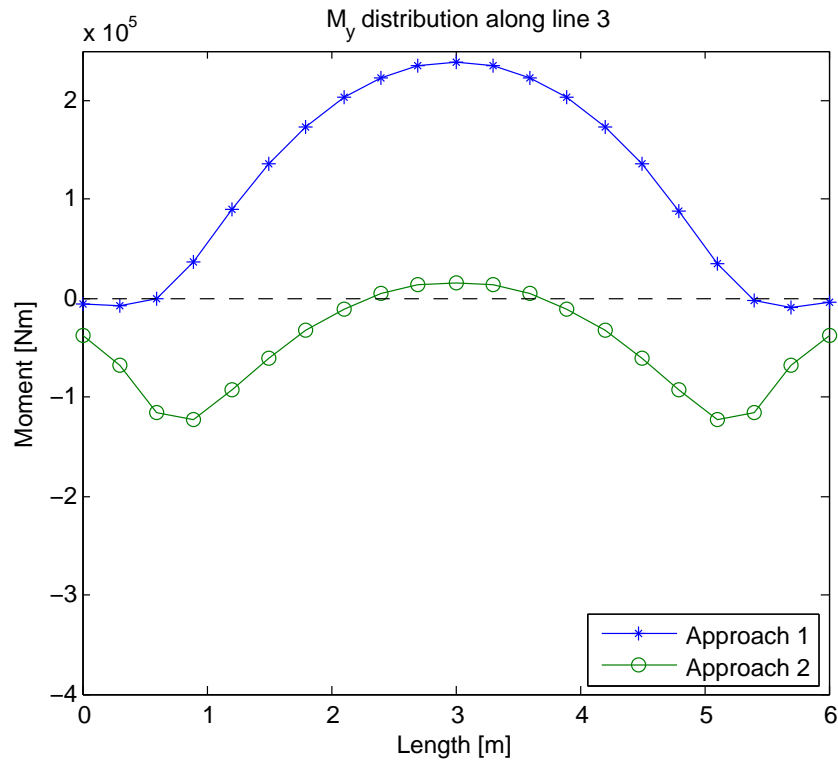


Figure B.12: Moment M_y distribution along line 3 with heating of the concrete bridge deck

B.2.1.2 Cooling of bridge deck

Following plots represents the section forces M_x and M_y as for the case of heating of the bridge deck.

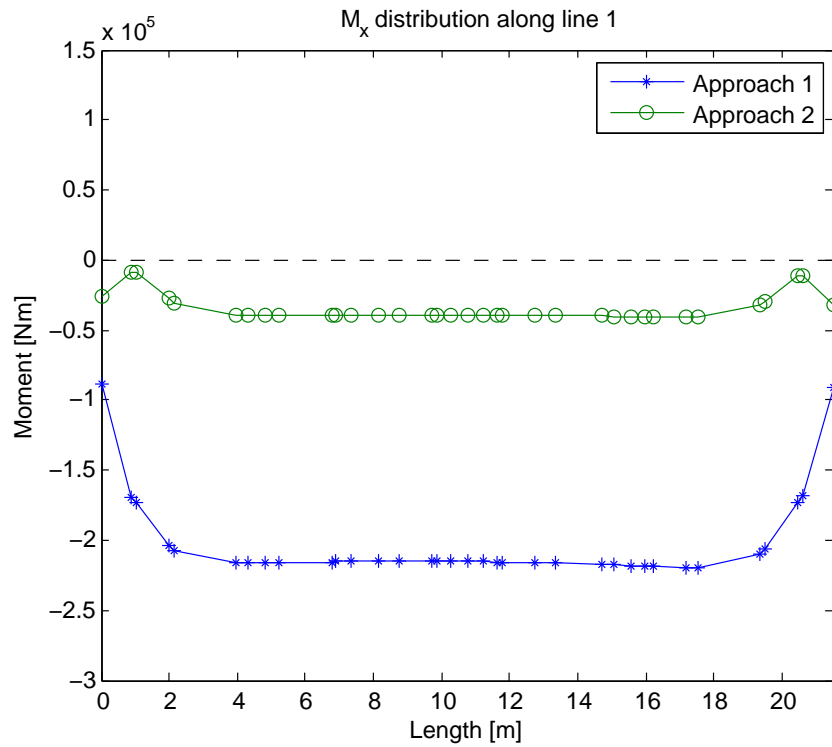


Figure B.13: Moment distribution along line 1 with cooling of the concrete bridge deck

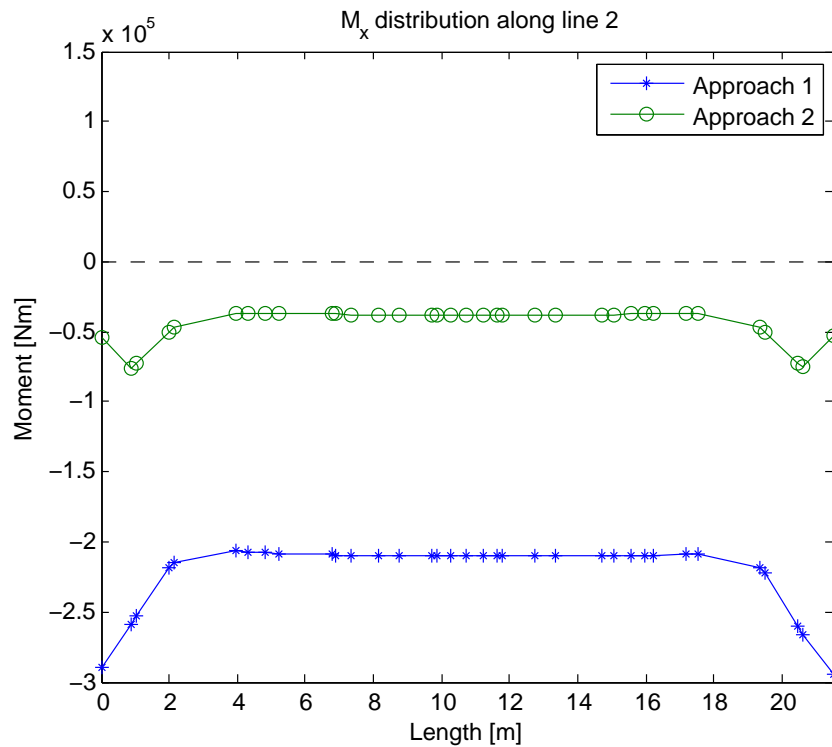


Figure B.14: Moment distribution along line 1 with cooling of the concrete bridge deck

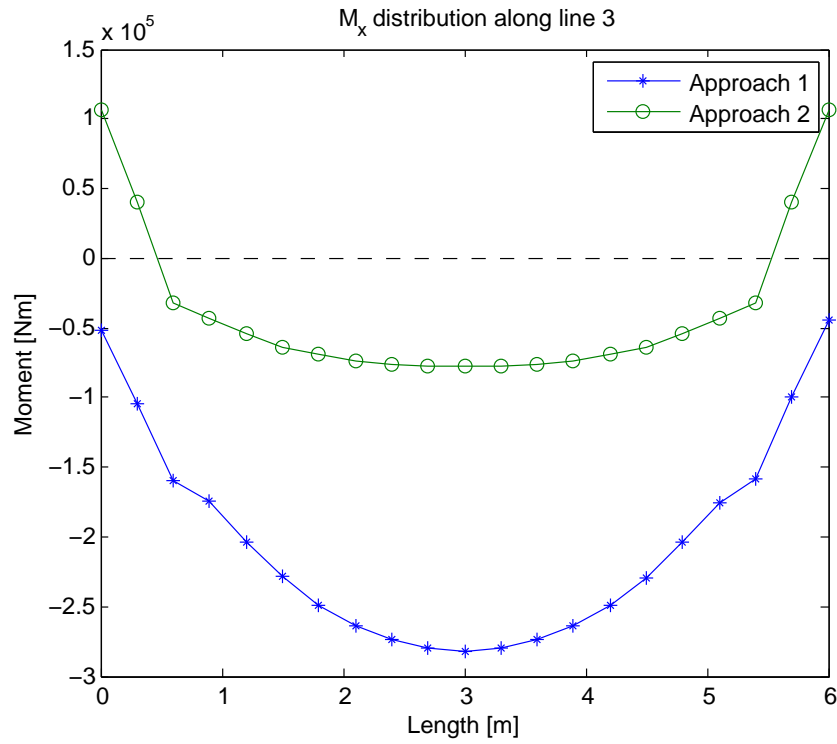


Figure B.15: Moment distribution along line 3 with cooling of the concrete bridge deck

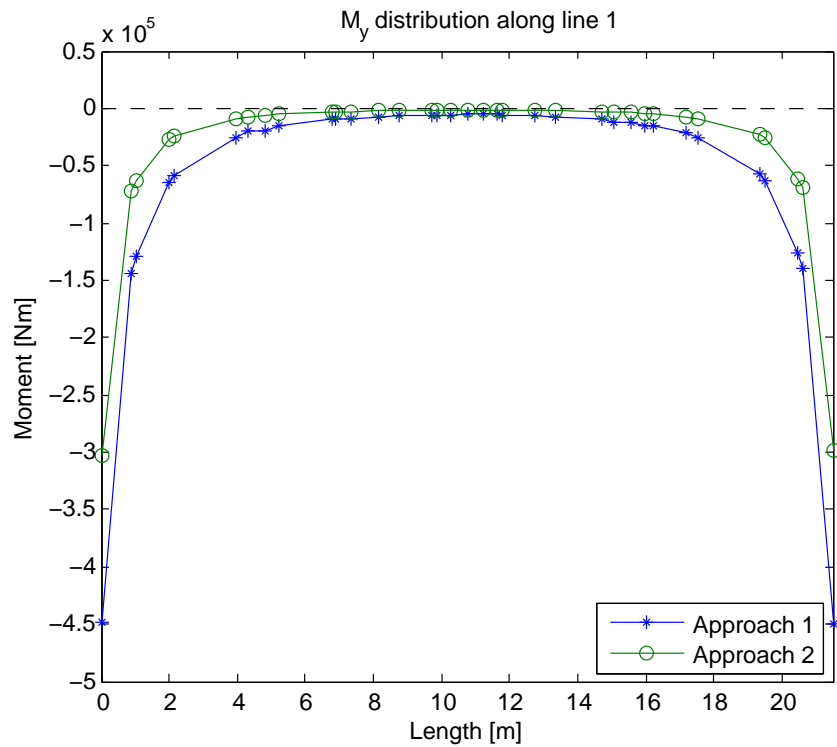


Figure B.16: Moment M_y distribution along line 1 with cooling of the concrete bridge deck

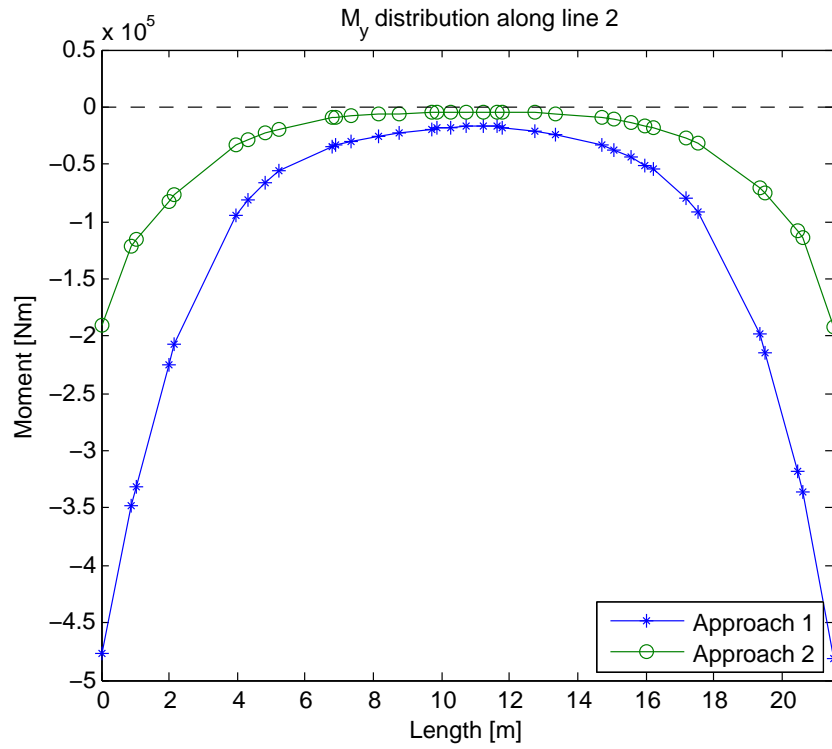


Figure B.17: Moment M_y distribution along line 2 with cooling of the concrete bridge deck

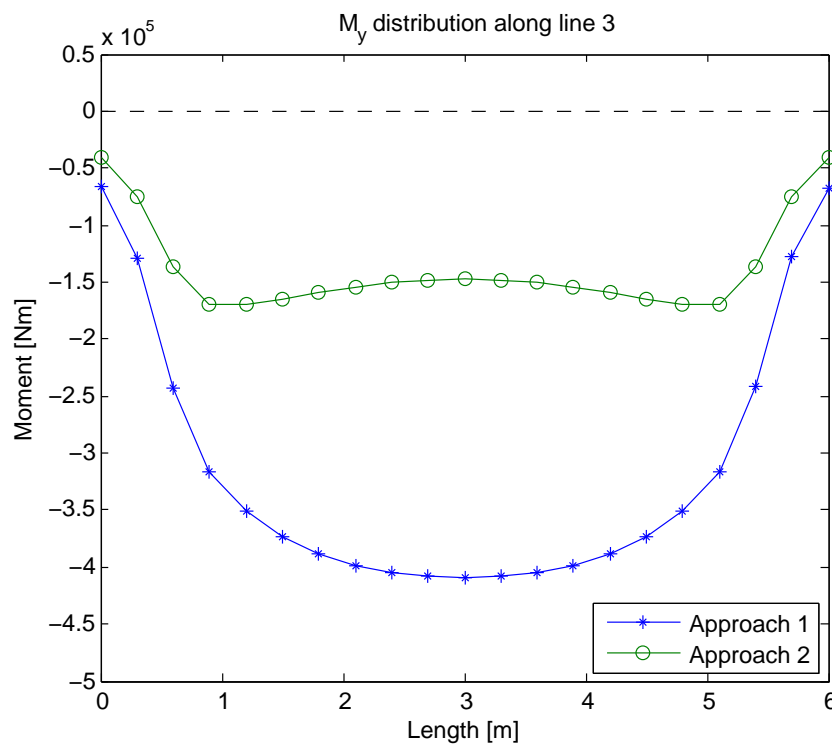


Figure B.18: Moment M_y distribution along line 3 with cooling of the concrete bridge deck

B.2.2 Section forces

Additional plots referred from chapter 6.2.2. The influence lines 1,2 and 3 is according to figure 6.6.

B.2.2.1 Heating of bridge deck

Following plots represents the section forces N_x , N_y , V_{xy} and V_{ys} as for the case of cooling of the bridge deck.

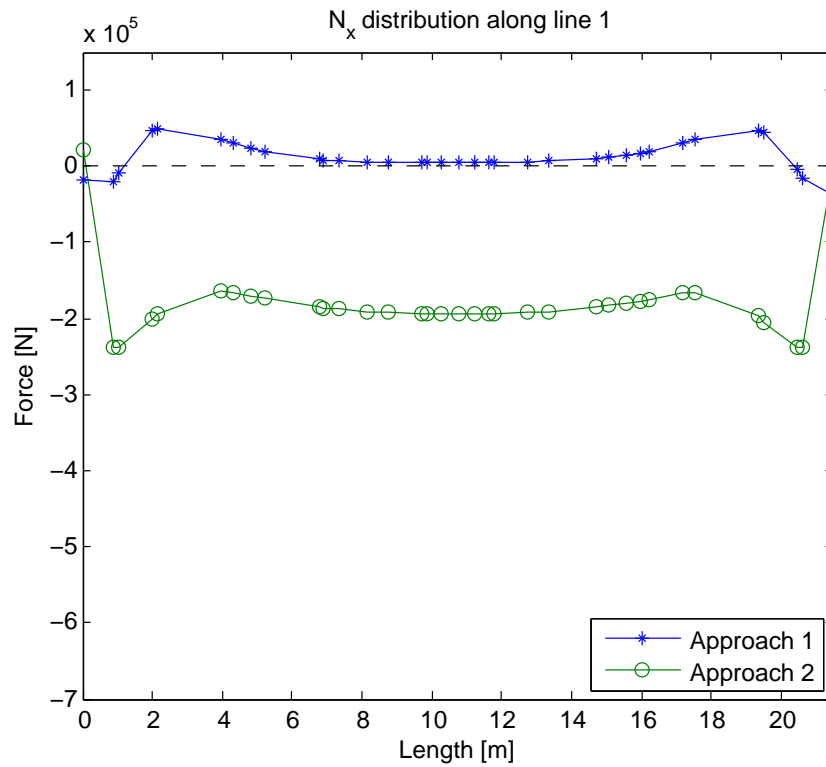


Figure B.19: Section forces N_x along line 1 with heating of the concrete bridge deck

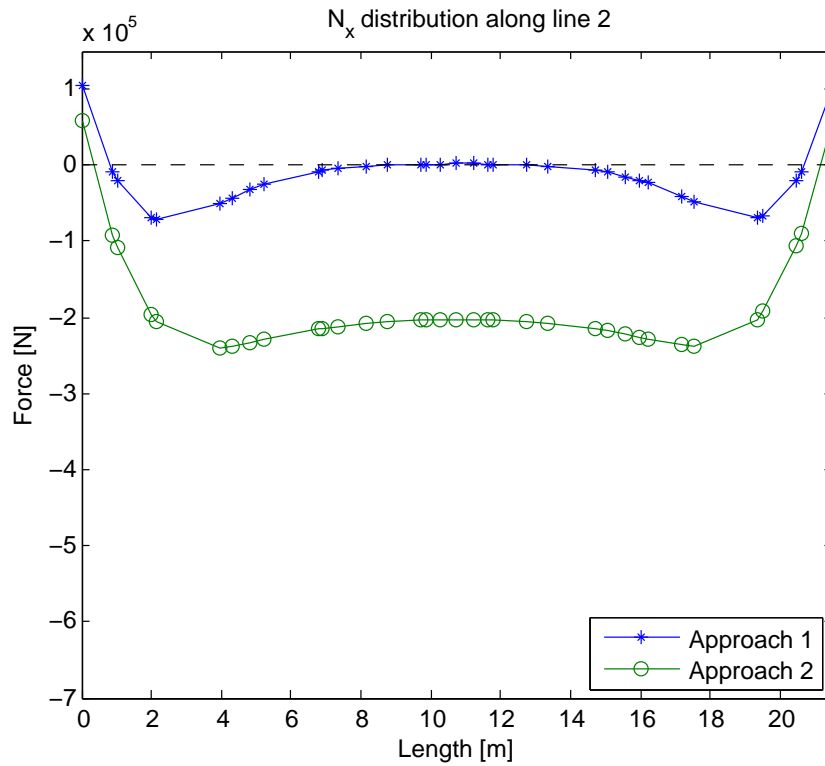


Figure B.20: Section forces N_x along line 2 with heating of the concrete bridge deck

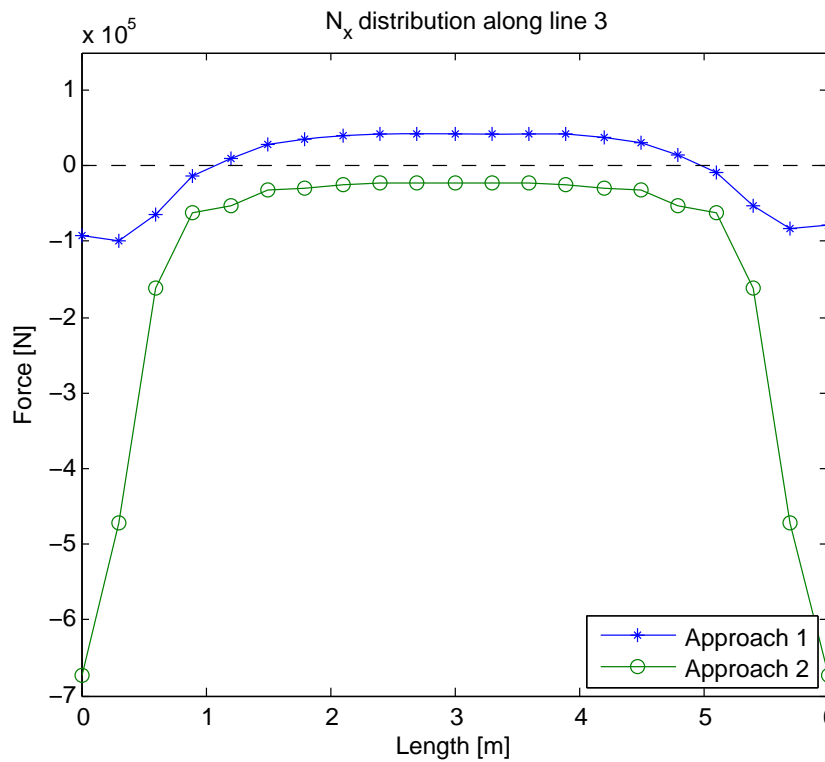


Figure B.21: Section forces N_x along line 3 with heating of the concrete bridge deck

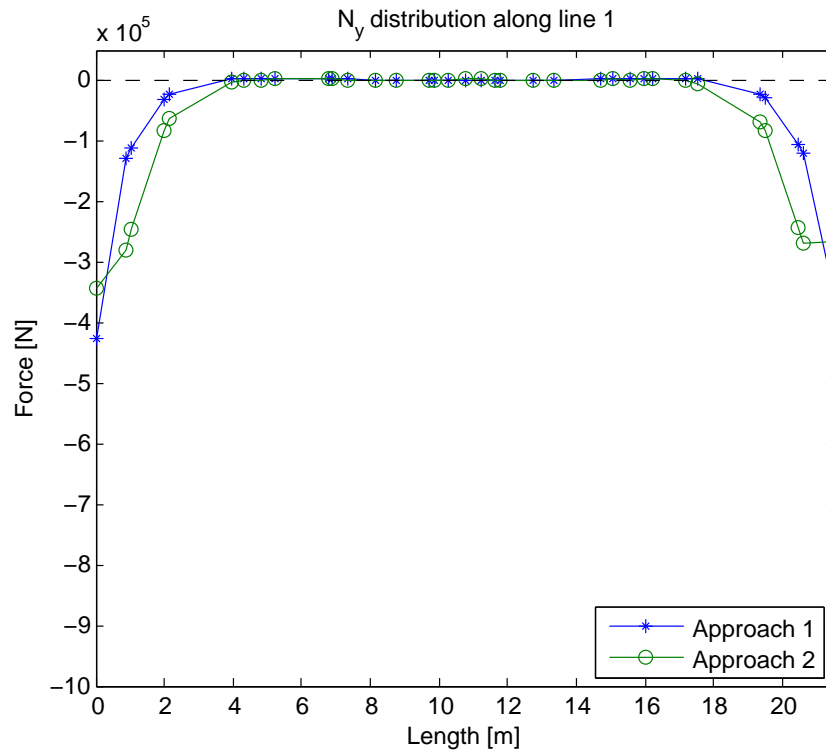


Figure B.22: Section forces N_y along line 1 with heating of the concrete bridge deck

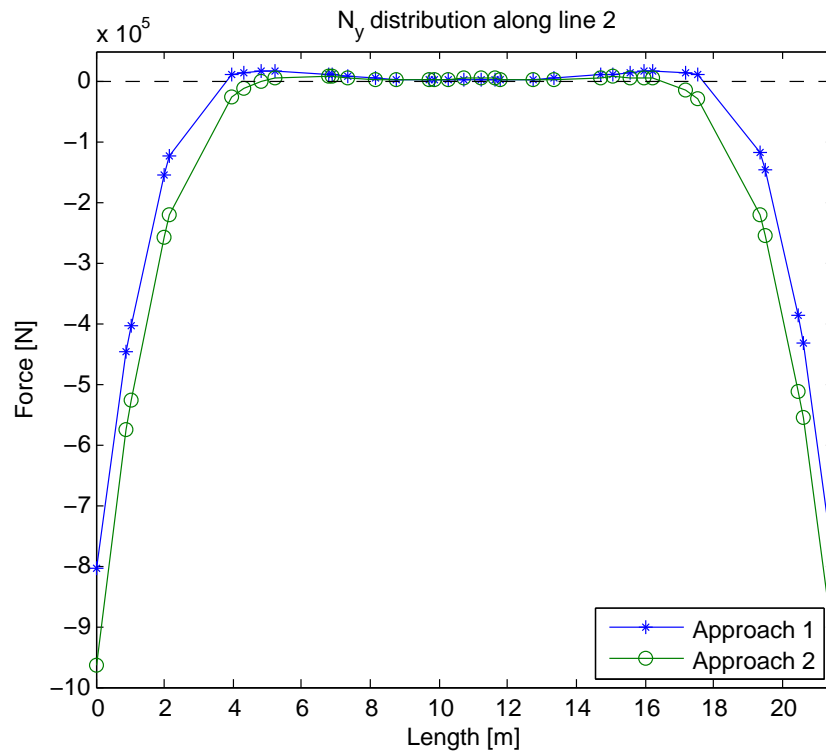


Figure B.23: Section forces N_y along line 2 with heating of the concrete bridge deck

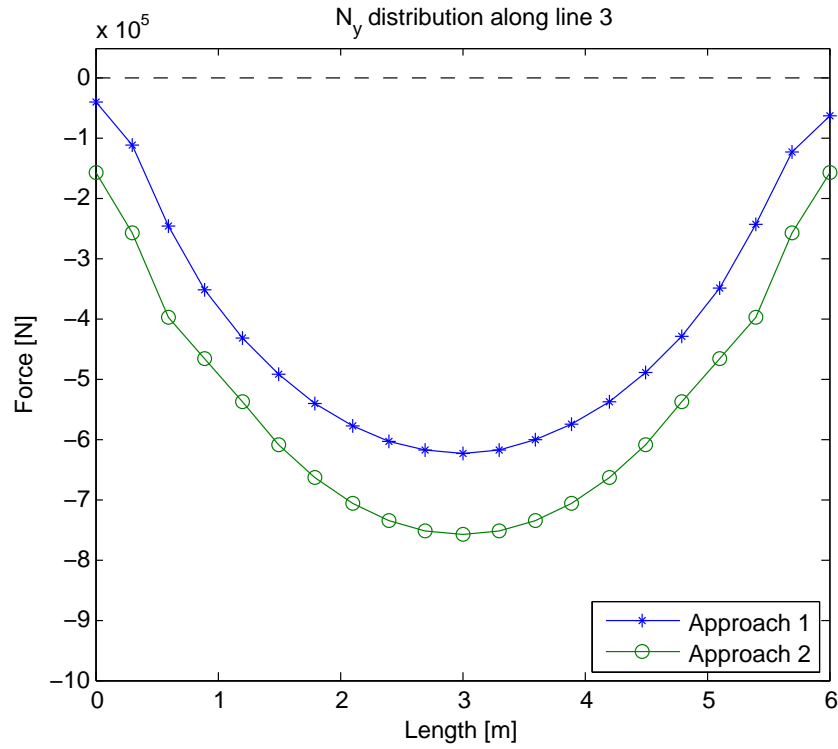


Figure B.24: Section forces N_y along line 3 with heating of the concrete bridge deck

B.2.2.2 Cooling of bridge deck

Following plots represents the section forces N_x , N_y , V_{xy} and V_{ys} as for the case of cooling of the bridge deck.

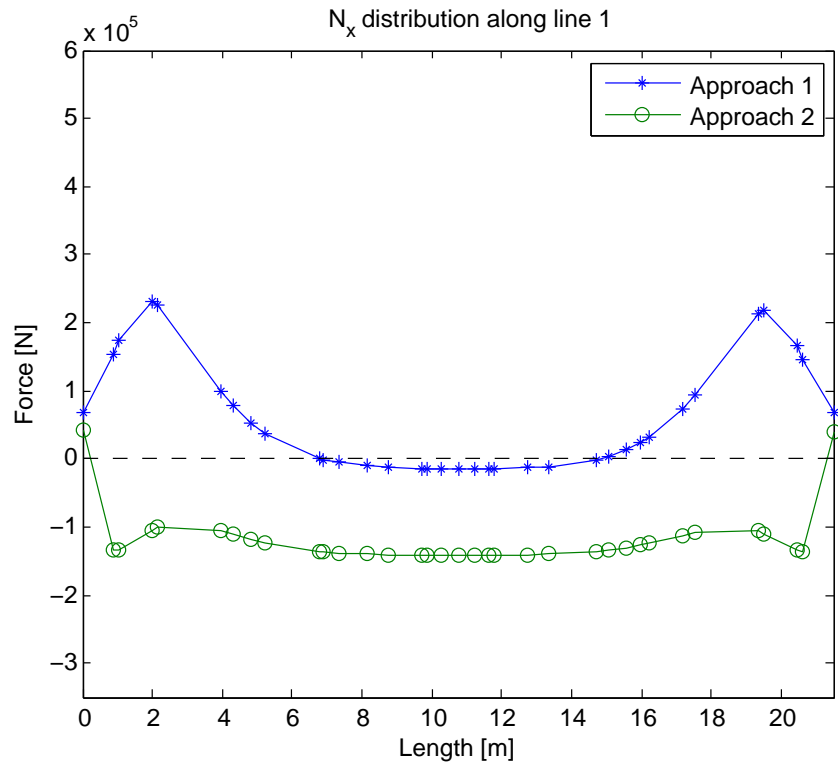


Figure B.25: Section forces N_x along line 1 with cooling of the concrete bridge deck

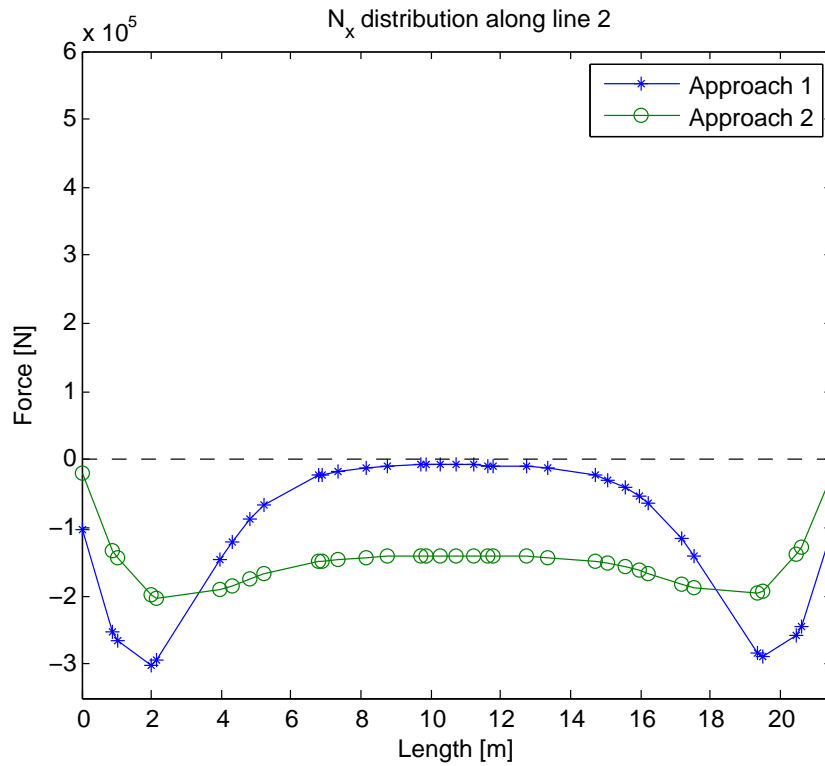


Figure B.26: Section forces N_x along line 2 with cooling of the concrete bridge deck

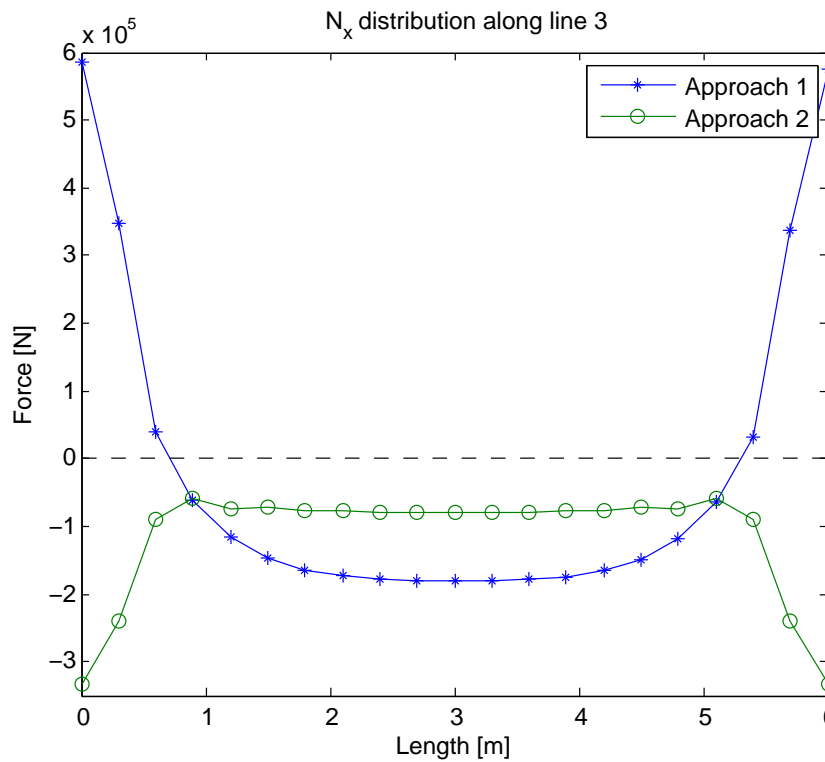


Figure B.27: Section forces N_x along line 3 with cooling of the concrete bridge deck

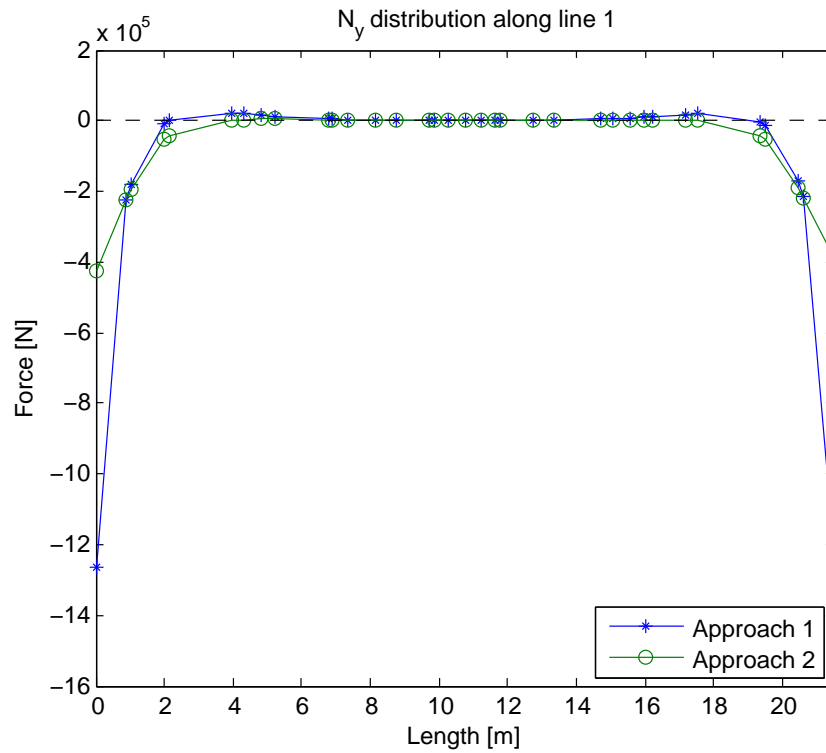


Figure B.28: Section forces N_y along line 1 with cooling of the concrete bridge deck

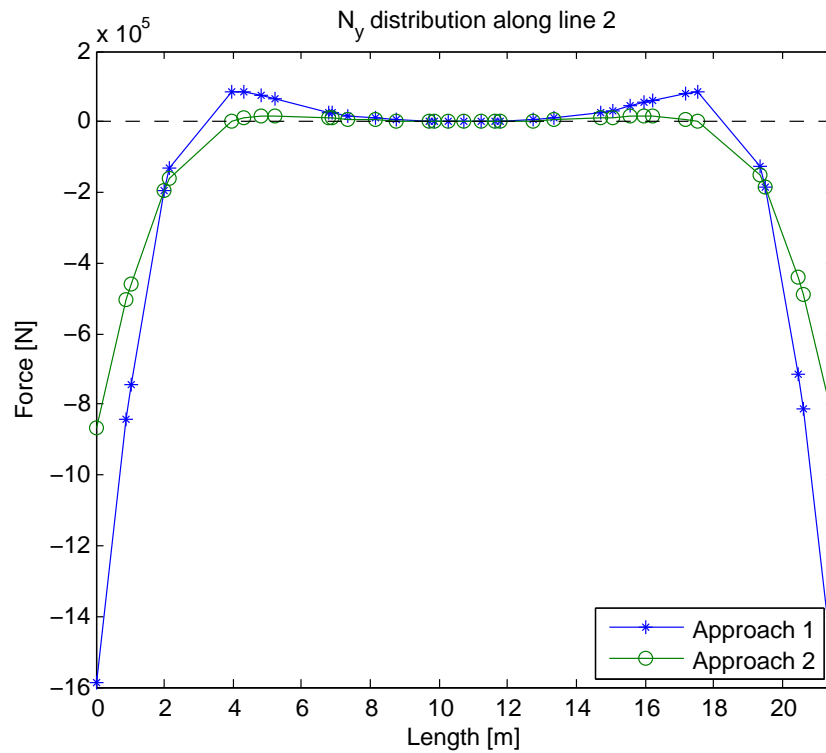


Figure B.29: Section forces N_y along line 2 with cooling of the concrete bridge deck

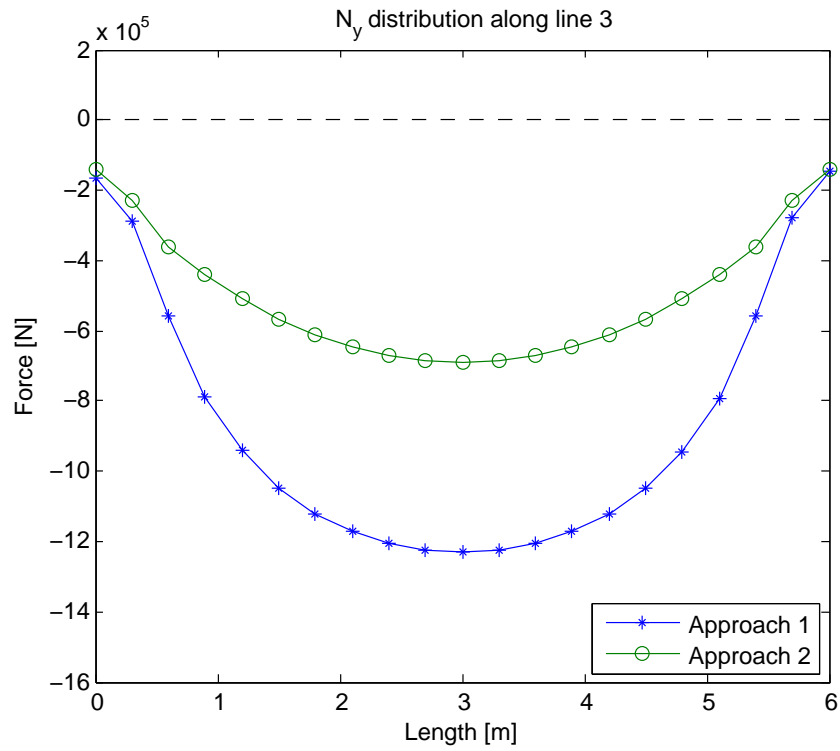


Figure B.30: Section forces N_y along line 3 with cooling of the concrete bridge deck

B.2.3 Results from climate simulation

Additional plots referred from chapter 6.2.3. The influence lines 1,2 and 3 is according to figure 6.6.

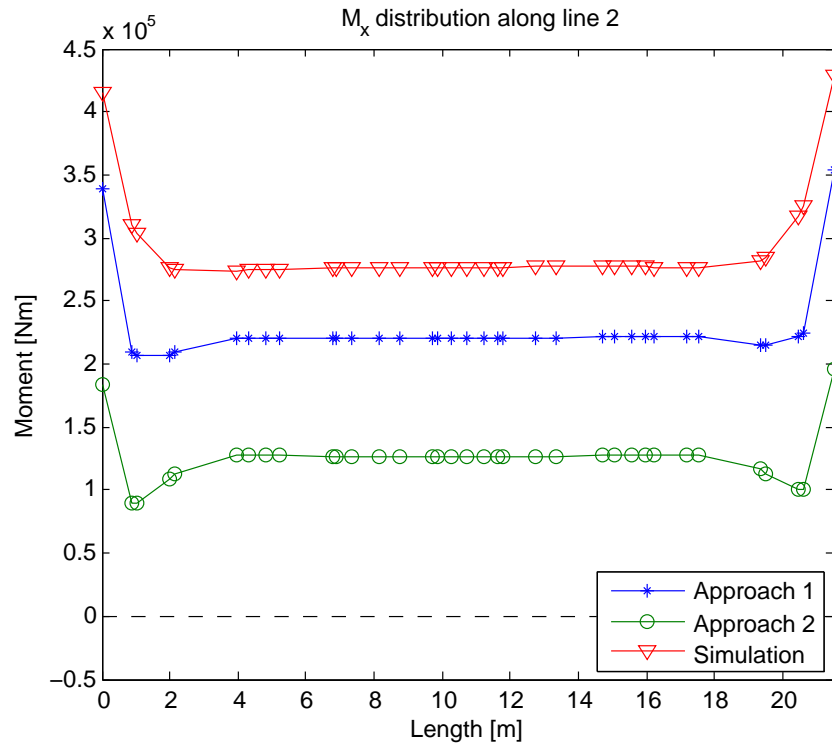


Figure B.31: Section moment M_x along line 2 with heating of the concrete bridge deck

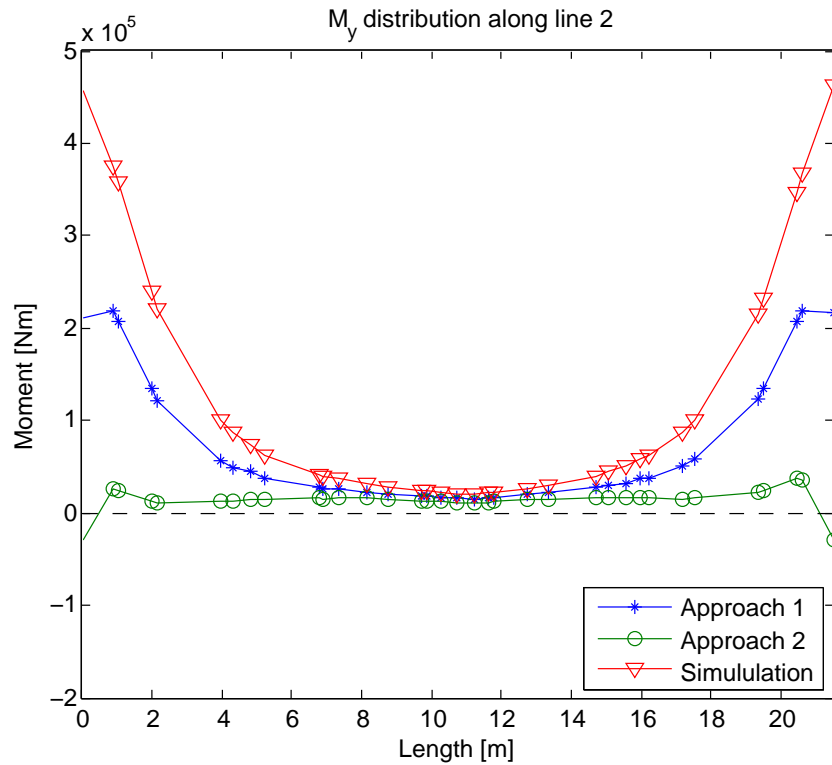


Figure B.32: Section moment M_y along line 2 with heating of the concrete bridge deck

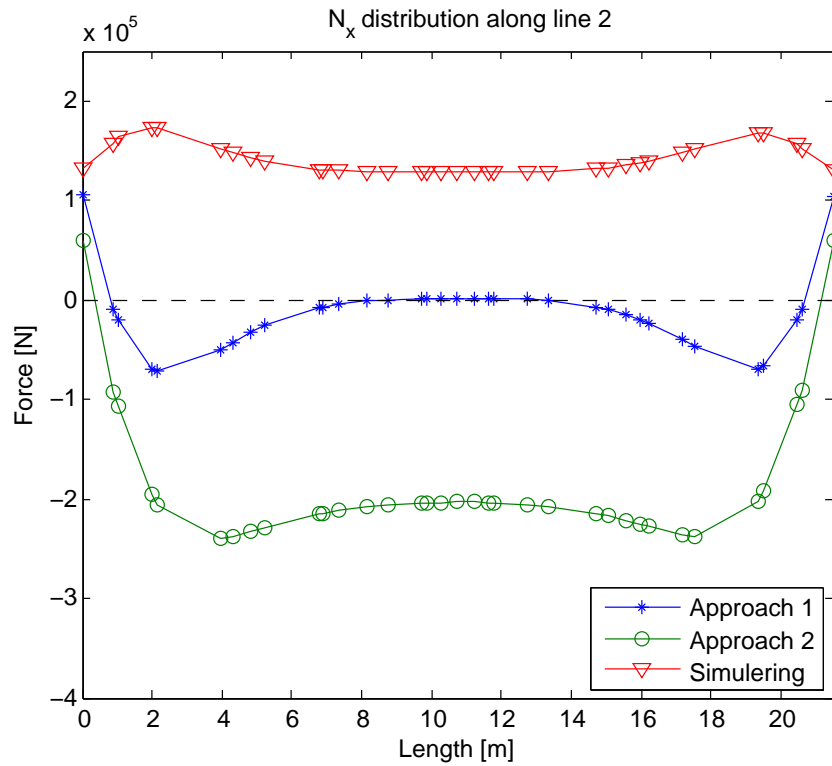


Figure B.33: Section force N_x along line 2 with heating of the concrete bridge deck

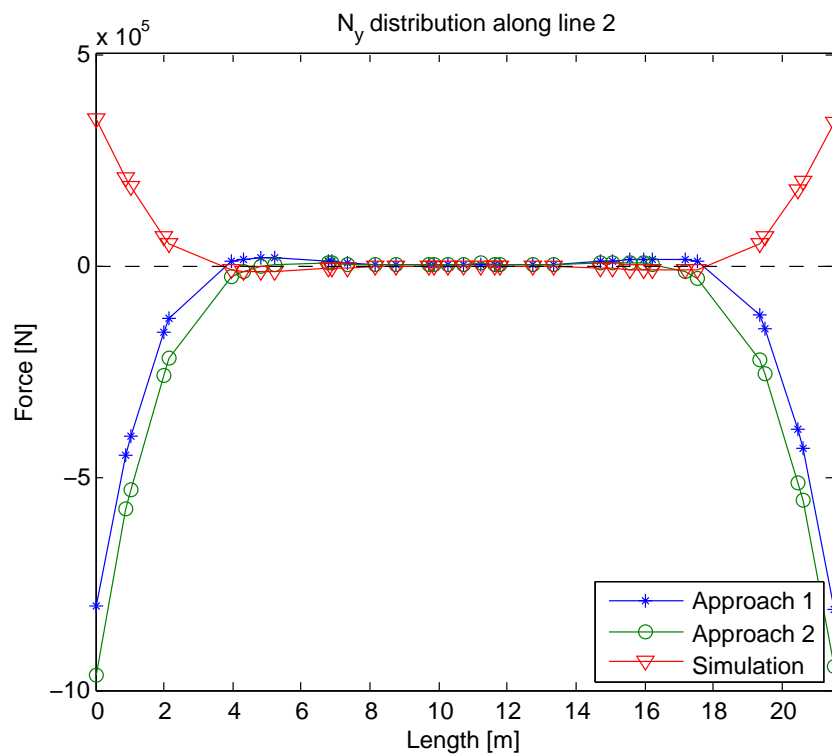


Figure B.34: Section force N_y along line 2 with heating of the concrete bridge deck

B.2.4 Stresses in cross section

Additional plots for element 2 from section 6.2.4.

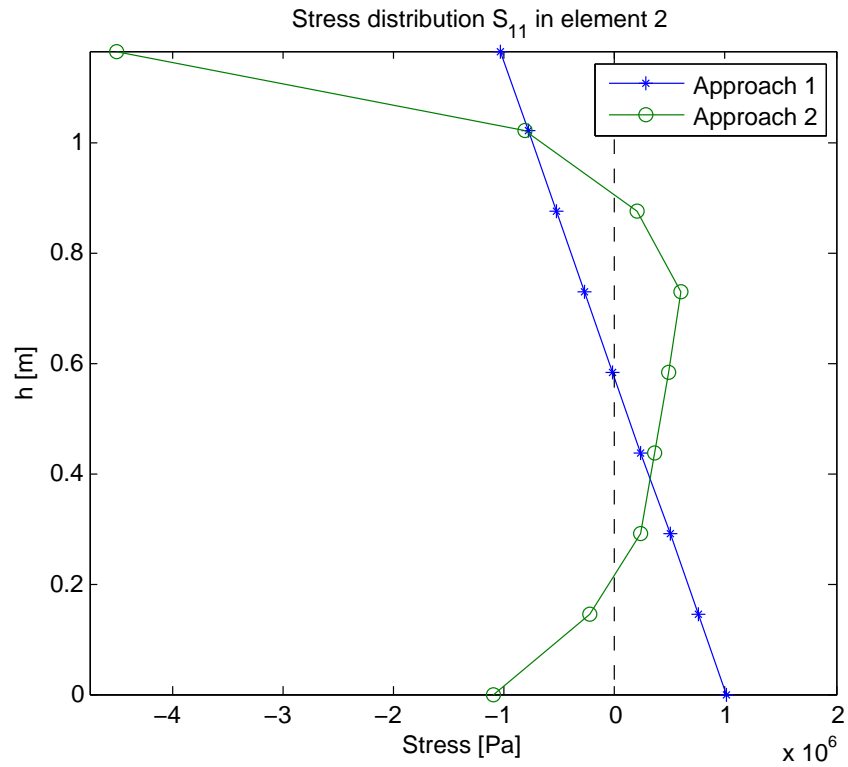


Figure B.35: Stress distribution in element 2, heating of bridge deck

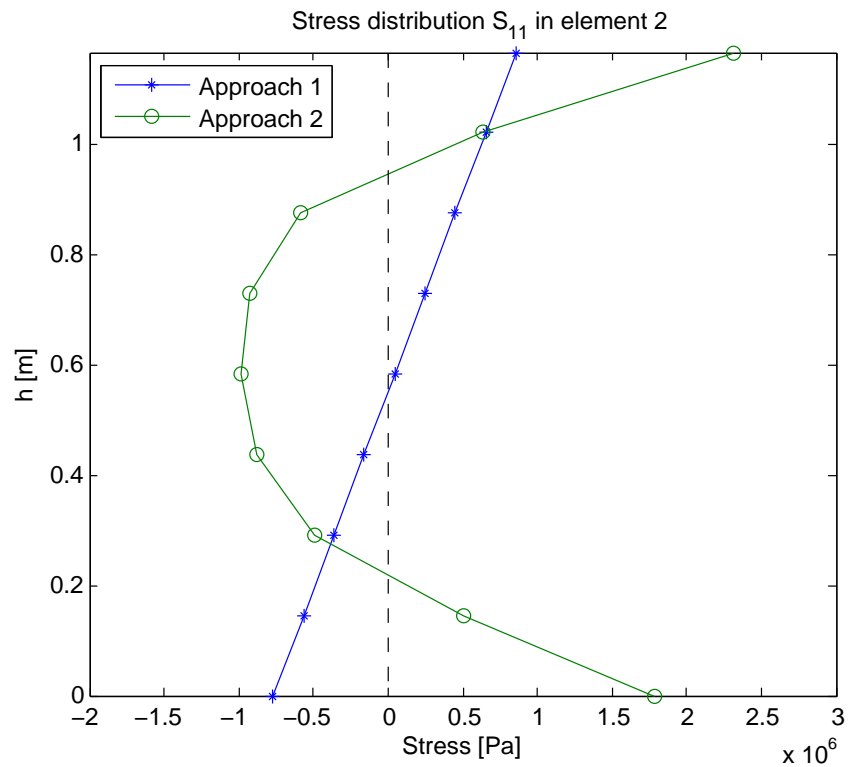


Figure B.36: Stress distribution in element 2, cooling of bridge deck

B.2.4.1 Stresses from self weight

As a comparison of the stresses from the temperature loads, plots showing stresses from the self weight load case is displayed here.

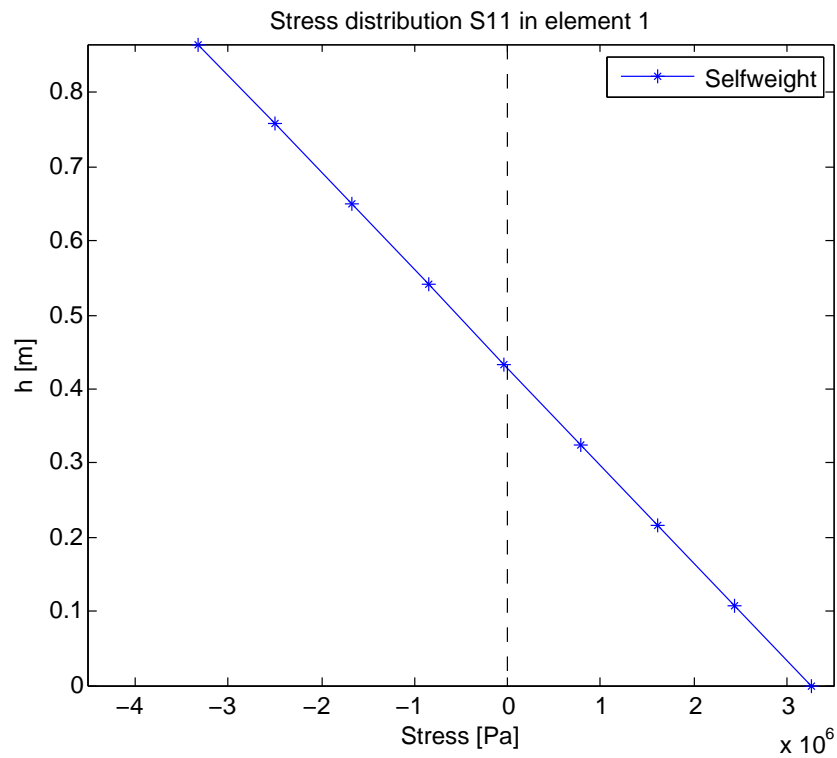


Figure B.37: Stress distribution in element 1, Self weight

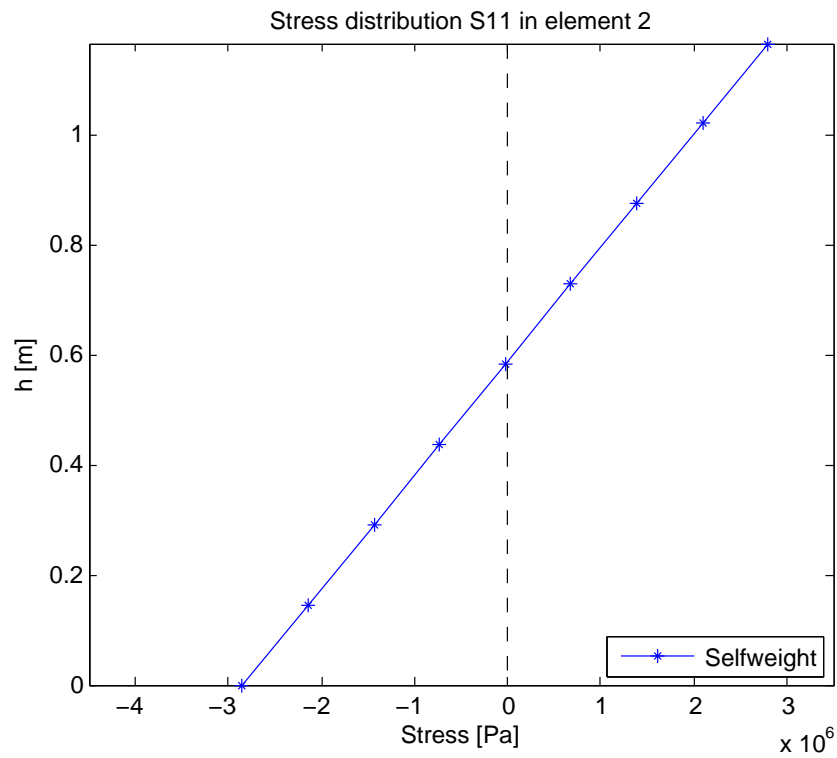


Figure B.38: Stress distribution in element 2, Self weight